（千葉大学学位申請論文）

Studies on function of Slingshot phosphatase during early development of *Xenopus laevis*

アフリカツメガエル初期発生における Slingshot フォスファターゼの機能に関する研究

2005 年 7 月

千葉大学大学院自然科学研究科
生命資源科学専攻生命機構学講座
田中健之

Table of contents

General abstract

ADF/cofilin is a key regulator for actin dynamics in cytokinesis and cell locomotion. Its activity is suppressed by phosphorylation and reactivated by dephosphorylation. First, I investigated dephosphorylation (activation) of ADF/cofilin during *Xenopus* cleavage. Since we found that ADF/cofilin was dephosphorylated at prophase and telophase, in cycling extracts. I examined the effect of Rho GTPase, which is activated at telophase, in CSF extracts. Addition of constitutively active Rho induced dephosphorylation of ADF/cofilin. This dephosphorylation was inhibited by Na_3VO_4 but not by other conventional phosphatase-inhibitors. I cloned a *Xenopus* homologue of slingshot phosphatase (XSSH), originally identified in *Drosophila* and human as an ADF/cofilin phosphatase, and raised antibody specific for the catalytic domain of XSSH. This inhibitory antibody significantly suppressed the Rho-induced dephosphorylation of ADF/cofilin in extracts, suggesting that the dephosphorylation at telophase is dependent on XSSH. XSSH bound to actin filaments with a dissociation constant of 0.4 μM, and the ADF/cofilin phosphatase activity was increased in the presence of F-actin. When latrunculin A, a G-actin-sequestering drug, was added to extracts, both Rho-induced actin polymerization and dephosphorylation of ADF/cofilin were markedly inhibited. Jasplakinolide, an actin filament-stabilizing drug, alone induced actin polymerization in the extracts and lead to dephosphorylation of ADF/cofilin. These results suggest that Rho-induced dephosphorylation of ADF/cofilin is dependent on the XSSH activation that is caused by increase in the amount of F-actin induced by Rho signaling. XSSH colocalized with both actin filaments and ADF/cofilin in the actin patches formed on the surface of the early cleavage furrow. Injection of inhibitory antibody blocked cleavage of blastomeres. Thus, XSSH may reorganize actin filaments through dephosphorylation and hence reactivation of ADF/cofilin at early stage of contractile ring formation.

Next, I investigated XSSH function on gastrulation movements of *Xenopus* embryos. Whole mount *in situ* hybridization showed XSSH transcripts in the blastopore lip and sensorial ectoderm at stage 11, and subsequently localized to developing brain, branchial arches, developing retina, otic

vesicle, cement gland, and spinal chord in neurula to tailbud embryos. Immunostaining of animal-vegetal sections of gastrula embryos demonstrated that both XAC and XSSH proteins are predominant in ectodermal and involuting mesodermal cells. Microinjection of either a wild type (thus induces overexpression) or a phosphatase-defective mutant (functions as dominantly negative form) caused defects in gastrulation, and often generated the spina bifida phenotype with reduced head structures. Interestingly, the ratio of phosphorylated XAC to dephosphorylated XAC markedly increased from the early gastrula stage (stage 10.5), although the amount of XSSH protein markedly increased from this stage. These results suggest that gastrulation movement requires ADF/cofilin activity through dynamic regulation of its phosphorylation state.

General introduction

Actin depolymerizing factor (ADF)/cofilin family of proteins, which has been shown to be essential in eukaryotes, enhances actin filament dynamics by depolymerizing and severing actin filaments (Bamburg, 1999; Bamburg *et al.*, 1999; Carlier *et al.*, 1999; Maciver and Hussey, 2002). The activity of this protein is inhibited by phosphorylation of an N-terminal serine residue (Agnew *et al.*, 1995; Moriyama *et al.*, 1996). In a wide variety of cells, ADF/cofilin exhibits rapid dephosphorylation in response to certain exogenous stimuli, for example, such as heat shock in cultured cells (Ohta *et al.*, 1989; Abe *et al.*, 1993) and formyl-methionyl-leucyl-phenylalanine (fMLP) in polymorphonuclear leukocytes (Suzuki *et al.*, 1995; Okada *et al.*, 1996), and the dephosphorylation accompanies dramatic changes in actin organization that are required for cellular function (Moon and Drubin, 1995). LIM kinases (Limks) (Arber *et al.*, 1998; Sumi *et al.*, 1999; Yang *et al.*, 1998), testicular protein kinases (TESKs) (Toshima *et al.*, 2001a, 2001b), and Nck-interacting kinase (NIK)-related kinase (NRK)/NIK-like embryo-specific kinase (NESK) (Nakano *et al.*, 2003) are responsible for phosphorylation of ADF/cofilin in vertebrates. Two types of Limks, designated by Limk 1 and Limk 2 are present in vertebrates (Mizuno *et al.*, 1994; Okano *et al.*, 1995; Nunoue *et al.*, 1995; Osada *et al.*, 1996; Cheng *et al.*, 1995; Koshimizu *et al.*, 1997; Takahashi *et al.*, 1997, 2001). Pioneering works (Arber *et al.*, 1998; Yang *et al.*, 1998) demonstrated that activation of Limk 1 is mediated by Rac1, and were followed by a study that activation of Pak1 through Rac1 or Cdc42 directly increases Limk 1 activity (Edwards *et al.*, 1999). Also, Limks activation occur downstream of Rho-Rho kinase (ROK/ROCK) signaling (Maekawa *et al.*, 1999; Sumi *et al.*, 1999; Ohashi *et al.*, 2000; Amano *et al.*, 2001). These studies all strongly suggest that phosphorylation, and thus inactivation, of ADF/cofilin proceeds through activation of Rho-GTPases. On the other hand, Slingshot (SSH) has been identified as an ADF/cofilin-specific phosphatase in *Drosophila* and human (Niwa *et al.*, 2002). SSH genetically interacts with the LIMK gene in *Drosophila*, and over-expression of SSH with Limk1 or Tesk1 suppresses formation of actin-rich structures induced by these kinases. Therefore, SSH might reactivate ADF/cofilin, phosphorylated by Limks, to increase

actin filament dynamics and/or to reorganize pre-existing actin cytoskeleton.

In *Xenopus*, ADF/cofilin is highly phosphorylated in oocytes and unfertilized eggs, and undergoes rapid dephosphorylation in response to the fertilization. Both overexpression and down-regulation of ADF/cofilin cause a defect in cytokinesis (Abe *et al.*, 1996). *Xenopus* Limk1 and 2 (Xlimk1 and 2) are shown to be functionally responsible for the completion of oocyte maturation (Takahashi *et al.*, 2001). These results suggest that phosphorylation-regulation of ADF/cofilin is tightly liked to actin-dependent cellular processes during *Xenopus* development. Therefore, I examined the biological significance of regulation of the ADF/cofilin activity during *Xenopus* early development.

Cytokinesis is the essential process to create two daughter cells. It begins at late anaphase to telophase and the contractile ring, the core components of which are actin filaments, is formed in the cortex of the cleavage furrow. Recent study demonstrated that actin dynamics in the contractile ring are critical for cytokinesis (Pelham and Chang, 2002). During cytokinesis, ADF/cofilin is concentrated in the cleavage furrow in mammalian cells and *Xenopus* zygotes (Nagaoka *et al.*, 1995; Abe *et al.*, 1996). Injection of the antibody specific for *Xenopus* ADF/cofilin (XAC) inhibits cleavage of zygotes, suggesting that XAC is required for the progression of cytokinesis (Abe *et al.*, 1996). Limk1 and SSH activities are differently regulated during cytokinesis of Hela cells: the activity of Limk1 is elevated at prometaphase to metaphase while the SSH activity increases at telophase to cytokinesis (Amano *et al.*, 2002; Kaji *et al.*, 2003). In addition, expression of dominantly negative form of SSH markedly increases multinucleated cells. These results strongly suggest that active ADF/cofilin is necessary for cytokinesis. On the other hand, the Rho GTPase is a key regulator for the contractile ring formation at cytokinesis (Mabuchi *et al.*, 1993; Kishi *et al.*, 1993; Drechsel *et al.*, 1997; Prokopenko *et al.*, 1999). GTP-bound Rho, which is the active form, increases at telophase, concentrated at the cleavage furrow and orchestrates various actin-binding proteins (Takaishi *et al.*, 1995; Kimura *et al.*, 2000; Yoshizaki *et al.*, 2003).

On the other hand, gastrulation is the most important morphogenetic process accompanied by dynamic cell migration. Rho family and the effector proteins are involved in the gastrulation movement (Marlow *et al.*, 2002; Tahinci and Symes, 2003). In *Xenopus*, the morphogenetic cell

behavior during gastrulation, such as epiboly of the ectoderm, rotation of the endoderm, involution of the mesoderm, and convergent extension of the dorsal mesoderm, is well defined by extensive studies (for reviews see Keller *et al.*, 2003; Duncan and Su, 2004). The molecular basis for these movements remains to be fully understood, while recent studies have considerably shed light on the molecular mechanism that underlies the convergent extension; non-canonical Wnt signaling is shown to play a central role in this process (Kuhl, 2002; Tada *et al.*, 2002) Rho is activated by Daam1 which binds to Dishevelled and might regulate the actin binding proteins (Habas *et al.*, 2003). ADF/cofilin activity and its regulation by Limks and SSH is significant for cell migration in cultured cells (Endo *et al.*, 2003; Pollard and Borisy, 2003; Ghosh *et al.*, 2004). Thus, it is of interest to examine whether the regulation of ADF/cofilin activity is involved in *Xenopus* gastrulation movements.

In the first chapter, I focused on dephosphorylation of XAC during *Xenopus* cleavage. I found that dephosphorylation of XAC was induced by addition of a constitutively active form of RhoA to the *Xenopus* egg extract which is able to reconstitute mitotic phases and cycles. Thus, I cloned a *Xenopus* homologue of SSH (XSSH) and investigated its involvement in dephosphorylation of XAC using *Xenopus* egg extracts. Finally, I concluded that Rho-induced XAC dephosphorylation is dependent on the XSSH activation that is caused by increase in the amount of F-actin induced by Rho signaling.

In the second chapter, I examined the significance of XAC phosphorylation-regulation by XSSH for *Xenopus* gastrulation movements. XSSH predominantly localize in ectodermal and involuting mesodermal cells, and overexpression or functionally inhibition by injection of XSSH mRNAs resulted in gastrulation defect. These results revealed that XSSH is functionally involved in the gastrulation. This finding provides novel insights into the regulatory mechanism of gastrulation movements from a cell biological aspect.

Chapter 1

Involvement of Slingshot in the Rho-mediated dephosphorylation of ADF/cofilin during *Xenopus* cleavage

Abstract

ADF/cofilin is a key regulator for actin dynamics during cytokinesis. Its activity is suppressed by phosphorylation and reactivated by dephosphorylation. Little is known, however, about regulatory mechanisms of ADF/cofilin function during formation of contractile ring actin filaments. Using *Xenopus* cycling extracts, we found that ADF/cofilin was dephosphorylated at prophase and telophase. In addition, constitutively active Rho GTPase induced dephosphorylation of ADF/cofilin in the egg extracts. This dephosphorylation was inhibited by Na_3VO_4 but not by other conventional phosphatase-inhibitors. I cloned a *Xenopus* homologue of Slingshot phosphatase (XSSH), originally identified in *Drosophila* and human as an ADF/cofilin phosphatase, and raised antibody specific for the catalytic domain of XSSH. This inhibitory antibody significantly suppressed the Rho-induced dephosphorylation of ADF/cofilin in extracts, suggesting that the dephosphorylation at telophase is dependent on XSSH. XSSH bound to actin filaments with a dissociation constant of 0.4 μM, and the ADF/cofilin phosphatase activity was increased in the presence of F-actin. When latrunculin A, a G-actin-sequestering drug, was added to extracts, both Rho-induced actin polymerization and dephosphorylation of ADF/cofilin were markedly inhibited. Jasplakinolide, an actin filament-stabilizing drug, alone induced actin polymerization in the extracts and lead to dephosphorylation of ADF/cofilin. These results suggest that Rho-induced dephosphorylation of ADF/cofilin is dependent on the XSSH activation that is caused by increase in the amount of F-actin induced by Rho signaling. XSSH colocalized with both actin filaments and ADF/cofilin in the actin patches formed on the surface of the early cleavage furrow. Injection of inhibitory antibody blocked cleavage of blastomeres. Thus, XSSH may reorganize actin filaments through dephosphorylation and hence reactivation of ADF/cofilin at early stage of contractile ring formation.

Introduction

Cytokinesis is the essential process to create two daughter cells. It begins at late anaphase to telophase and the contractile ring, the core components of which are actin filaments, is formed in the cortex of the cleavage furrow. Recent study demonstrated that actin dynamics in the contractile ring are critical for cytokinesis (Pelham and Chang, 2002). Actin filaments are dynamically regulated through interaction with various actin-binding proteins in cells. Among them, ADF/cofilin is the key regulator responsible for actin dynamics in cells (for reviews see Bamburg, 1999a; Bamburg *et al.*, 1999b; Carlier *et al.*, 1999; Maciver and Hussey, 2002).

ADF/cofilin is a ubiquitously expressed and highly conserved actin binding protein and also functions in cytokinesis (Gunsalus *et al.*, 1995; Nagaoka *et al.*, 1995; Abe *et al.*, 1996; Okada *et al.*, 1999; Nakano *et al.*, 2001; Ono *et al.*, 2003). ADF/cofilin binds to actin in a 1:1 molar ratio, alters the twist of F-actin and causes both depolymerization and severing of actin filaments (Nishida *et al.*, 1984; Carlier *et al.*, 1997; MacGough *et al.*, 1997). Acceleration of actin depolymerization by ADF/cofilin maintains the monomeric actin pool and thereby promotes actin filament turnover (for review see Pollard and Borisy, 2003). Severing of actin filaments by ADF/cofilin results in the generation of free barbed ends, which in turn is crucial for efficient enhancement of actin polymerization *in vivo* (Ghosh *et al.*, 2004). Both activities might be deeply involved in reorganization of actin filaments in cells.

These activities are suppressed by phosphorylation at Ser3 (Agnew *et al.*, 1995; Moriyama *et al.*, 1996). LIM kinases (Limks) (Arber *et al.*, 1998; Yang *et al.*, 1998; Sumi *et al.*, 1999), testicular protein kinases (TESKs) (Toshima *et al.*, 2001a, 2001b), and Nck-interacting kinase (NIK)-related kinase (NRK)/NIK-like embryo-specific kinase (NESK) (Nakano *et al.*, 2003) have been demonstrated to phosphorylate ADF/cofilin in vertebrates. Two types of Limks, designated by Limk 1 and Limk 2 are present in vertebrates (Mizuno *et al.*, 1994; Okano *et al.*, 1995; Nunoue *et al.*, 1995; Cheng and Robertson, 1995; Osada *et al.*, 1996; Koshimizu *et al.*, 1997; Takahashi *et al.*, 1997, 2001). Pioneering works (Arber *et al.*, 1998; Yang *et al.*, 1998) demonstrated that activation of Limk 1 is

mediated by a small GTPase Rac1, and were followed by a study that activation of p21-activated kinase (Pak1) through Rac1 or Cdc42 directly increases Limk 1 activity (Edwards *et al.*, 1999). Also, activation of Limks occurs downstream of Rho-Rho kinase (ROK/ROCK) signaling (Maekawa *et al.*, 1999; Sumi *et al.*, 1999; Ohashi *et al.*, 2000; Amano *et al.*, 2001). All of these studies strongly suggest that phosphorylation, and thus inactivation, of ADF/cofilin proceeds through activation of Rho-GTPases. On the other hand, ADF/cofilin is also dephosphorylated by extracellular stimuli (for review see Moon and Drubin, 1995). Recently, cofilin specific phosphatase, Slingshot (SSH), has been identified in *Drosophila*, human and mouse (Niwa *et al.*, 2002; Ohta *et al.*, 2003), which directly dephosphorylates and thus reactivates ADF/cofilin. This activity is also regulated downstream of PI3-kinase or Rac1 in lamellipodia of cultured mammalian cells and increased by binding to actin filaments (Nishita *et al.*, 2004; Nagata-Ohashi *et al.*, 2004).

During cytokinesis, ADF/cofilin is concentrated in the cleavage furrow in mammalian cells and *Xenopus* zygotes (Nagaoka *et al.*, 1995; Abe *et al.*, 1996). Injection of the antibody specific for *Xenopus* ADF/cofilin (XAC) inhibits cleavage of zygotes, suggesting that XAC is required for the progression of cytokinesis (Abe *et al.*, 1996). Limk1 and SSH activities are differently regulated during cytokinesis of Hela cells: the activity of Limk1 is elevated at prometaphase to metaphase while the SSH activity increases at telophase to cytokinesis (Amano *et al.*, 2002; Kaji *et al.*, 2003). In addition, expression of dominantly negative form of SSH markedly increases multinucleated cells. These results strongly suggest that active ADF/cofilin is necessary for cytokinesis. On the other hand, the Rho GTPase is a key regulator for the contractile ring formation at cytokinesis (Mabuchi *et al.*, 1993; Kishi *et al.*, 1993; Drechsel *et al.*, 1997; Prokopenko *et al.*, 1999). GTP-bound Rho, which is the active form, increases at telophase, concentrated at the cleavage furrow and orchestrates various actin-binding proteins (Takaishi *et al.*, 1995; Kimura *et al.*, 2000; Yoshizaki *et al.*, 2003). Therefore, it is important to examine whether the ADF/cofilin activity is regulated under the Rho GTPase during cytokinesis.

In this study, I found that dephosphorylation of XAC was induced by addition of a constitutively active form of RhoA to the *Xenopus* egg extract which is able to reconstitute mitotic phases and

cycles. Thus, I cloned a *Xenopus* homologue of SSH (XSSH) and investigated its involvement in dephosphorylation of XAC using *Xenopus* egg extracts. Finally, I concluded that Rho-induced XAC dephosphorylation is dependent on the XSSH activation that is caused by increase in the amount of F-actin induced by Rho signaling.

MATERIALS AND METHODS

Polyacrylamide gel electrophoresis and immunoblotting

SDS-polyacrylamide gel electrophoresis (SDS-PAGE) was carried out according to Laemmli (1970). Two-dimensional gel electrophoresis (2D-PAGE) was performed according to O'Farrell *et al.* (1977) using nonequilibrium-pH-gradient gel electrophoresis (NEpHGE) for the first dimension. Samples were dissolved in 2D-PAGE buffer composed of 9 M urea, 2% ampholine pH 3.5-10, 5% 2-mercaptoethanol, 0.1% SDS, 1% NP-40, and 10 mM Tris-HCl, pH 7.5. For immunoblotting, proteins were electrophoretically transferred from the SDS-gel to nitrocellulose paper by the method of Towbin *et al.* (1979). The paper was treated with 5% skimmed milk in PBS for 1 hr, and then incubated with the primary antibody followed by treatment with alkaline phosphatase-conjugated secondary antibody. The paper was thoroughly washed with PBS after each immunoreaction and stained with nitroblue tetrazolium chloride (NBT) and 5-bromo-4-chloro-3-indolylphosphate p-toluidine salt (BCIP) in alkaline phosphatase buffer (0.1 M NaCl, 5 mM $MgCl_2$, and 0.1 M Tris-HCl, pH 9.5), or detected by chemiluminescence with CDP-Star (Roche) using Light Capture (ATTO).

Preparation of egg extracts

Egg extracts (cycling extracts and cytostatic factor-arrested (CSF) extracts) were prepared from unfertilized eggs as described by Murray (1991) with some modifications. For cycling extracts, egg activation was carried out by treating eggs with 0.2 μg/ml calcium ionophore A23187 for 3 min at room temperature. Extracts were obtained by centrifugation in the absence of actin-depolymerizing drug such as cytochalasin B. Interphase extracts and re-entered mitotic extracts (prepared by adding ΔN85 cyclin B2 to interphase extracts; pGEX-ΔN85 cyclin B2 was kindly provided by Dr. Kishimoto, T of Tokyo Institute of Technology) were prepared according to Glotzer *et al.*, 1991.

Cloning of XSSH and construction of expression vectors

A stage 30 *Xenopus* embryo cDNA library in λZAPII was screened by polymerase chain reaction (PCR) with a degenerated primer set of 5'-CTKGGWAGYGARTGGAAYGC and 5'-ACWCCCATYTTRCARTGTAC, corresponding to the nucleotide sequence of 1177-1415 in the

Drosophila SSH catalytic domain that is highly homologous to human SSHs. A major band with about 240 bp was amplified and cloned into the EcoRV site of pBluescript II KS^+ vector. Sequencing of this PCR fragment exhibited about 70% identity with human SSH between their primary structures, suggesting a *Xenopus* homologue of SSH (XSSH). The PCR fragment was excised from pBluescript II KS^+ vector with EcoRI and XhoI and inserted into a pGEX-4T-1 vector digested with EcoRI and XhoI, and glutathione-S-transferase (GST)-fused catalytic domain was expressed. The anti-XSSH antibodies were obtained by immunizing the GST-catalytic domain to rabbits (see below). A full-length clone was isolated from a *Xenopus* ovary λZAPII cDNA library with anti-XSSH antibody (GenBank accession number AY 618876). A partial cDNA clone lacking N-terminus (pBluescript SK^--ΔN-XSSH) was also isolated from the stage 30 cDNA library, and used for expression of His-tagged ΔN-XSSH protein.

To produce the full-length XSSH as GST-fusion protein (GST-XSSH), the XSSH cDNA in pBluescript SK^- was first digested with KpnI and blunted by T4 polymerase, and then excised with EcoRI. This fragment was inserted into EcoRI and SmaI sites of pGEX-4T-3 vector. To produce catalytically inactive mutant (GST-CSXSSH), the catalytically essential Cys^{380} of GST-XSSH was changed to Ser by site-directed mutagenesis using complementary primers (5'-GTGTACTTGTGCACTCCAAGATGGGAGTCTCTC and 5'-GAGAGACTCCCATCTTGGAGTGCACAAGTACAC), and checked by sequencing. For GST-SSH A and B domains (GST-AB), the XSSH cDNA was digested with EcoRI and XhoI, and cloned into the same sites of pGEX-4T-3 vector. To produce GST-Tail, a novel EcoRI site was generated by site-directed mutagenesis using complementary primers (5'-CAAACATATCAAGGAATTCTAGGAGCCAGTAAGC and 5'-GCTTACTGGCTCCTAGAATTCCTTGATATGTTTG), and checked by sequencing. The tail region of mutagenized cDNA (EcoXSSH) was excised with EcoRI and inserted into the same site of pGEX-4T-2 vector. For the mutant possessing both SSH homology domain AB and DSPc domain (GST-ABP), the EcoXSSH cDNA was digested with EcoR1, and cloned into the same site of pGEX-4T-3 vector. For DSPc domain (GST-DSPc), the EcoXSSH cDNA was digested with Pst1 and

EcoR1, blunted by T4 polymerase, and cloned into Sma1 site of pGEX-4T-1. For expression of His-tagged ΔN-XSSH, ΔN-XSSH cDNA was excised with EcoRI and inserted into the same site of pRSET-A vector.

Preparation of proteins

pGEX expression plasmids carrying the XSSH full-length, CSXSSH, SSH A and B domains, DSPc domain, AB and DSPc domains, and tail region were transformed into BL21 (DE3) pLysS and the expression of recombinant proteins was induced by adding 0.1 mM IPTG for overnight at 13 °C. Cells were harvested and lysed by sonication in PBS containing 0.1% Triton X-100, and soluble fractions were obtained by centrifugation at 15,000 g for 20 min at 4 °C. Supernatants were added to glutathione-Sepharose 4B (Pharmacia) prewashed with PBS. Mixtures were incubated for 1 hr at 4 °C with gentle, continuous stirring, and then resins were poured into columns and thoroughly washed with PBS containing 0.1% Triton X-100. Proteins were eluted with PBS containing 50 mM Tris-HCl, pH 8.0 and 10 mM glutathione, and dialyzed against F-buffer (0.1 M KCl, 2 mM $MgCl_2$, 1 mM DTT, 20 mM HEPES-KOH, pH 7.2). BL21 (DE3) pLysS was also transformed by pRSET- ΔN-XSSH and the expression was induced by adding 0.5 mM IPTG for 3 hr at 37 °C. Inclusion bodies of ΔN-XSSH, washed with PBS containing 1% Triton X-100, was solubilized with 6 M urea containing 0.1 M Na-PO_4, pH 8.0, and applied to Ni-NTA column (QIAGEN). The column was washed with the same buffer, but at pH 6.5, and the same buffer containing 20 mM imidazole, pH 7.0. His-ΔN-XSSH was eluted by the same buffer containing 0.1 M imidazole, pH 7.0, dialyzed against coupling buffer (6M urea, 80 mM $CaCl_2$, 0.1 M HEPES-KOH, pH 7.4), and coupled to Affi-gel 10 (Bio-Rad).

GST-V14RhoA was prepared as described (Self and Hall, 1995). pGEX-human V14RhoA was a generous gift from Dr. Bamburg of Colorado States University. Purified GST-V14RhoA was concentrated to at least 4 mg/ml, dialyzed against 100 mM KCl, 2 mM $MgCl_2$, 50 mM sucrose, 10 mM HEPES-KOH, pH 7.7, and stored at –80 °C until use.

Actin was prepared from rabbit skeletal muscle by the method of Spudich and Watt (1971) and purified by gel filtration on a Sephadex G-200 column pre-equilibrated with G-buffer composed of 0.2 mM $CaCl_2$, 0.1 mM DTT, 0.2 mM ATP, 0.01% NaN_3, and 2.5 mM Tris-HCl, pH 8.0. 100 μl

portions of G-actin were quick-frozen in liquid nitrogen and stored at –80 °C.

The phosphorylated XAC fraction was prepared from *Xenopus* ovaries. *Xenopus* ovaries were homogenized in 5 volumes of buffer A (0.1 M KCl, 2 mM EGTA, 2 mM DTT, 50 mM NaF, and 20 mM HEPES-KOH, pH 7.2) containing 40% saturation of ammonium sulfate, 20 μg/ml leupeptin, and 1 mM PMSF. After centrifugation at 15,000 g for 20 min at 4 °C, the supernatant was further fractionated by 60-90% saturation with ammonium sulfate. The precipitate was collected by centrifugation at 15,000 g for 30 min at 4 °C, and solubilized and dialyzed to buffer A. The dialysate was gel-filtrated on a Sephadex G-75 column, and fractions containing XAC were applied to a hydroxyapatite column pre-equilibrated with buffer A, followed by washing thoroughly with buffer A and buffer A containing 0.6 M KCl. XAC was eluted with buffer A containing 0.6 M KCl and 10 mM K-PO4, pH 7.5, and dialyzed against 20 mM NaCl, 2 mM DTT, and 20 mM Tris-HCl (pH 7.5). Finally, the flow-through fraction from a DE52 ion exchange column pre-equilibrated with the same buffer was concentrated, dialyzed against F-buffer, and stored at –80 °C until use.

Assays for dephosphorylation of XAC

Cycling extracts were incubated at 23 °C and 5 μl of the extract was removed and immediately added to 100 μl of 10% trichloroacetic acid (TCA) every 5 min to stop reaction and precipitate proteins. Samples were centrifuged at 15,000 g for 15 min at 4 °C, and pellets were once rinsed with 50% acetone and dried for 2D-PAGE. Progression of cell cycle was monitored by checking sperm morphology as described by Murray (1991).

1/20 volume of GST-V14RhoA or buffer alone was added to CSF extracts, interphase extracts or re-entered mitotic extracts at a final concentration of 4.2 μM, and incubated at 22 °C for 1 hr. When phosphatase inhibitors, Y-27632 (kindly provided by Yoshitomi Pharmaceutical Industries, Ltd), latrunculin A, jasplakinolide, or 10 mg/ml of affinity-purified antibody were used, adding volume was fixed at 1/20 to the extract. Final concentrations of each drug are shown in figure legends. At the end of incubation, 10% TCA was added to the samples to stop reaction and proteins were precipitated, rinsed and dried as described above.

For in vitro phosphatase assay, various forms of XSSH or GST was incubated with the

phosphorylated XAC (pXAC) fraction (the final concentration of pXAC was estimated to be 5.5 μM by densitometry) for 1 hr at room temperature in F-buffer. To examine the effect of F-actin, pXAC fraction was pre-incubated with F-actin in the absence or presence of latrunculin A (50 μM) for 30 min at room temperature in F-buffer, and then GST-XSSH, GST-ABP or GST was added and incubated for additional 1 hr at room temperature. Reactions were stopped by addition of 10% TCA to samples and proteins were precipitated, rinsed and dried as described above.

Samples were solubilized in 2D-PAGE buffer and subjected to 2D-PAGE and immunoblotting. XAC spots were detected by chemiluminescence using Light Capture (ATTO) and analyzed by densitometry with a software of ATTO Lane Analyzer 10H.

Co-sedimentation assay of XSSH with F-actin

Binding of XSSH to actin filaments was examined by pelleting assay. Various amounts of GST-tagged full-length XSSH or truncated mutants were incubated with 3.0 μM F-actin, which had been polymerized in F-buffer for 1 hr at room temperature, for 3 hr at 4 °C. Samples were centrifuged at 400,000 g for 20 min and the supernatants and pellets were subjected to SDS-PAGE. Gels were stained with Coomassie Blue G-250 and destained in 7% acetic acid. Protein bands were quantified by densitometry using Light Capture (ATTO) and a software, ATTO Lane Analyzer 10H.

Antibodies

Inclusion bodies of GST-fused XSSH catalytic domain, as described above, was thoroughly washed with PBS containing 1% Triton X-100, and with 3M urea, and then solubilized with SDS-sample buffer (4% SDS, 5% 2-mercaptoethanol, 10% glycerol and 25 mM Tris-HCl, pH 6.8). After centrifugation at 15,000 g for 15 min, the supernatant was subjected to SDS-PAGE, stained with Coomassie Blue R-250 and the protein band corresponding to GST-catalytic domain was excised with a razor blade. GST-catalytic domain was electrophoretically eluted from gel slices, dialyzed to PBS, and used to immunize rabbits to produce polyclonal antibody. Antisera were purified by His-XSSH-coupled Affi-gel 10 column chromatography.

Anti-XAC monoclonal antibody was previously prepared (Okada *et al.*, 1999). Anti-actin polyclonal and monoclonal (AC-40) antibodies were kindly provided by Dr. K. Iida of the Tokyo

Metropolitan Institute of Medical Science and purchased from Sigma, respectively. Anti-phosphorylated ADF/cofilin-specific antibody was kindly provided by Dr. Bamburg of Colorado State University. Fluorescein or rhodamine-labeled goat anti-mouse or rabbit IgG was purchased from TAGO Inc. Alkaline phosphatase-conjugated goat anti-mouse or rabbit IgG was purchased from Bio-Rad.

Microinjection

Affinity-purified anti-XSSH IgG, concentrated to 10 mg/ml and dialyzed against the injection buffer consisting of 60 mM KCl, 2 mM $MgCl_2$, 5 mM HEPES-KOH, pH 7.2, was injected into one blastomere of two-cell stage embryos. Injection volumes from each pipette from a pressure injector (CIJ-1, Shimadzu, Kyoto) were calibrated by measuring the volume of an aqueous drop delivered into mineral oil. Control injections with injection buffer alone and the same amount of non-immune IgG were also done (Abe *et al.*, 1996; Okada *et al.*, 1999).

Immunofluorescence microscopy

Xenopus embryos were fixed in MEMFA (3.7% formaldehyde, 2 mM $MgSO_4$, 1 mM EGTA, and 0.1 M MOPS, pH 7.4) containing 1% TCA, embedded in paraffin, and sectioned as described elsewhere (Okada *et al.*, 1999). *Xenopus* cleavage furrows were manually isolated and fixed according to Noguchi and Mabuchi (2000). After blocking with 20% goat serum in PBS for 1 hr at room temperature, specimens were incubated with primary antibodies or Alexa 488-wheatgerm agglutinin (WGA) for 1 hr at room temperature, and then with appropriate fluorochrome-conjugated secondary antibodies. After each immunoreaction step, specimens were rinsed and washed with PBS, and mounted in PBS containing 1 mg/ml p-phenylenediamine and 90 % glycerol.

RESULTS

XAC is dephosphorylated at prophase and telophase during cell cycle

In order to address whether the phosphorylation state of XAC is altered during mitosis of *Xenopus* zygotes, we first quantified changes of the ratio of phosphorylated XAC (pXAC) to unphosphorylated XAC using cycling extracts prepared from *Xenopus* unfertilized eggs. Progression of the cell cycle was monitored by morphological changes of added sperm nuclei. pXAC and unphosphorylated XAC were separated and detected by a combination of 2D-PAGE and immunoblotting using a monoclonal antibody specific for XAC. The signal intensity of each spots was quantified by densitometry. As shown in Fig. 1A, the amount of dephosphorylated XAC increased at prophase and telophase when actin filaments are thought to be drastically reorganized. Dephosphorylation of XAC (thus, reactivation of XAC) at telophase might exhibit necessity of XAC for contractile ring formation, since we have previously demonstrated that XAC is essential for the progression of cleavage of *Xenopus* zygotes. Therefore, I next examined effects of RhoA, a key regulator of the contractile ring formation, on the phosphorylation state of XAC using *Xenopus* mitotic extracts.

RhoA induces dephosphorylation of XAC in Xenopus egg extracts

Extracts, to which V14RhoA, a constitutively active form of RhoA, was added, were incubated for 1 hr at 22 °C, and analyzed by 2D-PAGE and immunoblotting. As shown in Fig. 1B and C, although about 55% of endogenous XAC was phosphorylated in a control CSF extract, addition of V14RhoA decreased pXAC to about 30%. Similar results were obtained by using either interphase extracts or mitotic extracts reentered to anaphase by addition of undegradable cyclin B (delta-N cyclin B) to the interphase extract (data not shown). In order to examine whether RhoA signaling correlates with this dephosphorylation, Y-27632, a ROCK-specific inhibitor, was added to extracts. As shown in Fig.1C, Y-27632 partially suppressed the V14RhoA-induced dephosphorylation of XAC. Therefore, activation of Rho seems to induce dephosphorylation of XAC in *Xenopus* zygotes.

To determine which phosphatase is responsible for the dephosphorylation of XAC, effects of

various phosphatase inhibitors were examined. V14RhoA was added to CSF extracts in the presence of okadaic acid (OA), a phosphatase inhibitor specific for phosphatase type 1 and type 2A (PP1 and PP2A), cypermethrin (specific for PP2B), or sodium orthovanadate (Na_3VO_4, specific for protein tyrosine phosphatases (PTP) and dual-specificity phosphatases (DSP)). Changes in the amount of pXAC were monitored chemiluminescently by immunoblotting using an antiserum that specifically recognizes the phosphorylated form of ADF/cofilin (Fig. 2A). Total amounts of XAC on each lane were confirmed by immunoblotting on the same membrane using a monoclonal antibody specific for XAC. Neither OA nor cypermethrin suppressed dephosphorylation of XAC induced by addition of V14RhoA (Fig. 2, B and C), whereas Na_3VO_4 completely blocked it (Fig. 2D). Thus, the results suggest that XAC phosphatase is a DSP but not a conventional Ser/Thr phosphatase.

XSSH is responsible for the dephosphorylation of XAC in the extracts

Slingshot (SSH) was recently identified as a cofilin-specific phosphatase and is a candidate for the XAC phosphatase, since it possesses a DSP-catalytic domain (DSPc). Therefore, I cloned a *Xenopus* homologue of SSH (XSSH, accession number AY618876) and raised a polyclonal antibody specific for the DSPc domain. This antibody, as shown in Fig. 3A, specifically reacted with bacterially expressed XSSH (His-ΔN–XSSH, see *Materials and Methods*) and a single band of an apparent molecular mass of 78 kDa in the egg extract, well corresponding to the calculated value from the deduced amino acid sequence. In addition, this antibody also reacted the XSSH that was expressed in reticulocyte lysates. Thus, I concluded that this antibody specifically recognizes DSPc domain of XSSH. When V14RhoA was added to the CSF extract in the presence of this antibody, dephosphorylation of XAC was inhibited as shown in Fig. 3B and C. This inhibitory effect strongly suggests that XSSH is responsible for the dephosphorylation of XAC induced by RhoA.

XSSH is activated by actin polymerization induced by RhoA

Since purified SSH is shown to be activated by the presence of actin filaments (Nagata-Ohashi *et al.*, 2004), I hypothesized that RhoA-induced dephosphorylation of XAC in egg extracts may also be affected by the increasing amount of F-actin triggered by the active RhoA. In order to elucidate this point, I first quantified F-actin contents in extracts. As shown in Fig. 3D, addition of V14RhoA

markedly decreased the amount of actin in the supernatant and hence increased that in the pellet, although a significant amount of actin was present in the supernatant in control extracts. Therefore, RhoA induces actin polymerization in this extract. When latrunculin A alone was added to extracts, the amount of F-actin decreased. V14RhoA did not antagonize this effect of latrunculin A because of no increase in the amount of F-actin in the pellet. Next, as shown in Fig. 3E, I examined phosphorylation states of XAC in the respective extracts and found that dephosphorylation of XAC by RhoA was suppressed in the presence of latrunculin A. In addition, the dephosphorylation effect of an exogenous GST-XSSH (see Fig. 4) was also inhibited to some extent by the presence of latrunculin A. It should be noted that addition of latrunculin A alone effectively increased the phosphorylation level of XAC in the extract, and staurosporine, a broad kinase inhibitor, did not repress this increase in the amount of pXAC (data not shown). Whether *Xenopus* Limks are involved in this phosphorylation remains to be elucidated.

Since repression of actin polymerization by latrunculin A prevented XAC dephosphorylation induced by RhoA, it is possible that increasing amount of F-actin directly causes dephosphorylation of XAC in the extract. To clarify this point, jasplakinolide, which promotes actin polymerization, was added to the extract. As shown in Fig. 3D and F, F-actin was increased in the high-speed precipitate and dephosphorylation of XAC was induced by addition of this drug. Na_3VO_4 completely inhibited this dephosphorylation.

XSSH tightly binds to actin filaments to increase dephosphorylation activity

In order to examine the binding property of XSSH to actin filaments, I prepared GST-tagged XSSH (full-length, GST-XSSH) and two mutants of XSSH, the SSH domain (GST-AB), and the tail region (GST-Tail) (Fig. 4, A and B). Pelleting assays revealed that both full-length and each mutants were cosedimented with F-actin (Fig. 4, C and D). Dissociation constants (Kd) of GST-XSSH and GST-AB for actin were calculated by Scatchard analyses to be 0.4 and 0.5 μM, respectively (Fig. 4E). In addition, their binding to actin was saturated at a molar ratio of 1:6.5 and 1:8.7, respectively. On the other hand, in vitro phosphatase activity of XSSH was examined with GST-XSSH and phosphorylated XAC (pXAC) fraction. As shown in Fig. 4F, the pXAC fraction contained more than

85% of pXAC, and no kinase, phosphatase, and proteinase activities were detected (data not shown). GST-XSSH dephosphorylated XAC and its activity was markedly increased in the presence of F-actin, while the addition of F-actin preincubated with latrunculin A antagonized this effect (Fig. 4G). Taken all together, it is reasonable to conclude that XSSH activity increases by binding to F-actin, of which polymerization is induced by RhoA signaling.

Domain analyses of XSSH

To determine domains required for XAC dephosphorylation, I also prepared three mutants of XSSH recombinant proteins (Fig. 5A), and carried out phosphatase assay. GST-XSSH and GST-ABP, both of which possess SSH homology domain AB and DSPC domain, dephosphorylated XAC, but GST-DSPc and GST-CSXSSH (phoshatase inactive mutant) did not (Fig. 5B; *left*). Na_3VO_4 inhibited XAC dephosphorylation by purified GST-XSSH. In addition, it is of interest that GST-ABP showed higher activity for dephosphorylation of XAC than GST-XSSH did. On the other hand, pNPP hydorolytic assay revealed that GST-DSPc can dephosphorylate pNPP as a substrate (Fig. 5B; *right*). This indicates that GST-DSPc was functionally active. Thus, the AB domain of XSSH seems to be necessary for recognition of XAC for its dephosphorylation.

Since AB domain and tail region of XSSH bind to F-actin and F-actin binding elevates the dephosphorylation activity of GST-XSSH (Fig.4), I next examined the effect of F-actin on dephosphorylation activity of GST-ABP. As shown in Fig. 5C, although GST-ABP exhibited potent dephosphorylation activity for XAC, its activity was not increased by the presence of F-actin. In contrast, GST-XSSH, showing lower activity than GST-ABP in the absence of F-actin, was markedly activated by the addition of F-actin. These results suggest that (or I assume that) the tail region potentially functions as a weak inhibitory domain for XAC dephosphorylation, whereas F-actin binding to the tail region releases the inhibitory effect and increases the dephosphorylation activity.

Phosphorylation of XSSH does not affect its activities for F-actin and XAC

Recently, it was reported that hSSH-1L, the human slingshot type 1 long form, was down-regulated by phosphorylation (Nagata-Ohashi *et al.*, 2004; Soosairajah *et al*, 2005; Wang *et al*, 2005). I previously confirmed that XSSH in CSF-extracts is phosphorylated and addition of V14RhoA to

extracts does not affect the phosphorylation state of XSSH itself. Then, to examine effects of phosphorylation of XSSH on its F-actin-binding and XAC dephosphorylation activities, I first treated extracts with alkaline phosphatase. As shown in Fig. 6A *left*, the phosphorylated XSSH in the extract was dephosphorylated by alkaline phosphatase (AP) treatment. By addition of GST-XSSH to the extract, the exogenous XSSH also phosphorylated efficiently (Fig. 6A *right*). Phosphrylated or dephosphorylated form of GST-XSSH in extracts was collected by pull down using glutathione beads, and their affinity for F-actin were analyzed by F-actin co-sedimentation assay (Fig. 6B) and their phosphatase activities were assayed using the pXAC fraction as a substrate (Fig. 6C). In either case, I could not find any differences between phosphorylated and dephosphorylated form of XSSH.

Inhibition of cleavage by injection of anti-XSSH antibody

I injected affinity-purified anti-XSSH antibody into one blastomere of 2-cell stage embryos. Injection of more than 100 ng of anti-XSSH IgG arrested the cleavage of blastomeres (Fig. 7B, arrows), but control injection of neither buffer alone nor non-immune IgG arrested development (Fig. 7A, arrowheads). Injection of less than 100 ng scarcely affected cleavage. The processes of the cleavage of antibody-injected blastomeres were monitored (Fig. 7C). De-vitellinized embryos were used to observe blastomeres clearly and the antibody was injected into one blastomere at the 2-cell stage. Buffer-injected control embryos normally divided and each blastomere separated (Fig. 7C, arrowhead). In contrast, the antibody-injected blastomere exhibited abnormal cleavage (Fig. 7C, arrow): the furrow ingress occurred partially, did not deepen, and sometimes regressed.

Distribution of XSSH in cleaving zygotes and its localization at the cleavage furrow

Cleaving zygotes were fixed, sectioned, and stained with anti-XSSH and anti-XAC antibodies. As shown in Fig. 8 A and B, both proteins were diffusely distributed in the cytoplasm in addition to the localization at the cortex. XSSH also accumulated deeper in the cleavage furrow and its immunofluorescence was found in the midbody structure (Fig. 8C). These distributions of XSSH were very similar to those of XAC (Fig. 8D; Abe *et al.*, 1996).

The localization of XSSH at the cleavage furrow was further observed with isolated cleavage furrows. In the early stage of furrowing, as has been shown by Noguchi and Mabuchi (2000), bleb-

like structures, which were detected by binding of wheatgerm agglutinin (WGA), formed on the surface of the furrow region (Fig. 8E), and the F-actin patch was present underneath these structures (Fig. 8F). Immunofluorescent microscopy revealed that XAC colocalized with F-actin patches, but not with F-actin bundles (Fig. 8, G and H). Both XSSH and XAC colocalized in F-actin patches (Fig. 8, I and J).

Discussion

Here I cloned a *Xenopus* homologue of slingshot ADF/cofilin phosphatase and characterized its biochemical properties for dephosphorylation of XAC by using *Xenopus* egg extracts and demonstrated its biological significance for the cleavage of *Xenopus* zygotes. *Xenopus* egg extracts are primarily powerful materials for analyses of cell cycle progression and mitosis. In addition, recent studies provide the advantages of their usage in studies on the cytoskeletal organization, since extracts contains almost all materials, such as proteins, RNAs, and membranous vesicles, essential for reproduction of intracellular events without any novel gene expression. Therefore I chose the extract system to examine the dephosphorylation pathway of XAC.

XAC dephosphorylation downstream of RhoA in Xenopus egg extracts

Spikes in dephosphorylation (activation) of XAC were observed twice during mitotic phase, once in prophase and again in telophase. Generally in cultured animal cells, actin cytoskeleton that has been organized in interphase dramatically disassembles and cells round at prophase (for review see Glotzer 2001). At telophase, when cytokinesis begins, actin cytoskeleton is also reorganized to form contractile ring at the cleavage furrow. Since ADF/cofilin essentially possesses severing and depolymerizing activities for actin filaments, this protein could act in the opposite situation, i.e., disassemble actin filaments at prophase but function as a reorganizer to enhance turnover of actin filaments at telophase. It is necessary to confirm whether disassembly of actin filaments really arises at prophase in *Xenopus* zygotes. Rho protein is a key regulator of cytokinesis, since C3 exoenzyme, a Rho specific ADP-ribosyl transferase, blocks the cytokinesis and GTP-bound RhoA is increased at telophase and concentrated in the cleavage furrow (Kishi *et al.*, 1993; Mabuchi *et al.*, 1993; Takahashi *et al.*, 1995; Drechsel *et al.*, 1997; Prokopenko *et al.*, 1999; Kimura *et al.*, 2000; Yoshizaki *et al.*, 2003). The downstream protein kinases of Rho family GTPases, such as ROCK and PAK, phosphorylate and activate Limks (Edwards *et al.*, 1999; Maekawa *et al.*, 1999; Ohashi *et al.*, 2000; Amano *et al.*, 2001; Sumi *et al.*, 2001a, b). Thus, I focused my study on XAC dephosphorylation at telophase.

Interestingly, constitutively active RhoA induced XAC dephosphorylation, and this dephosphorylation was suppressed by addition of Na_3VO_4 (a PTP and DSP inhibitor), but not okadaic acid (a PP1 and PP2A inhibitor) and cypermethrin (a PP2B inhibitor). ADF/cofilin phosphatases were previously characterized by addition of phosphatase-type specific inhibitors, and suggested to be PP1 and PP2A in T lymphocytes, PP1 and PP2B in cultured neurons, and PP2C and/or other type phosphatase in neutrophils (Meberg *et al.*, 1998; Ambach *et al.*, 2000; Zhan *et al.*, 2003). However, since conventional phosphatase inhibitors except Na_3VO_4 did not inhibit dephosphorylation of XAC in the extract, I assumed my phosphatase to be a novel one and began to explore it. Recently, however, SSH was identified as a cofilin specific phosphatase in *Drosophila*, human and mouse (Niwa *et al.*, 2002; Ohta *et al.*, 2003). SSH has DSPc domain in the central portion, and this activity is inhibited by addition of Na_3VO_4 (Niwa *et al.*, 2002). Together, I predicted that XSSH might be involved in RhoA induced XAC dephosphorylation in the extracts. Therefore, I cloned a *Xenopus* homologue of SSH and raised an inhibitory antibody specific for XSSH DSPc domain. Finally, since addition of this antibody suppressed the RhoA-induced XAC dephosphorylation in extracts, I concluded that XSSH dephosphorylates and activates XAC downstream of Rho signaling at telophase.

Regulation of XSSH activity

SSH phosphatases consists of N-terminal SSH homology domain A and B, DSPc domain and tail region. Primary structures of N-terminal half, A, B, and catalytic domains, were well conserved in vertebrates, whereas the tail regions were less homologous between *Xenopus* and mammals. Bacterially expressed GST-ABP exhibited XAC dephosphorylation activity but GST-DSPc did not (Fig. 5), suggesting that AB domain is necessary for XAC dephosphorylation activity of XSSH. Previous work demonstrated that the tail region more tightly binds to F-actin than the N-terminal half without the tail region does (Ohta *et al.*, 2003). Interestingly, however, the A and B domains of XSSH possessed much higher affinity for F-actin with Kd value of 0.5 μM than the tail region. The full length XSSH with Kd of 0.4 μM suggests that the tail region also participates in binding to F-actin. Several isoforms of mammalian SSH have S domain in the tail region. However, XSSH does not

possess this domain in its tail region. This might be the reason for lower affinity of the tail region of XSSH for F-actin.

The phosphatase activity of purified XSSH markedly increased by binding of F-actin to the tail region (Fig. 5C). This result corresponds well to the case of mammalian SSH (Nagata-Ohashi *et al.*, 2004). Mammalian SSH exhibits dephosphorylation activity toward ADF/cofilin with or without tail region in the absence of F-actin. However, the truncated SSH without tail is scarcely activated by F-actin and decreased the affinity for F-actin. Tail region of human SSH (hSSH-1L) is phosphorylated and possesses two 14-3-3 binding motifs, and dephosphorylated form of hSSH-1L exhibits higher activity (Nagata-Ohashi *et al.*, 2004; Soosairajah *et al*, 2005; Wang *et al*, 2005). In this study, however, XSSH was also phosphorylated but showed no differences for activity toward pXAC between the two forms. The discrepancy may be due to the difference of animals examined, but two explanations might be possible. 1) Phospho-regulation of XSSH is restricted within binding to some partners (for example, 14-3-3 or the other un-identified proteins) and/or localization in cells not to be involved in the regulation of phosphatase activity. 2) There are some phosphorylation sites on XSSH, one of which is up-regulation site and the other is down-regulation site. Indeed, I confirmed that AB domain and the tail region of XSSH are phosphorylated (data not shown). It is important to identify the phosphorylated residues and their regulatory functions.

V14RhoA induced both XAC dephosphorylation and actin polymerization in the egg extracts. Latrunculin A, an actin monomer sequestering drug, suppressed XAC dephosphorylation induced by V14RhoA in egg extracts. On the other hand, addition of jasplakinolide, an actin-stabilizing drug, into the egg extracts caused F-actin accumulation and XAC dephosphorylation, and this effect was blocked in the presence of Na_3VO_4. These results suggest that XSSH is activated by its binding to actin filaments which are induced to polymerize by RhoA signaling, and dephosphorylates XAC. Actually, when ROCK, one of RhoA effectors that promote actin polymerization, was inhibited by Y-27632, V14RhoA-induced dephosphorylation of XAC was partially blocked. Originally, ROCK activates Limk to increase phosphorylated ADF/cofilin in mammalian cultured cells (Maekawa *et al.*, 1999), but Y-27632 alone scarcely affected phosphorylation states of XAC in the extract. In addition,

Amano *et al.* (2002) reported that Limk is not activated by ROCK during mitotic phase. Therefore, this partial inhibition of V14RhoA-induced dephosphorylation of XAC by Y27632 might be caused by suppression of novel actin polymerization mediated by ROCK.

More of interest is that addition of latrunculin A alone caused increase in phosphorylated XAC compared with addition of vehicle alone. The basal level of phosphorylated XAC in extracts was scarcely affected in the presence of phosphatase inhibitors or anti-XSSH antibody alone (Fig. 2 and 3). Therefore, I speculate that depolymerization of actin has driven the unknown machinery which leads to phosphorylation of XAC. This latrunculin A-induced XAC phosphorylation was not suppressed by staurosporine, a broad kinase inhibitor. Whether or not Limk is involved in this phosphorylation remains to be addressed.

Possible function of XSSH during cytokinesis

Immunofluorescence microscopy revealed that XSSH localizes to the midbody and actin patches on the surface of the furrow with XAC and actin. Noguchi and Mabuchi (2000) have shown that actin patches are fused with each other and with myosin spots and then simultaneously reorganized to form the contractile ring actin bundles. XSSH may dephosphorylate and activate XAC in these patches to reorganize actin filaments. Genetic studies using model animals demonstrated that ADF/cofilin mutants form unusual actin aggregates in cells and blockage of regular actin filament bundles (Gunsalus *et al.*, 1995; Ono *et al.*, 1999). In addition, inactivation of ADF/cofilin by expression of active Limk also induced to form actin aggregates (Sumi *et al.*, 1999). Thus, ADF/cofilin may be required for the regular actin assembly in cells. The present result that injection of inhibitory antibody prevented cleavage of blastomeres suggests functional significance of XSSH for dephosphorylation of XAC at actin patches.

On the other hand, roles of ADF/cofilin in membrane protrusion and lamellipodia formation were reported (Chan *et al.*, 2000; Zebda *et al.*, 2000; Kempiak *et al.*, 2003; DesMarais *et al.*, 2004; Mounelimne *et al.*, 2004;). A recent study using caged cofilin directly showed that cofilin activation induces actin polymerization, cell protrusion and determine the direction of cell migration (Ghosh *et al.*, 2004). These reports suggest that cofilin generates free barbed ends, which in turn are necessary

for polymerization of actin *in vivo*. In *Xenopus* zygotes, it was reported that exogenous G-actin was incorporated into contractile ring (Noguchi and Mabuchi 2000). It is possible that XAC, reactivated through dephosphorylation by XSSH, severs actin filaments to generate free barbed ends, sites for novel actin polymerization.

Together with previous works by Kaji *et al.* (2003), the present study provided evidence that dephosphorylation and hence reactivation of ADF/cofilin is critical for cytokinesis. Most recently, a novel ADF/cofilin-specific phosphatase, designated as chronophin (CIN), has been reported (Gohla *et al.*, 2005). This phosphatase regulates ADF/cofilin dephosphorylation during mitosis and is activated differently from SSH. In my present study, XAC dephosphorylation occurred twice at prophase and telophase, and I suggested the later dephosphorylation is Rho-dependent. Consistently with my results, mammalian SSH activity is also elevated at telophase to cytokinesis (Kaji *et al.*, 2003). The first dephosphorylation peak at prophase is possibly dependent on *Xenopus* CIN, because it has been shown that CIN dephosphorylates ADF/cofilin prior to SSH activation. *Xenopus* egg extracts may offer an excellent experiment system in which to further examine their regulation and role during cytokinesis.

References

Abe, H., Obinata, T., Minamide, L. S. and Bamburg, J. R. (1996). Xenopus laevis actin-depolymerizing factor/cofilin: a phosphorylation-regulated protein essential for development. *J Cell Biol* **132**, 871-85.

Agnew, B. J., Minamide, L. S. and Bamburg, J. R. (1995). Reactivation of phosphorylated actin depolymerizing factor and identification of the regulatory site. *J Biol Chem* **270**, 17582-7.

Amano, T., Tanabe, K., Eto, T., Narumiya, S. and Mizuno, K. (2001). LIM-kinase 2 induces formation of stress fibres, focal adhesions and membrane blebs, dependent on its activation by Rho-associated kinase-catalysed phosphorylation at threonine-505. *Biochem J* **354**, 149-59.

Amano, T., Kaji, N., Ohashi, K. and Mizuno, K. (2002). Mitosis-specific activation of LIM motif-containing protein kinase and roles of cofilin phosphorylation and dephosphorylation in mitosis. *J Biol Chem* **277**, 22093-102. Epub 2002 Mar 29.

Ambach, A., Saunus, J., Konstandin, M., Wesselborg, S., Meuer, S. C. and Samstag, Y. (2000). The serine phosphatases PP1 and PP2A associate with and activate the actin-binding protein cofilin in human T lymphocytes. *Eur J Immunol* **30**, 3422-31.

Arber, S., Barbayannis, F. A., Hanser, H., Schneider, C., Stanyon, C. A., Bernard, O. and Caroni, P. (1998). Regulation of actin dynamics through phosphorylation of cofilin by LIM-kinase. *Nature* **393**, 805-9.

Bamburg, J. R. (1999). Proteins of the ADF/cofilin family: essential regulators of actin dynamics. *Annu Rev Cell Dev Biol* **15**, 185-230.

Bamburg, J. R., McGough, A. and Ono, S. (1999). Putting a new twist on actin: ADF/cofilins modulate actin dynamics. *Trends Cell Biol* **9**, 364-70.

Carlier, M. F., Laurent, V., Santolini, J., Melki, R., Didry, D., Xia, G. X., Hong, Y., Chua, N. H. and Pantaloni, D. (1997). Actin depolymerizing factor (ADF/cofilin) enhances the rate of filament turnover: implication in actin-based motility. *J Cell Biol* **136**, 1307-22.

Carlier, M. F., Ressad, F. and Pantaloni, D. (1999). Control of actin dynamics in cell motility. Role

of ADF/cofilin. *J Biol Chem* **274**, 33827-30.

Chan, A. Y., Bailly, M., Zebda, N., Segall, J. E. and Condeelis, J. S. (2000). Role of cofilin in epidermal growth factor-stimulated actin polymerization and lamellipod protrusion. *J Cell Biol* **148**, 531-42.

Cheng, A. K. and Robertson, E. J. (1995). The murine LIM-kinase gene (limk) encodes a novel serine threonine kinase expressed predominantly in trophoblast giant cells and the developing nervous system. *Mech Dev* **52**, 187-97.

DesMarais, V., Macaluso, F., Condeelis, J. and Bailly, M. (2004). Synergistic interaction between the Arp2/3 complex and cofilin drives stimulated lamellipod extension. *J Cell Sci* **117**, 3499-510.

Drechsel, D. N., Hyman, A. A., Hall, A. and Glotzer, M. (1997). A requirement for Rho and Cdc42 during cytokinesis in Xenopus embryos. *Curr Biol* **7**, 12-23.

Edwards, D. C., Sanders, L. C., Bokoch, G. M. and Gill, G. N. (1999). Activation of LIM-kinase by Pak1 couples Rac/Cdc42 GTPase signalling to actin cytoskeletal dynamics. *Nat Cell Biol* **1**, 253-9.

Endo, M., Ohashi, K., Sasaki, Y., Goshima, Y., Niwa, R., Uemura, T. and Mizuno, K. (2003). Control of growth cone motility and morphology by LIM kinase and Slingshot via phosphorylation and dephosphorylation of cofilin. *J Neurosci* **23**, 2527-37.

Ghosh, M., Song, X., Mouneimne, G., Sidani, M., Lawrence, D. S. and Condeelis, J. S. (2004). Cofilin promotes actin polymerization and defines the direction of cell motility. *Science* **304**, 743-6.

Glotzer, M., Murray, A. W. and Kirschner, M. W. (1991). Cyclin is degraded by the ubiquitin pathway. *Nature* **349**, 132-8.

Glotzer, M. (2001). Animal cell cytokinesis. *Annu Rev Cell Dev Biol* **17**, 351-86.

Gohla, A., Birkenfeld, J. and Bokoch, G. M. (2005). Chronophin, a novel HAD-type serine protein phosphatase, regulates cofilin-dependent actin dynamics. *Nat Cell Biol* **7**, 21-9. Epub 2004 Dec 5.

Gunsalus, K. C., Bonaccorsi, S., Williams, E., Verni, F., Gatti, M. and Goldberg, M. L. (1995). Mutations in twinstar, a Drosophila gene encoding a cofilin/ADF homologue, result in defects in centrosome migration and cytokinesis. *J Cell Biol* **131**, 1243-59.

Kaji, N., Ohashi, K., Shuin, M., Niwa, R., Uemura, T. and Mizuno, K. (2003). Cell cycle-

associated changes in Slingshot phosphatase activity and roles in cytokinesis in animal cells. *J Biol Chem* **278**, 33450-5. Epub 2003 Jun 14.

Kempiak, S. J., Yip, S. C., Backer, J. M. and Segall, J. E. (2003). Local signaling by the EGF receptor. *J Cell Biol* **162**, 781-7.

Kimura, K., Tsuji, T., Takada, Y., Miki, T. and Narumiya, S. (2000). Accumulation of GTP-bound RhoA during cytokinesis and a critical role of ECT2 in this accumulation. *J Biol Chem* **275**, 17233-6.

Kishi, K., Sasaki, T., Kuroda, S., Itoh, T. and Takai, Y. (1993). Regulation of cytoplasmic division of Xenopus embryo by rho p21 and its inhibitory GDP/GTP exchange protein (rho GDI). *J Cell Biol* **120**, 1187-95.

Koshimizu, U., Takahashi, H., Yoshida, M. C. and Nakamura, T. (1997). cDNA cloning, genomic organization, and chromosomal localization of the mouse LIM motif-containing kinase gene, Limk2. *Biochem Biophys Res Commun* **241**, 243-50.

Laemmli, U. K. (1970). Cleavage of structural proteins during the assembly of the head of bacteriophage T4. *Nature* **227**, 680-5.

Mabuchi, I., Hamaguchi, Y., Fujimoto, H., Morii, N., Mishima, M. and Narumiya, S. (1993). A rho-like protein is involved in the organisation of the contractile ring in dividing sand dollar eggs. *Zygote* **1**, 325-31.

Maciver, S. K. and Hussey, P. J. (2002). The ADF/cofilin family: actin-remodeling proteins. *Genome Biol* **3**, reviews3007. Epub 2002 Apr 26.

Maekawa, M., Ishizaki, T., Boku, S., Watanabe, N., Fujita, A., Iwamatsu, A., Obinata, T., Ohashi, K., Mizuno, K. and Narumiya, S. (1999). Signaling from Rho to the actin cytoskeleton through protein kinases ROCK and LIM-kinase. *Science* **285**, 895-8.

McGough, A., Pope, B., Chiu, W. and Weeds, A. (1997). Cofilin changes the twist of F-actin: implications for actin filament dynamics and cellular function. *J Cell Biol* **138**, 771-81.

Meberg, P. J., Ono, S., Minamide, L. S., Takahashi, M. and Bamburg, J. R. (1998). Actin depolymerizing factor and cofilin phosphorylation dynamics: response to signals that regulate neurite extension. *Cell Motil Cytoskeleton* **39**, 172-90.

Moon, A. and Drubin, D. G. (1995). The ADF/cofilin proteins: stimulus-responsive modulators of actin dynamics. *Mol Biol Cell* **6**, 1423-31.

Moriyama, K., Iida, K. and Yahara, I. (1996). Phosphorylation of Ser-3 of cofilin regulates its essential function on actin. *Genes Cells* **1**, 73-86.

Mouneimne, G., Soon, L., DesMarais, V., Sidani, M., Song, X., Yip, S. C., Ghosh, M., Eddy, R., Backer, J. M. and Condeelis, J. (2004). Phospholipase C and cofilin are required for carcinoma cell directionality in response to EGF stimulation. *J Cell Biol* **166**, 697-708.

Murray, A. W. (1991). Cell cycle extracts. *Methods Cell Biol* **36**, 581-605.

Nagaoka, R., Abe, H., Kusano, K. and Obinata, T. (1995). Concentration of cofilin, a small actin-binding protein, at the cleavage furrow during cytokinesis. *Cell Motil Cytoskeleton* **30**, 1-7.

Nagata-Ohashi, K., Ohta, Y., Goto, K., Chiba, S., Mori, R., Nishita, M., Ohashi, K., Kousaka, K., Iwamatsu, A., Niwa, R. et al. (2004). A pathway of neuregulin-induced activation of cofilin-phosphatase Slingshot and cofilin in lamellipodia. *J Cell Biol* **165**, 465-71.

Nakano, K., Kanai-Azuma, M., Kanai, Y., Moriyama, K., Yazaki, K., Hayashi, Y. and Kitamura, N. (2003). Cofilin phosphorylation and actin polymerization by NRK/NESK, a member of the germinal center kinase family. *Exp Cell Res* **287**, 219-27.

Nakano, K., Satoh, K., Morimatsu, A., Ohnuma, M. and Mabuchi, I. (2001). Interactions among a fimbrin, a capping protein, and an actin-depolymerizing factor in organization of the fission yeast actin cytoskeleton. *Mol Biol Cell* **12**, 3515-26.

Nishida, E., Maekawa, S. and Sakai, H. (1984). Cofilin, a protein in porcine brain that binds to actin filaments and inhibits their interactions with myosin and tropomyosin. *Biochemistry* **23**, 5307-13.

Nishita, M., Wang, Y., Tomizawa, C., Suzuki, A., Niwa, R., Uemura, T. and Mizuno, K. (2004). Phosphoinositide 3-kinase-mediated activation of cofilin phosphatase Slingshot and its role for insulin-induced membrane protrusion. *J Biol Chem* **279**, 7193-8. Epub 2003 Nov 26.

Niwa, R., Nagata-Ohashi, K., Takeichi, M., Mizuno, K. and Uemura, T. (2002). Control of actin reorganization by Slingshot, a family of phosphatases that dephosphorylate ADF/cofilin. *Cell* **108**,

233-46.

Noguchi, T. and Mabuchi, I. (2001). Reorganization of actin cytoskeleton at the growing end of the cleavage furrow of Xenopus egg during cytokinesis. *J Cell Sci* **114**, 401-12.

Nunoue, K., Ohashi, K., Okano, I. and Mizuno, K. (1995). LIMK-1 and LIMK-2, two members of a LIM motif-containing protein kinase family. *Oncogene* **11**, 701-10.

O'Farrell, P. Z., Goodman, H. M. and O'Farrell, P. H. (1977). High resolution two-dimensional electrophoresis of basic as well as acidic proteins. *Cell* **12**, 1133-41.

Ohashi, K., Nagata, K., Maekawa, M., Ishizaki, T., Narumiya, S. and Mizuno, K. (2000). Rho-associated kinase ROCK activates LIM-kinase 1 by phosphorylation at threonine 508 within the activation loop. *J Biol Chem* **275**, 3577-82.

Ohta, Y., Kousaka, K., Nagata-Ohashi, K., Ohashi, K., Muramoto, A., Shima, Y., Niwa, R., Uemura, T., Mizuno, K. and Takeichi, M. (2003). Differential activities, subcellular distribution and tissue expression patterns of three members of Slingshot family phosphatases that dephosphorylate cofilin

Control of actin reorganization by Slingshot, a family of phosphatases that dephosphorylate ADF/cofilin. *Genes Cells* **8**, 811-24.

Okada, K., Obinata, T. and Abe, H. (1999). XAIP1: a Xenopus homologue of yeast actin interacting protein 1 (AIP1), which induces disassembly of actin filaments cooperatively with ADF/cofilin family proteins. *J Cell Sci* **112**, 1553-65.

Okano, I., Hiraoka, J., Otera, H., Nunoue, K., Ohashi, K., Iwashita, S., Hirai, M. and Mizuno, K. (1995). Identification and characterization of a novel family of serine/threonine kinases containing two N-terminal LIM motifs. *J Biol Chem* **270**, 31321-30.

Pantaloni, D., Le Clainche, C. and Carlier, M. F. (2001). Mechanism of actin-based motility. *Science* **292**, 1502-6.

Pelham, R. J. and Chang, F. (2002). Actin dynamics in the contractile ring during cytokinesis in fission yeast. *Nature* **419**, 82-6.

Pollard, T. D. and Borisy, G. G. (2003). Cellular motility driven by assembly and disassembly of

actin filaments. *Cell* **112**, 453-65.

Prokopenko, S. N., Brumby, A., O'Keefe, L., Prior, L., He, Y., Saint, R. and Bellen, H. J. (1999). A putative exchange factor for Rho1 GTPase is required for initiation of cytokinesis in Drosophila. *Genes Dev* **13**, 2301-14.

Self, A. J. and Hall, A. (1995). Purification of recombinant Rho/Rac/G25K from Escherichia coli. *Methods Enzymol* **256**, 3-10.

Soosairajah, J., Maiti, S., Wiggan, O., Sarmiere, P., Moussi, N., Sarcevic, B., Sampath, R., Bamburg, J. R. and Bernard, O. (2005). Interplay between components of a novel LIM kinase-slingshot phosphatase complex regulates cofilin. *Embo J* **24**, 473-86. Epub 2005 Jan 20.

Spudich, J. A. and Watt, S. (1971). The regulation of rabbit skeletal muscle contraction. I. Biochemical studies of the interaction of the tropomyosin-troponin complex with actin and the proteolytic fragments of myosin. *J Biol Chem* **246**, 4866-71.

Sumi, T., Matsumoto, K., Takai, Y. and Nakamura, T. (1999). Cofilin phosphorylation and actin cytoskeletal dynamics regulated by rho- and Cdc42-activated LIM-kinase 2. *J Cell Biol* **147**, 1519-32.

Sumi, T., Matsumoto, K. and Nakamura, T. (2001a). Specific activation of LIM kinase 2 via phosphorylation of threonine 505 by ROCK, a Rho-dependent protein kinase. *J Biol Chem* **276**, 670-6.

Sumi, T., Matsumoto, K., Shibuya, A. and Nakamura, T. (2001b). Activation of LIM kinases by myotonic dystrophy kinase-related Cdc42-binding kinase alpha. *J Biol Chem* **276**, 23092-6. Epub 2001 May 04.

Takaishi, K., Sasaki, T., Kameyama, T., Tsukita, S. and Takai, Y. (1995). Translocation of activated Rho from the cytoplasm to membrane ruffling area, cell-cell adhesion sites and cleavage furrows. *Oncogene* **11**, 39-48.

Takahashi, T., Aoki, S., Nakamura, T., Koshimizu, U. and Matsumoto, K. (1997). Xenopus LIM motif-containing protein kinase, Xlimk1, is expressed in the developing head structure of the embryo. *Dev Dyn* **209**, 196-205.

Takahashi, T., Koshimizu, U., Abe, H., Obinata, T. and Nakamura, T. (2001). Functional involvement of Xenopus LIM kinases in progression of oocyte maturation. *Dev Biol* **229**, 554-67.

Toshima, J., Toshima, J. Y., Amano, T., Yang, N., Narumiya, S. and Mizuno, K. (2001a). Cofilin phosphorylation by protein kinase testicular protein kinase 1 and its role in integrin-mediated actin reorganization and focal adhesion formation. *Mol Biol Cell* **12**, 1131-45.

Toshima, J., Toshima, J. Y., Takeuchi, K., Mori, R. and Mizuno, K. (2001b). Cofilin phosphorylation and actin reorganization activities of testicular protein kinase 2 and its predominant expression in testicular Sertoli cells. *J Biol Chem* **276**, 31449-58. Epub 2001 Jun 19.

Towbin, H., Staehelin, T. and Gordon, J. (1979). Electrophoretic transfer of proteins from polyacrylamide gels to nitrocellulose sheets: procedure and some applications. *Proc Natl Acad Sci U S A* **76**, 4350-4.

Wang, Y., Shibasaki, F. and Mizuno, K. (2005). Calcium signal-induced cofilin dephosphorylation is mediated by Slingshot via calcineurin. *J Biol Chem* **280**, 12683-9. Epub 2005 Jan 24.

Yang, N., Higuchi, O., Ohashi, K., Nagata, K., Wada, A., Kangawa, K., Nishida, E., Mizuno, K., Arber, S., Barbayannis, F. A. et al. (1998). Cofilin phosphorylation by LIM-kinase 1 and its role in Rac-mediated actin reorganization

Regulation of actin dynamics through phosphorylation of cofilin by LIM-kinase. *Nature* **393**, 809-12.

Yoshizaki, H., Ohba, Y., Kurokawa, K., Itoh, R. E., Nakamura, T., Mochizuki, N., Nagashima, K. and Matsuda, M. (2003). Activity of Rho-family GTPases during cell division as visualized with FRET-based probes. *J Cell Biol* **162**, 223-32. Epub 2003 Jul 14.

Zebda, N., Bernard, O., Bailly, M., Welti, S., Lawrence, D. S. and Condeelis, J. S. (2000). Phosphorylation of ADF/cofilin abolishes EGF-induced actin nucleation at the leading edge and subsequent lamellipod extension. *J Cell Biol* **151**, 1119-28.

Zhan, Q., Bamburg, J. R. and Badwey, J. A. (2003). Products of phosphoinositide specific phospholipase C can trigger dephosphorylation of cofilin in chemoattractant stimulated neutrophils. *Cell Motil Cytoskeleton* **54**, 1-15.

Figure legends

Figure 1. Dephosphorylation of XAC at prophase and telophase in cycling extracts (A) and induction of dephosphorylation of XAC by V14RhoA in CSF extracts (B and C). (A) Time course of changes in the amount of phosphorylated XAC is shown after incubation of cycling extracts at 23 °C. Samples were collected every 5 minutes. pXAC and XAC were separated and detected by a combination of 2D-PAGE and immunoblotting using anti-XAC antibody. Times from 30 to 60 min and from 85 to 130 min were in mitotic phase (M phase), and time points entered in prophase and telophase are shown, respectively. The results were obtained from at least three independent experiments. (B) CSF extracts were incubated in the presence of buffer alone or V14RhoA for 1 hr at 22 °C, and, and XAC spots were detected by 2D-immunobloting. Right spots and left spots indicate phosphorylated XAC (pXAC) and dephosphorylated XAC (XAC), respectively. (C) Changes in the percentage of phosphorylated XAC were quantified after addition of V14RhoA in the presence or absence of Y-27632. Control, addition of buffer alone; V14RhoA, addition of 4.2 μM V14RhoA; Y-27632, addition of 10 μM Y-27632; Y-27632+V14RhoA, addition of both Y-27632 and V14RhoA at the same concentration as above. The results were obtained from at least three independent experiments. Error bars represent S.E.M.

Figure 2. RhoA-induced XAC dephosphorylation was suppressed by addition of Na_3VO_4, but not okadaic acid (OA) and cypermethrin. (A) Effects of various concentration of okadaic acid (shown under the bottom panel) on RhoA-induced XAC dephosphorylation (+ indicates V14RhoA addition). *Top panel*, immunoblots using anti-phospho-cofilin antibody; *bottom panel*, immunoblots on the same membrane using anti-XAC antibody. (B) The amount of pXAC in A is quantified and shown with the ratio of addition of buffer alone (OA 0 nM) without V14RhoA (-) taken as 1.0. Effects of 1.0 nM cypermethrin (C) and 1.0 mM Na_3VO_4 (D) on XAC dephosphorylation in the presence (+) or absence (-) of V14RhoA are shown as percentage of pXAC with the means ± S.E.M. of three independent experiments.

Figure 3. XSSH is involved in the XAC dephosphorylation induced by V14RhoA. (A) Specificity of the anti-XSSH antibody. Bacterially expressed XSSH (His-ΔN-XSSH, lanes 1 and 1'), CSF-extracts (lanes 2 and 2'), reticulocyte lysates expressing XSSH (lanes 3 and 3'), and reticulocyte lysates alone (lanes 4 and 4') were electrophoresed on SDS-polyacrylamide gels. Proteins were transferred to nitrocellulose membrane. Coomassie Blue-stained gels (lanes 1-4) and immunoblots with anti-XSSH antibody (lanes 1'-4') are shown. (B) Typical patterns of immunoblot analysis of the RhoA-induced XAC dephosphorylation in the presence of affinity-purified anti-XSSH antibody. Addition of buffer alone (control), 4.2 μM V14RhoA, 200 ng of anti-XSSH antibody alone, or both anti-XSSH antibody and V14RhoA into CSF extracts were subjected to 2D-PAGE and immunoblotting using anti-XAC antibody. Arrows indicate phosphorylated XAC spots. (C) Quantification of the amounts of phosphorylated XAC in CSF extracts treated with (+) or without (-) V14RhoA in the presence (anti-XSSH) or absence of affinity-purified anti-XSSH antibody. All experimental conditions and procedures were the same as in B. (D) Polymerization of actin filaments in CSF extracts. CSF extracts were incubated with buffer alone (control), 4.2 μM V14RhoA (V14RhoA), 50 μM latrunculin A (LatA), both 50 μM latrunculin A and 4.2 μM V14RhoA (Lat A+V14RhoA), or 30 μM jasplakinolide (Jas), and then were ultracentrifuged. The supernatant (sup) and pellet (ppt) were subjected to SDS-PAGE and immnoblotting using anti-actin antibody. (E) Suppression of V14RhoA-induced XAC dephosphorylation by the presence of latrunculin A. Amounts of phosphorylated XAC in CSF extracts were quantified in the presence (+) or absence (-) of V14RhoA, latrunculin A (Lat A), or GST-XSSH. Concentrations of V14RhoA and latrunculin A added to the extract are the same as in D, and the concentration of GST-XSSH is 2 μM. (F) Effects of addition of jasplakinolide into CSF extracts on XAC dephosphorylation in the presence (+) or absence (-) of Na_3VO_4. Amounts of phosphorylated XAC were quantified in the presence (Jas, +) or absence (-) of 30 μM jasplakinolide. All error bars represent S.E.M.

Figure 4 Recombinant XSSH binds to F-actin and dephosphorylates pXAC. (A) Schematic

representation of XSSH recombinant protein constructs. All constructs were GST-tagged at the N-terminus. XSSH possesses SSH homology domains A and B, catalytic domain (DSPc) and tail region. Numbers on the bars show amino acid residues flanking each domain in addition to N- and C-terminal residues. (B) Coomassie Blue staining of purified XSSH recombinant proteins. Numbers at left denote positions of molecular mass markers. (C) Co-sedimentation assay of the respective XSSH recombinant proteins with F-actin. 3.0 μM F-actin and various concentrations of recombinant proteins (as indicated at the top of the each panel) were mixed and incubated at 4°C for 3 hours and then ultracentrifuged. The supernatant (s) and pellet (p) were subjected to SDS-PAGE. *Top panel,* GST-XSSH; *middle panel,* GST-AB; *bottom panel,* GST-Tail. Recombinant proteins and actin are indicated by arrowheads and arrows, respectively. (D) Direct plots of bound versus free for binding of different concentrations of the three recombinant proteins to fixed concentration of F-actin under the same condition as in C. *Top panel,* GST-XSSH (open squares); *middle panel,* GST-AB (closed triangles); *bottom panel,* GST-Tail (closed circles). (E) The affinity of GST-XSSH and GST-AB for actin filaments was analyzed by Scatchard plots, respectively. (F) The phosphorylated XAC (pXAC) fraction prepared from *Xenopus* oocytes was subjected to SDS-PAGE (upper panel). pXAC is shown by an asterisk. This fraction was subjected to 2D-immunoblot (lower panel). Since more than 85% of XAC is phosphorylated in this fraction (arrow), dephosphorylated XAC is scarcely detected (arrowhead). (G) Increase in XSSH activity in the presence of F-actin. Phosphatase assays were carried out using pXAC fraction and purified 2 μM GST-XSSH in the presence (+) or absence (-) of 3 μM F-actin, with (+) or without (-) 50 μM latrunculin A. Addition of buffer alone (buffer) or GST alone (GST) into pXAC fraction was also performed as control experiments. The results were obtained from at least three independent experiments. Error bars represent S.E.M.

Figure 5. Domain analyses of XSSH. (A) Schematic representation of XSSH recombinant protein constructs. Cys-380 in XSSH was replaced by Ser to construct catalytically inactive form (CSXSSH). ABP is composed of both SSH homology domain A B and DSPc domain. All constructs were tagged with GST. (B) The functional significance of AB domain for XAC dephosphorylation. *left*;

Phosphatase assay with pXAC fraction as a substrate. Final concentration of each XSSHs was 1 μM and Na_3VO_4 was adding to 1mM. *right*; Hydrolysis of *p*-nitrophenyl phosphate (pNPP) by 0.15 μM various XSSH recombinant proteins during 80 min incubation at 30 °C. Optical densities were measured at 405 nm. XSSH recombinant proteins examined are indicated under the pannel. (C) Increase in XSSH activity by F-actin is dependent on the tail region. Phosphatase assays were performed with 1 μM GST-XSSH (lane 1, 2) or GST-ABP (lane 3, 4) in the presence (+) or absence (-) of 3 μM F-actin.

Figure 6. Phosphorylated and dephosphorylated forms of XSSH exhibit the same activities for both F-actin binding and XAC dephosphorylation (A) Alkaline phosphatase (AP) treatment induced gel mobility shift of endogenous and exogenous XSSH in the extract. *left*; Extract was incubated with (+) or without (-) calf intestinal alkaline phosphatase (CIP) , and subjected to immnoblotting with anti-XSSH antibody. *right*; The extracts, to which GST-XSSH was added, were incubated with or without CIP, and immunoblotted with anti-GST antibody. (B) Phosphorylated or dephosphorylated form of GST-XSSH was collected by pull down using gltathione-beads , eluted by addition of 5 mM glutathione, and F-actin binding activities were examined by co-sedimentation assay. Both forms of XSSH equally bound to F-actin. (C) Time course of XAC dephosphorylation activity of phosphorylated and dephosphorylated XSSH in the presence or absence of F-actin. *closed diamonds*; AP un-treated GST-XSSH, *closed squares*; AP treated GST-XSSH, *open diamonds*; AP un-treated GST-XSSH with 3 μM F-actin, *open squares*; AP treated GST-XSSH with 3 μM F-actin

Figure 7. The significance of XSSH activity for complete cytokinesis. Control IgG (A) or affinity purified anti-XSSH antibody (B; 140 ng) was injected into one blastomere of *Xenopus* embryo at the 2-cell stage. Four representative examples are shown with allowheads or allows pointing to the injected blastomere. (C) Time course of the cleavage after injection. *Xenopus* eggs were fertilized, dejellied, and then vitelline membranes were removed manually with watchmaker's forceps. After the first cleavage, 20 nl of affinity purified anti-XSSH antibody (allows) or same volume of buffer

(allowheads) was injected into one blastomere. Times after injection are shown at the upper right.

Figure 8. Distribution and localization of XSSH in *Xenopus* zygotes and isolated cleavage furrows. Paraffin sections of the first cleaving embryos were immunostained dually with anti-XSSH antibody (A and C) and anti-XAC monoclonal antibody (B and D), respectively. The midbody region was amplified in C and D. Bar, 100 μm. (E-J) Isolated cleavage furrows were dually stained with Alexa-488-WGA (E) and anti-actin antibody (F), anti-XAC antibody (G) and anti-actin antibody (H), or anti-XSSH antibody (I) and anti-XAC antibody (J). The inserts show the enlarged image of actin patches. Arrowheads in H show long F-actin bundles. Bar, 20 μm.

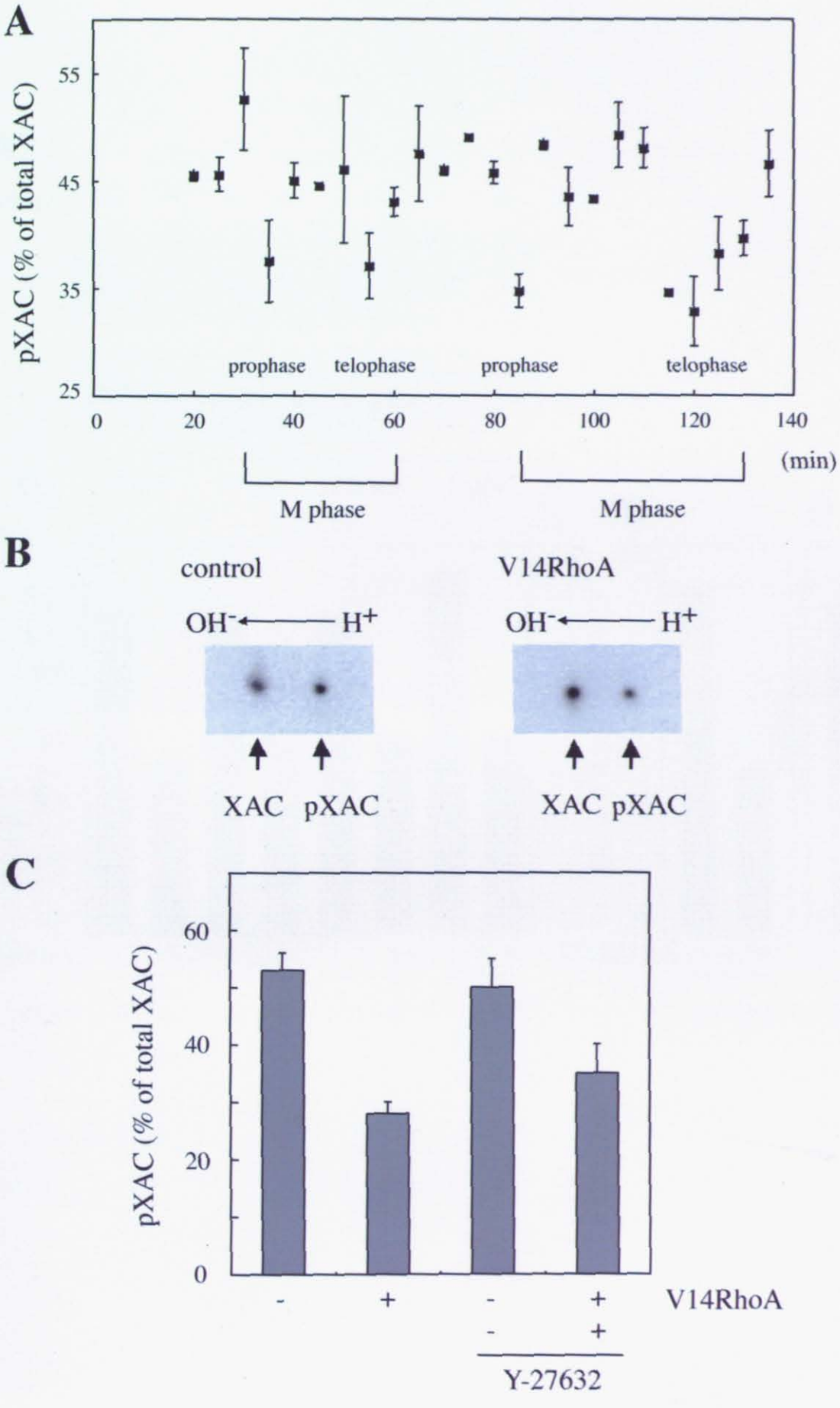
A
pXAC (% of total XAC)
55
45
35
25
prophase
telophase
prophase
telophase
0
20
40
60
80
100
120
140
(min)
M phase
M phase
B
control
V14RhoA
OH⁻ ← H⁺
OH⁻ ← H⁺
XAC pXAC
XAC pXAC
C
pXAC (% of total XAC)
60
40
20
0
-
+
-
+
V14RhoA
-
+
Y-27632

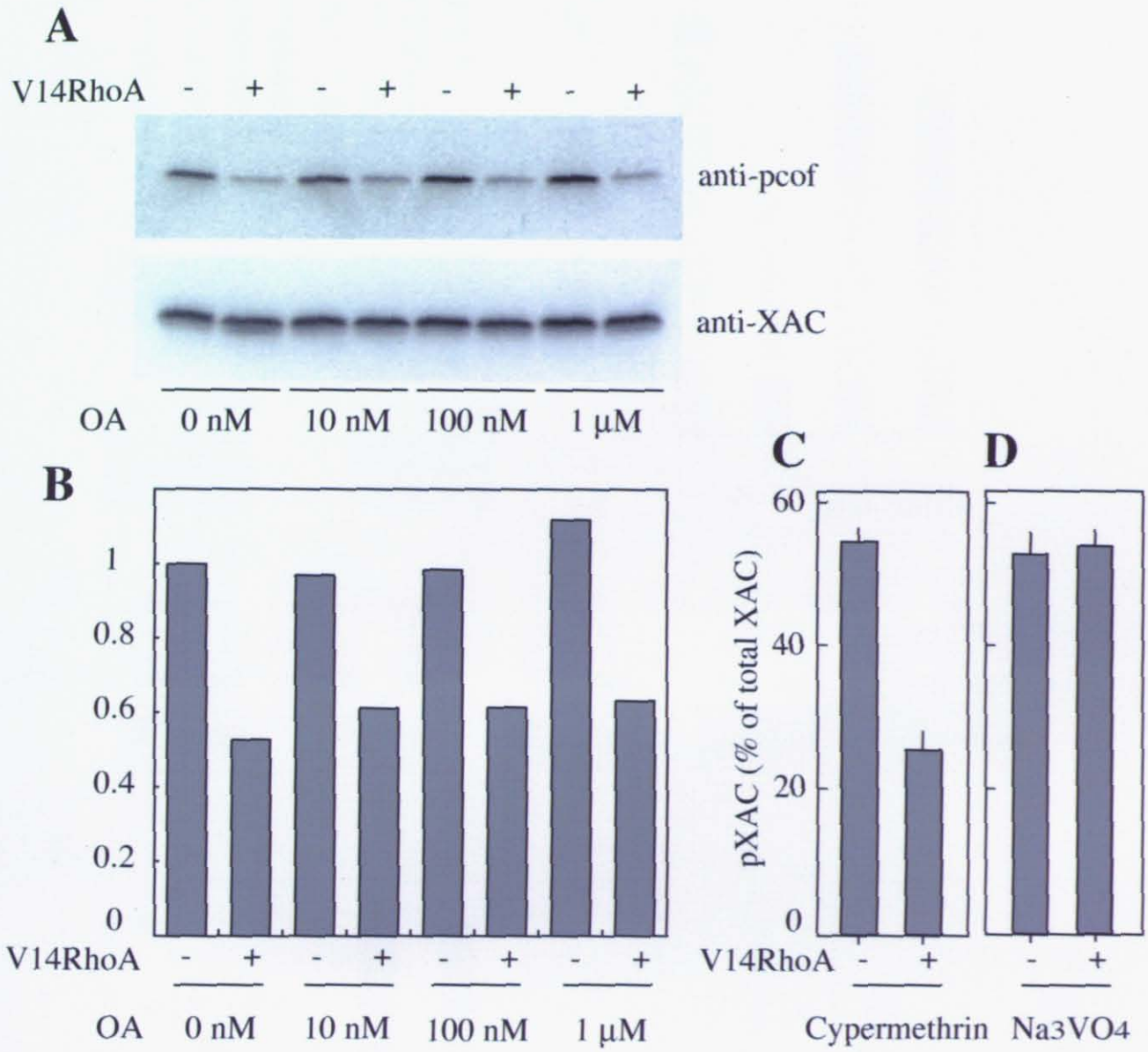
A
V14RhoA - + - + - + - +
anti-pcof
anti-XAC
OA 0 nM 10 nM 100 nM 1 μM
B
1
0.8
0.6
0.4
0.2
0
V14RhoA - + - + - + - +
OA 0 nM 10 nM 100 nM 1 μM
C
D
60
40
20
0
pXAC (% of total XAC)
V14RhoA - + - +
Cypermethrin Na3VO4

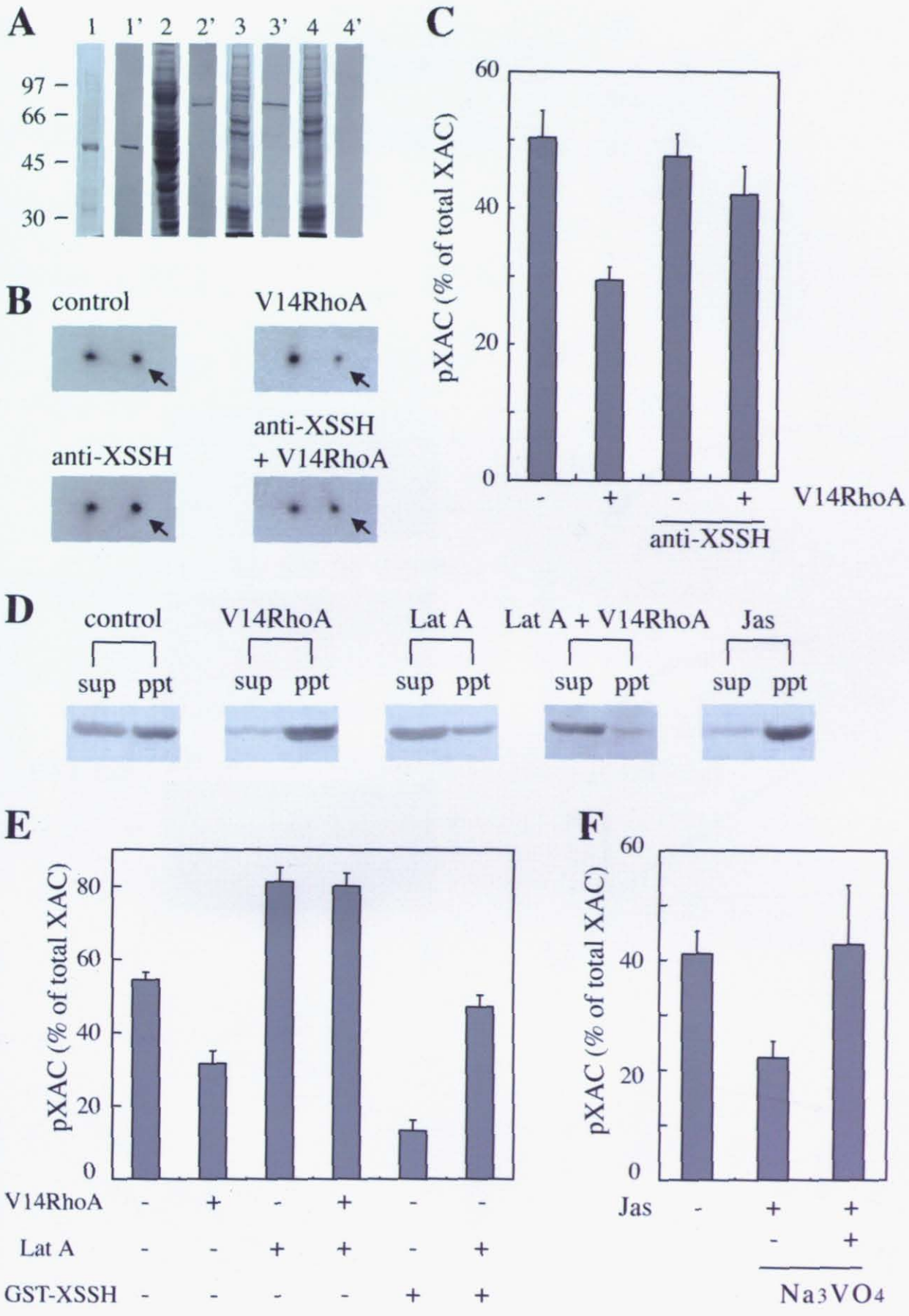
A
1 1' 2 2' 3 3' 4 4'
97
66
45
30
B
control
V14RhoA
anti-XSSH
anti-XSSH
+ V14RhoA
C
pXAC (% of total XAC)
60
40
20
0
- + - +
V14RhoA
anti-XSSH
D
control
V14RhoA
Lat A
Lat A + V14RhoA
Jas
sup ppt
sup ppt
sup ppt
sup ppt
sup ppt
E
pXAC (% of total XAC)
80
60
40
20
0
V14RhoA - + - + - -
Lat A - - + + - +
GST-XSSH - - - - + +
F
pXAC (% of total XAC)
60
40
20
0
Jas - + +
- +
Na3VO4

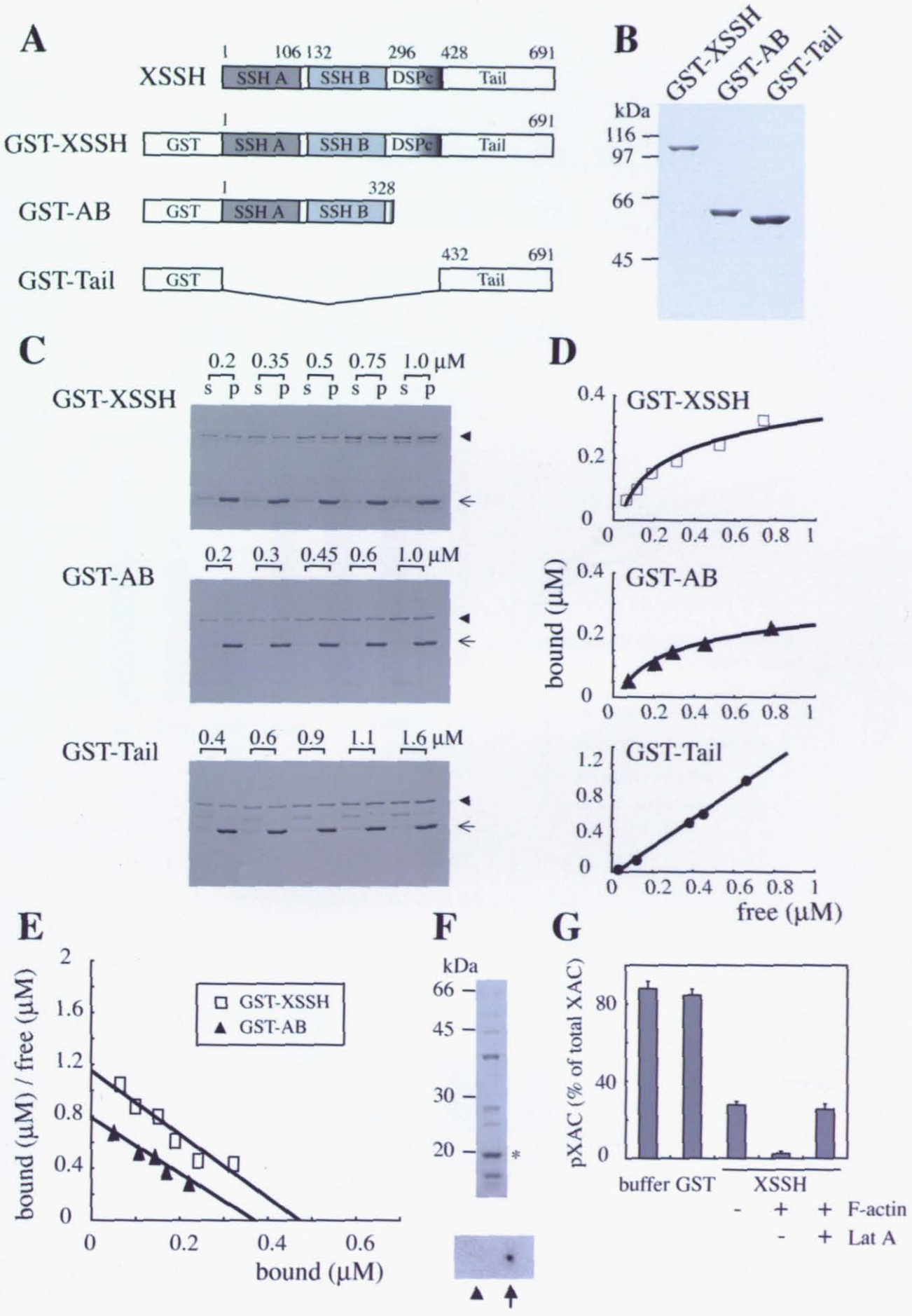
A
XSSH
GST-XSSH
GST-AB
GST-Tail
SSH A
SSH B
DSPc
Tail
GST
1
106
132
296
428
691
328
432
B
GST-XSSH
GST-AB
GST-Tail
kDa
116
97
66
45
C
GST-XSSH
GST-AB
GST-Tail
s p
D
bound (μM)
free (μM)
E
bound (μM) / free (μM)
bound (μM)
F
kDa
66
45
30
20
G
pXAC (% of total XAC)
buffer
GST
XSSH
F-actin
Lat A

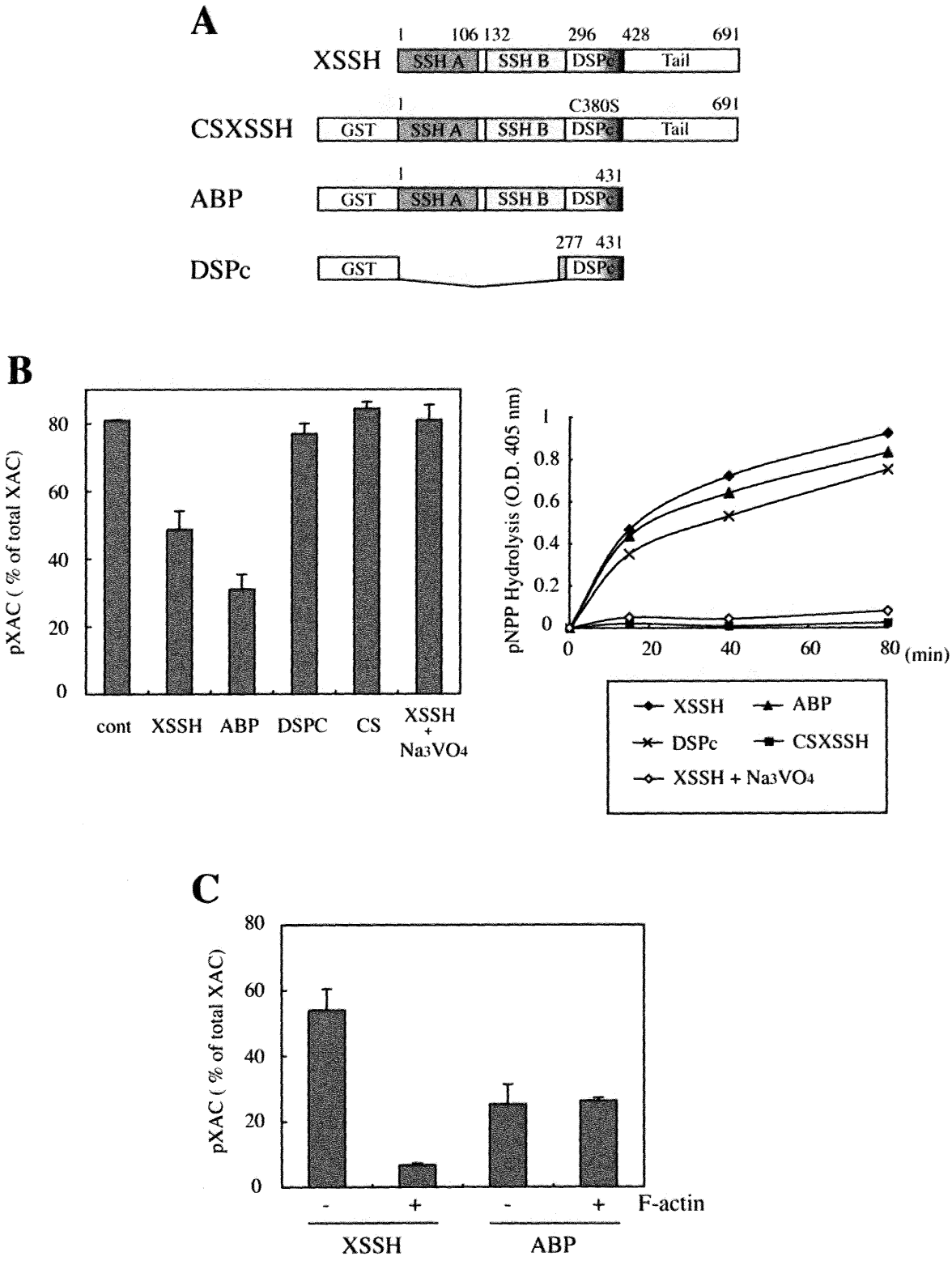
A
XSSH
1
106 132
296
428
691
SSH A
SSH B
DSPc
Tail
CSXSSH
GST
C380S
ABP
431
DSPc
277 431
B
pXAC (% of total XAC)
cont
XSSH
ABP
DSPC
CS
XSSH + Na3VO4
pNPP Hydrolysis (O.D. 405 nm)
(min)
XSSH
ABP
DSPc
CSXSSH
XSSH + Na3VO4
C
pXAC (% of total XAC)
F-actin
XSSH
ABP

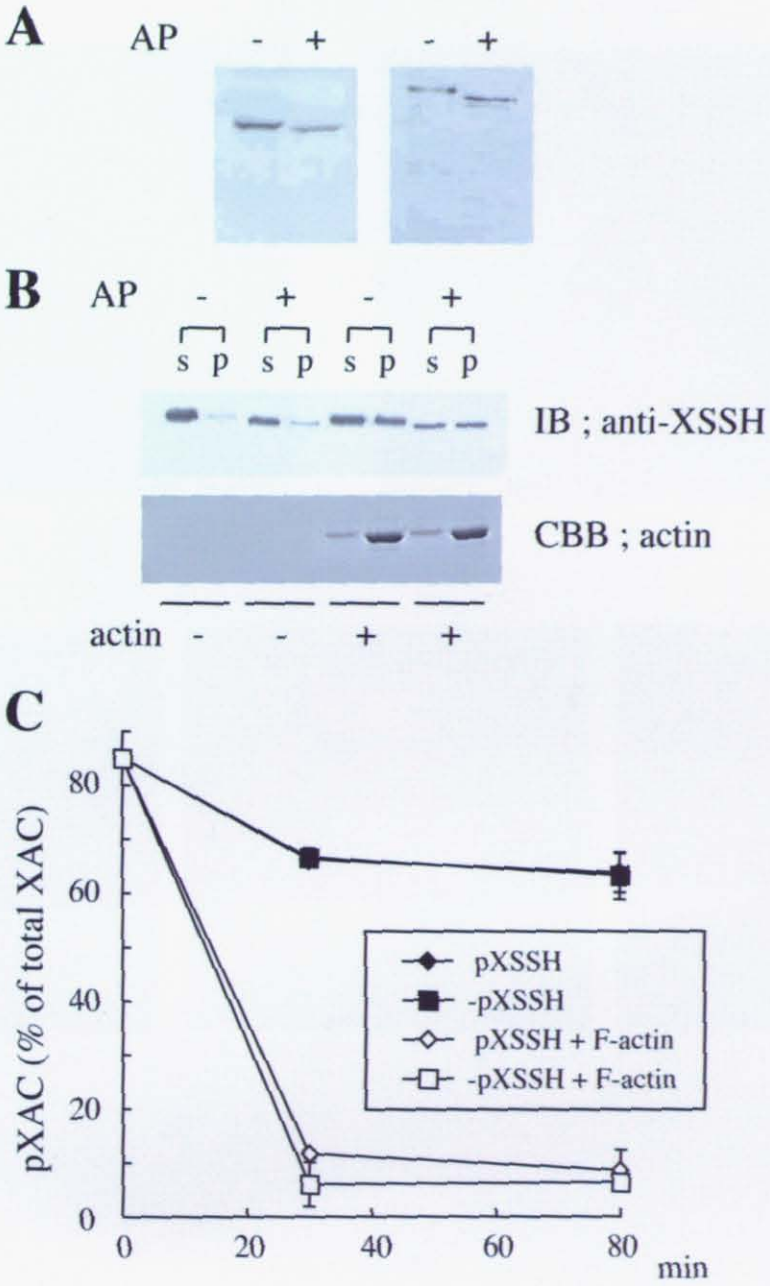
A
AP
- + - +
B
AP
- + - +
s p s p s p s p
IB ; anti-XSSH
CBB ; actin
actin - - + +
C
pXAC (% of total XAC)
0
20
40
60
80
0
20
40
60
80
min
pXSSH
-pXSSH
pXSSH + F-actin
-pXSSH + F-actin

A control IgG

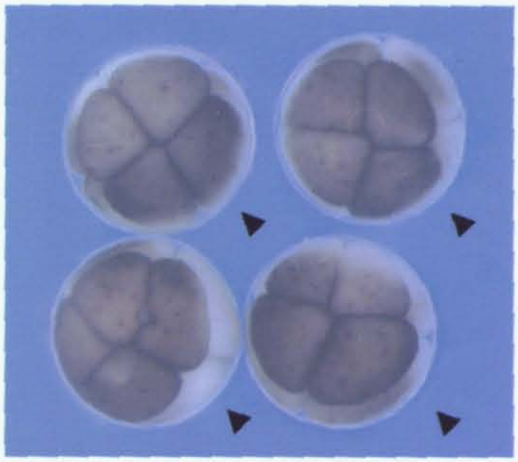

B anti-XSSH antibody

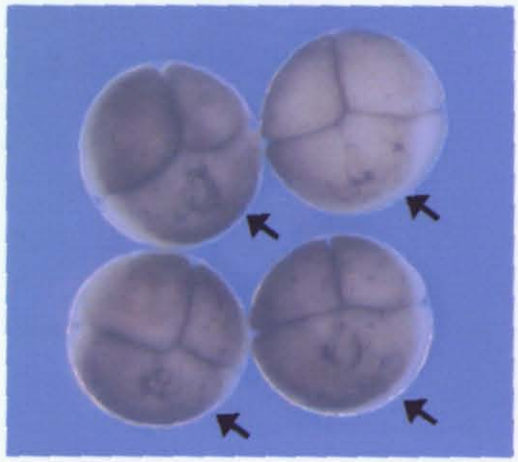

C

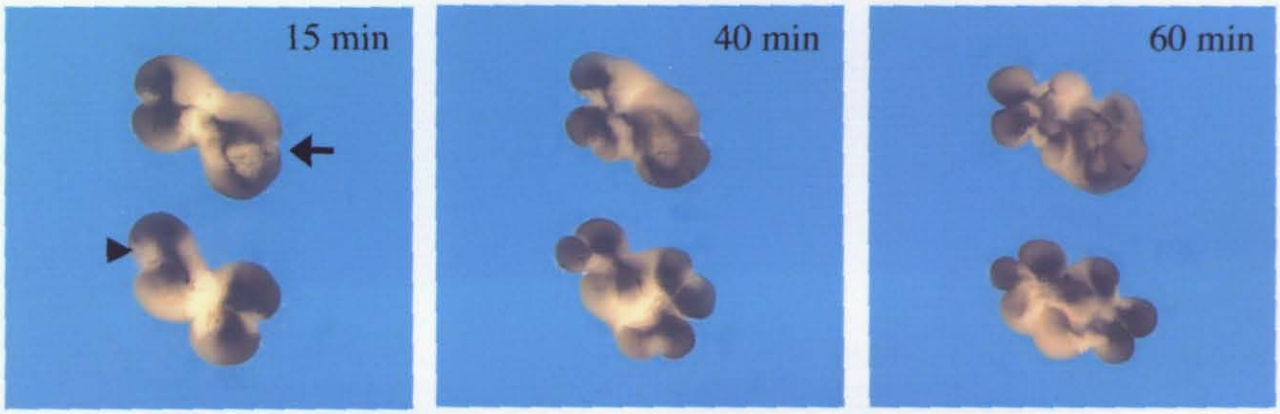

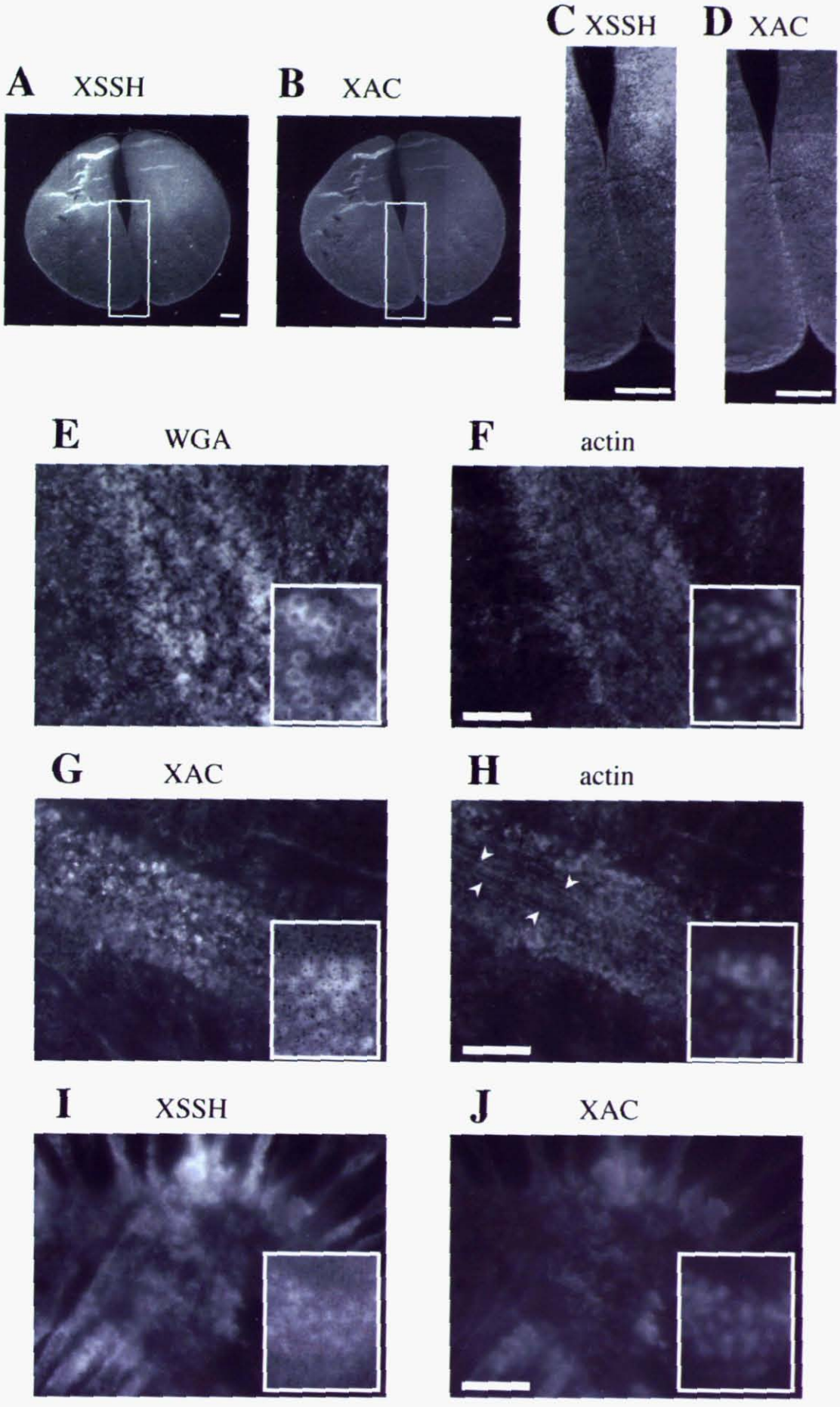
A XSSH
B XAC
C XSSH
D XAC
E WGA
F actin
G XAC
H actin
I XSSH
J XAC

Chapter 2

Functional involvement of *Xenopus* homologue of ADF/cofilin phosphatase, Slingshot (XSSH), in the gastrulation movement

Abstract

ADF/cofilin is a phosphorylation-regulated protein essential for actin filament dynamics in cells. Here, I cloned a cDNA encoding *Xenopus* ADF/cofilin (XAC)-specific phosphatase, slingshot (XSSH). Whole mount *in situ* hybridization showed XSSH transcripts in the blastopore lip and sensorial ectoderm at stage 11, and subsequently localized to developing brain, branchial arches, developing retina, otic vesicle, cement gland, and spinal chord in neurula to tailbud embryos. Immunostaining of animal-vegetal sections of gastrula embryos demonstrated that both XAC and XSSH proteins are predominant in ectodermal and involuting mesodermal cells. Microinjection of either a wild type (thus induces overexpression) or a phosphatase-defective mutant (functions as dominantly negative form) resulted in defects in gastrulation, and often generated the spina bifida phenotype with reduced head structures. Interestingly, the ratio of phosphorylated XAC to dephosphorylated XAC markedly increased from the early gastrula stage (stage 10.5), although the amount of XSSH protein markedly increased from this stage. These results suggest that gastrulation movement requires ADF/cofilin activity through dynamic regulation of its phosphorylation state.

Introduction

Gastrulation, a complex process essential for the development of most animals to establish their body plans, comprises coordinated regulation of several distinct types of cell movements. In *Xenopus*, the morphogenetic cell behavior during gastrulation, such as epiboly of the ectoderm, rotation of the endoderm, involution of the mesoderm, and convergent extension of the dorsal mesoderm, is well defined by extensive studies (for reviews see Keller *et al.*, 2003; Duncan and Su, 2004). The molecular basis for these movements remains to be fully understood, while recent studies have considerably shed light on the molecular mechanism that underlies the convergent extension; non-canonical Wnt signaling is shown to play a central role in this process (Kuhl, 2002; Tada *et al.*, 2002)

Dynamic changes in cell polarity, adhesion, morphology and motility are well known to be directly dependent on the actin cytoskeleton, and remodeling and reorganization of actin filaments in cells are regulated by Rho family small GTPases, Rho, Rac, and Cdc42 (Nobes and Hall, 1995). It has been shown that Rho and Rac participate in several developmental processes, including planar cell polarity pathway in *Drosophila* (Eaton *et al.*, 1996; Strutt *et al.*, 1997; Fanto *et al.*, 2000; Winter *et al.*, 2001) and convergent extension in *Xenopus* (Habas *et al.*, 2001, 2003; Tahinci and Symes, 2003). Dishevelled (Dvl), a scaffold protein possessing multi-functional domains, mediates coactivation of Rho and Rac but the respective activities are differently regulated; Rho but not Rac activation requires the Formin-homology protein Daam1 which binds to both Rho and Dvl. (Habas *et al.*, 2003). In addition, Rho and Rac coordinately control dynamic properties and polarity of lamellipodia formation in axial mesodermal cells to promote convergent extension (Tahinci and Symes, 2003). Several downstream effectors for Rho-GTPases are also reported to be involved in vertebrate gastrulation. Rac activation that proceeds from Dvl resulted in the activation of the JUN N-terminal kinase (JNK) (Kuhl, 2002; Habas *et al.*, 2003). Rho kinase 2, one of downstream effectors of Rho, is shown to be involved in the cell polarity and motility during convergent extension movements of Zebrafish (Marlow *et al.*, 2002).

The actin depolymerizing factor (ADF)/cofilin family of proteins, which has been shown to be

essential in eukaryotes, enhances actin filament dynamics by depolymerizing and severing actin filaments (Bamburg, 1999; Bamburg *et al.*, 1999; Carlier *et al.*, 1999; Maciver and Hussey, 2002). The activity of this protein is inhibited by phosphorylation of an N-terminal serine residue (Agnew *et al.*, 1995; Moriyama *et al.*, 1996). In a wide variety of cells, ADF/cofilin exhibits rapid dephosphorylation in response to certain exogenous stimuli, for example, such as heat shock in cultured cells (Ohta *et al.*, 1989; Abe *et al.*, 1993) and formyl-methionyl-leucyl-phenylalanine (fMLP) in polymorphonuclear leukocytes (Suzuki *et al.*, 1995; Okada *et al.*, 1996), and the dephosphorylation accompanies dramatic changes in actin organization that are required for cellular function (Moon and Drubin, 1995). LIM kinases (Limks) (Arber *et al.*, 1998; Sumi *et al.*, 1999; Yang *et al.*, 1998), testicular protein kinases (TESKs) (Toshima *et al.*, 2001a, 2001b), and Nck-interacting kinase (NIK)-related kinase (NRK)/NIK-like embryo-specific kinase (NESK) (Nakano *et al.*, 2003) are responsible for phosphorylation of ADF/cofilin in vertebrates. Two types of Limks, designated by Limk 1 and Limk 2 are present in vertebrates (Mizuno *et al.*, 1994; Okano *et al.*, 1995; Nunoue *et al.*, 1995; Osada *et al.*, 1996; Cheng *et al.*, 1995; Koshimizu *et al.*, 1997; Takahashi *et al.*, 1997, 2001). Pioneering works (Arber *et al.*, 1998; Yang *et al.*, 1998) demonstrated that activation of Limk 1 is mediated by Rac1, and were followed by a study that activation of Pak1 through Rac1 or Cdc42 directly increases Limk 1 activity (Edwards *et al.*, 1999). Also, Limks activation occur downstream of Rho-Rho kinase (ROK/ROCK) signaling (Maekawa *et al.*, 1999; Sumi *et al.*, 1999; Ohashi *et al.*, 2000; Amano *et al.*, 2001). These studies all strongly suggest that phosphorylation, and thus inactivation, of ADF/cofilin proceeds through activation of Rho-GTPases. On the other hand, Slingshot (SSH) has been identified as an ADF/cofilin-specific phosphatase in *Drosophila* and human (Niwa *et al.*, 2002). SSH genetically interacts with the LIMK gene in *Drosophila*, and over-expression of SSH with Limk1 or Tesk1 suppresses actin-rich structures induced by these kinases. Therefore, SSH might reactivate ADF/cofilin, phosphorylated by Limks, to increase actin filament dynamics and/or to reorganize pre-existing actin cytoskeleton.

In *Xenopus*, ADF/cofilin is highly phosphorylated in oocytes and unfertilized eggs, and undergoes rapid dephosphorylation in response to the fertilization. Both overexpression and down-regulation of

ADF/cofilin cause a defect in cytokinesis (Abe *et al.*, 1996). *Xenopus* Limk1 and 2 (Xlimk1 and 2) are shown to be functionally responsible for the completion of oocyte maturation (Takahashi *et al.*, 2001). These results suggest that phosphorylation-regulation of ADF/cofilin is tightly regulated during actin-dependent cellular processes. To understand the biological significance of regulation of the ADF/cofilin activity, I cloned *Xenopus* SSH (XSSH) and examined its functions during *Xenopus* early development. Here I report that XSSH is functionally involved in the gastrulation. This finding provides novel insights into the regulatory mechanism of gastrulation movements from a cell biological aspect.

MATERIALS AND METHODS

Polyacrylamide gel electrophoresis and immunoblotting

SDS-polyacrylamide gel electrophoresis (SDS-PAGE), two-dimensional gel electrophoresis (2D-PAGE), and immunoblotting were performed as indicated in chapter 1.

Plasmid construction

Plasmids for XSSH, GST-XSSH (WT) and GST-XSSH (CS) were constructed as described in chapter 1.

Xenopus brachyury (Xbra) and α-cardiac actin cDNA fragments were obtained by PCR using *Xenopus* stage 30 cDNA library and primer sets of 5'-GAGTCACTACCTGCCGATCA and 5'-TCTCCAGTGGGCTCCAAAG for Xbra and 5'-GATCTGGCACCACACCTTCT and 5'-CATAGCTCTTCTCCAGGG for actin. The amplified 533 bp fragment of Xbra and 470 bp fragment of actin were cloned into EcoRV site of pBluescript II KS^+ vector, respectively and confirmed by sequencing.

RT-PCR samples and primers

mRNAs were extracted from *Xenopus* embryos using a QuickPrep MicromRNA purification kit (Amersham Bioscience, UK) and were reverse-transcripted with oligo-dT primers. PCR was carried out using a primer set of 5'-ATATCGCTTGGAGTCCCTGTGACATGG and 5'-CCCCTTCATCCTGCAGAAGAAGTGCTG.

Preparation of mRNA and proteins

For mRNA production, the XSSH and XSSH (CS) cDNA in pBluescript SK^- were digested with KpnI and EcoRI, blunted with T4 DNA polymerase, and inserted into the EcoRV site of pBluescript II KS^+ vector, respectively. Each constract was linearized with SalI, and mRNA was generated by T7 RNA polymerase using an mMESSAGE mMachine T7 kit (Ambion Inc.).

Preparations of GST-XSSH (WT), GST-XSSH (CS), and pXAC fraction were described in chapter 1.

In vitro phosphatase assay

This assay was performed as described in chapter 1 using 2 μM GST-XSSH or GST and 5.5 μM pXAC.

Antibodies

Anti-XSSH antibody was prepared as described in chapter 1. Anti-XAC monoclonal antibody was previously prepared (Okada *et al.*, 1999). Anti-phosphorylated ADF/cofilin-specific antibody was kindly provided by Dr. Bamburg of Colorado State University. The monoclonal antibody specific for both α-cardiac and α-skeletal muscle actin (SKA-06) was used as described in elsewhere (Hayakawa *et al.*, 1996). anti-tubulin monoclonal antibody (DM1A) was purchased from Sigma. Fluorescein or rhodamine-labeled goat anti-mouse or rabbit IgG was purchased from TAGO Inc. Alkaline phosphatase-conjugated goat anti-mouse or rabbit IgG was purchased from Bio-Rad.

Microinjection

0.05 or 0.1 μg/μl mRNA was injected into each blastomere of two-cell stage embryos. Injection volumes from each pipette from a pressure injector (CIJ-1, Shimadzu, Kyoto) were calibrated by measuring the volume of an aqueous drop delivered into mineral oil. Control injections with H_2O alone or the same amount of β-galactosidase mRNA was also done.

***In situ* hybridization and immunofluorescence microscopy**

For *in situ* hybridization, digoxigenin-labeled single strand RNA probes were prepared using the DIG RNA Labeling Kit (Roche). 420 bp of 3'-sequence of XSSH was amplified by PCR using 3'-primer (GCTATGCATGCCAGAAGATAC) and T7 primer with λZAPII-XSSH as a template. Amplified fragments were digested with XhoI and inserted into EcoRV and XhoI sites of pBluescript II KS^+ vector. To generate RNA probes, this construct was linearized either with EcoRI for the antisense probe or with XhoI for the sense probe. For Xbra RNA probe production, pBluescript II KS^+-Xbra was linearized by XhoI for the antisense probe or with EcoRI for the sense probe. *In situ* hybridization was done according to Harland (1991).

For immunofluorescence microscopy, *Xenopus* embryos were fixed in MEMFA (3.7% formaldehyde, 2 mM $MgSO_4$, 1 mM EGTA, and 0.1 M MOPS, pH 7.4) containing 1% TCA,

embedded in paraffin, and sectioned as described elsewhere (Okada *et al.*, 1999). After blocking with 20% goat serum in PBS for 1 hr at room temperature, specimens were incubated with primary antibodies for 1 hr at room temperature, and then with appropriate fluorochrome-conjugated secondary antibodies. After each immunoreaction step, specimens were rinsed and washed with PBS, and mounted in PBS containing 1 mg/ml p-phenylenediamine and 90 % glycerol. Samples were examined with an Axioskop (Carl Zeiss, Germany) with a cooled charge-coupled devise camera, CoolSNAP (Nippon ROPER, Japan).

Results

Expression and phosphorylation of XSSH during development

I raised antibodies specific for XSSH by immunizing rabbits with GST-tagged XSSH catalytic domain. The specificity of the antibody was examined by immunoblotting (Fig. 1A). The antibody specifically recognized the protein with expected mobility in the whole lysates from stage 35 embryos. In addition, XSSH protein translated in rabbit reticulocyte lysates was specifically reacted with the antibody. Thus, this antibody is specific for the XSSH protein.

As shown in Fig. 1B, immunoblotting of whole lysates from unfertilized eggs and different stages of embryos showed that XSSH is present as a maternal protein and remained unchanged in amount during cleavage. The amount of the XSSH protein markedly increased from stage 10.5 when the gastrulation movement dynamically occurs, and persisted hereafter. On the other hand, as shown in Fig. 1C, RT-PCR revealed that XSSH transcripts markedly increase from stage 8 when the mid-blastula transition occurs. Although this time lag of expression between the transcript and the protein is unknown, XSSH function is assumed to be required for the gastrulation movements.

The mobility sift on an SDS-gel was a remarkable feature of this protein (Fig. 1B). In addition to a major band (shown by an open arrowhead), faint bands showing lower mobility (shown by a small arrow) were detected during cleavage, while those faint bands disappeared from the gastrula stage (stage 10.5) and a novel band with higher mobility (shown by a closed arrowhead) gradually increased and became a major form from late neurula stage (stage 23). In unfertilized eggs (lane 1), however, the major band (shown by a large arrow) showed the mobility much lower than that of 2 cell stage embryos. As shown in Fig. 1D, the faint bands were disappeared and shifted to the position of the major band of the cleaving stage embryos when cell lysates of unfertilized eggs were treated with an alkaline phosphatase. Therefore, the faint bands with the lower mobility are suggested to be the phosphorylated form of XSSH. However, this mobility sift by alkaline phsphatase did not change any more to the position of that of tail-bud stage embryos (stage 35, Fig. 1D, lane 2 and 3). In addition, it should be noted that phosphorylation of XSSH is prominent during cleavage, but not during

morphogenetic movements.

Spatial expression of XSSH in embryos

Whole mount *in situ* hybridization showed that XSSH transcripts concentrate at blastopore lips and the dorsal side of stage 11 embryos (Fig. 2A). In the neurula stage, XSSH was present in the head structures and the dorsal part of trunk, and these patterns became clear in the tailbud stage (Fig 2, B, C and D). mRNA of XSSH predominantly expressed in brain, optic and otic vesicles, hyoid and branchial arches, and spinal cords. The striped pattern in the dorsal part of trunk was also obvious and was well correspondent with that of XAC (Fig. 2, E and F). When these stripes of XSSH were compared to the staining pattern of somites by cardiac actin probe (Fig. 2, G and H), stripes of XSSH were more narrow and appeared to position at the regions between somites, or at the restricted region in somites (compare C with G, and E with H)

We next examined expression patterns of both XSSH and XAC proteins by immunofluorescence microscopy of animal-vegetal sections of early gastrula stage embryos. As shown in Fig. 3, A and B, both proteins predominantly expressed in the involuting mesodermal cells and ectodermal cells. XAC accumulated to the cortical region of cells, while XSSH showed rather diffuse in cells (inserts). When distribution of phosphorylated XAC (pXAC) in embryos was examined by the antiserum specific for pXAC, both mesodermal and ectodermal cells were also stained diffusely by this antiserum and it is characteristic of pXAC staining to show that cells scarcely stained by the pXAC antiserum were scattered among staining-positive cells (Fig. 3, C and D; two serial sections with an interval of six sections). Therefore, cells with faint staining might be promoting dephosphorylation of pXAC. The circumferential strong staining by this antiserum is non-specific binding of antibody to the vitellin membrane surrounding embryos. Since the amount of XSSH increased from the early gastrula stage, changes in ratio of pXAC to XAC from blastula to gastrula were examined by a combination of 2D-PAGE and immunoblotting. Unexpectedly, the amount of pXAC drastically increased at stage 10.5 when gastrulation movements have just begun (Fig. 3G). I assume that activation of both phosphorylation and dephosphorylation might require for the gastrulation movements.

On the other hand, additional immunofluorescence staining for XSSH was done on sections from embryos at stage 33. Anterior and posterior dorsal parts of the trunk of a single embryo were shown in Fig. 3, E and F. Cells within the neural tube, notochord, and epidermis were brightly stained, and bright patches were often observed in the somite regions (shown by arrows). These patches are likely to be correspondent to the striped pattern shown by *in situ* hybridization.

XSSH is required for the gastrulation movements

In order to clarify the significance of XSSH activity during gastrulation, I constructed a phosphatase-inactive mutant of XSSH (XSSH (CS)). The wild type XSSH (XSSH (WT)) and XSSH (CS) were expressed in *E. coli* and purified, and their phosphatase activities were assayed using partially purified pXAC fraction. As shown in Fig. 4A, partially purified pXAC fraction contained many other proteins, but any phosphatase or kinase activities, or 14-3-3 family proteins were never detected (data not shown). A combination of 2D-PAGE and immunoblotting (Fig. 4, B and C) showed that XSSH dephosphorylates pXAC, whereas XSSH (CS) completely lacks phosphatase activity. Sodium orthovanadate inhibited XSSH phosphatase activity.

Effects of ectopic expression of XSSH on gastrulation movements were then examined. Injection of either wild type XSSH or XSSH (CS) mRNA impaired gastrulation movements (Fig. 4D). As summarized in Table I, these effects were dependent on the concentration of injected mRNA and significant amounts of embryos injected with 1 ng mRNAs showed the defective phenotypes. I confirmed the protein expression from ectopic mRNAs by immunoblotting of whole lysates of 1 ng mRNA-injected embryos. Fig. 4E clearly demonstrated about two- to three-fold increase in amount of ectopically expressed proteins. The phosphorylation state of XAC in injected embryos was also examined by 2D-PAGE when control embryos developed to reach stage 12. The amount of pXAC was decreased by injection of wild type XSSH mRNA, and was markedly increased when XSSH (CS) mRNA was injected (Fig. 4, F and G). These results strongly suggest that XSSH (CS) functions as a dominantly negative form in embryos as reported in mammalian cultured cells transfected by SSH (CS) (see *discussion*). Time-lapse images of XSSH (CS) injected embryos were shown in Fig.

5A. At the onset of gastrulation, the blastopore lip formed more equatorially in XSSH (CS) injected embryos, suggesting that pregastrula epiboly is inhibited. Although the gastrulation of control embryos progressed, XSSH (CS) injected embryos showed neither involution nor epiboly and finally formed spina bifida which resulted from the inability of the blastopore to close. Animal-vegetal sections of control (stage 11), XSSH (WT)- and XSSH (CS)-injected embryos were shown in Fig. 5B. The control embryo formed two cell layers at the animal cap, the epithelial and sensorial layers of cells. In XSSH (WT)- and XSSH (CS)-injected embryos, however, animal cap cells might be defective in epiboly, since the animal cap region constituted five to six layers of cells. In addition, injected embryos often showed expanded blastocoels and incomplete involution without any formation of archenterons (data not shown). These results strongly suggest that intracellular perturbation of phosphorylation state of XAC entirely disrupts the gastrulation movement.

Injected embryos developed until tailbud stage with a light phenotype, possibly generated by lower expression level from ectopic mRNA, often showed shortening of the anteroposterior axis and reduction of head structures including a defect in the eye development (Fig. 6A). Immunofluorescence staining of XSSH in vertical sections of control and XSSH (CS)-injected embryos (Fig. 6B) showed that the forebrain, formed in the control embryo (indicated by an arrow), completely disappeared in the XSSH (CS)-injected embryo and instead, notochord was still observed (indicated by an arrow). In addition, one of eyes (the right side in this case) failed to form.

Finally, to exclude the possibility that the gastrulation-defective phenotypes resulted from indirect effects by suppression of the mesoderm induction but not inhibition of a normal cell migration, I examined the expression of the mesoderm marker *Xenopus* brachyury (Xbra) by whole mount *in situ* hybridization and of the muscle-specific α-actin by immunoblotting in control and XSSH (CS) injected embryos. As shown in Fig. 6C, whole mount *in situ* hybridization clearly demonstrated that Xbra expression was obvious surrounding blastopores in both control and injected stage 10.5 embryos, while the staining in XSSH (CS) injected embryos localized to more equatorial region compared with that in control embryos, according to the position of blastopore lip formation (Fig. 5A). Expression of the muscle specific α-actin was also confirmed in XSSH (CS) injected embryos (Fig.

6D). Together, these results suggest that mesoderm induction and differentiation are not influenced by XSSH (CS)-injection and that cell migration itself is disrupted in XSSH (CS)-injected embryos.

Discussion

In the present study, I confirmed that a *Xenopus* homologue of SSH possesses an activity to dephosphorylate *Xenopus* ADF/cofilin. Thus, XSSH is structurally and functionally identical to *Drosophila* and mammalian SSHs. By injection of XSSH mRNAs, I found that ectopic expression of XSSH (CS), the phosphatase-inactive mutant, caused severe defects in gastrulation. Over-expression of XSSH also inhibited gastrulation movements. These results suggest that gastrulation movement requires proper regulation of XAC activity in cells. After the gastrula stage, a novel XSSH band, exhibiting the highest mobility on an SDS gel, appeared and gradually became the major band. Since the mobility of XSSH in egg extracts did not sift to the position of this novel band after treatment by alkaline phosphatase, it is possible that the XSSH showing highest mobility is an isoform, or XSSH at cleaving stage is likely to be modified by phosphorylation at a specific residue where the alkaline phosphatase can not associate. Furthermore, I cannot deny that the other modification could regulate the XSSH activity until early neurula stage.

The expression pattern of XSSH was well correspondent to that of XAC during early embryogenesis (Abe *et al*, 1996). Both were predominantly expressed in neural tissues. The striped pattern at dorsal side of trunk was also characteristic to both staining by *in situ* hybridization. These stripes were apparently narrow in width in comparison with somites stained by alpha-cardiac actin probe and seemed to position between somites. Supporting these *in situ* hybridization images, immunofluorescence microscopy of vertical sections revealed that somites were patched with fluorescence, but never stained entirely with anti-XSSH antibody. Recently, knock out study demonstrated that non-muscle type cofilin is essential for neural crest cell migration as well as other cell types in the paraxial mesoderm in mice (Gurniak *et al*, 2005). Together, I assume that the striped region might contain neural crest cells. Experiments with probes specific for each type of mesodermal cells may confirm cell types in these striped regions.

The full-length XSSH tagged with GST was successfully purified from *E. coli*, and possessed XAC dephosphorylation activity that was inhibited by Na_3VO_4. And the mutant (GST-XSSH (CS)),

the essential Cys residue of which was substituted by Ser, completely lost dephosphorylation activity. These results were well corresponding to studies with *Drosophila* and mammalian SSH (Niwa *et al.*, 2002). Previous studies demonstrated that SSH (CS) functions as a dominantly negative form to prevent cofilin dephosphorylation when expressed in cultured cells (Kaji *et al.*, 2003; Nagata-Ohashi *et al.*, 2004; Wang *et al.*, 2005). In this study, ectopic expression of XSSH (CS) also increased the level of XAC phosphorylation and over-expression of wild type XSSH decreased the total amount of phosphorylated XAC (pXAC). Therefore, I conclude that XSSH (CS) functions as a dominantly negative form in embryos.

pXAC level was kept lower in the blastula stage, while, in the gastrula stage, its level markedly increased. Since the amount of XAC did not alter during these stages (Okada *et al.*, 1999), it is suggested that XAC phosphorylation activity is elevated at the gastrula stage. On the other hand, the amount of XSSH protein apparently increased from the gastrula stage. *In situ* hybridization and immunofluorescence microscopy indicate that this increased expression of XSSH occur in ectodermal and mesodermal cells in gastrula embryos. In these cells, however, staining by anti-pXAC antibody was not uniform and not weak, and cells with faint staining by anti-pXAC antibody are scattered in ectodermal and mesodermal cells with clear staining. The respective cells may not wholly decrease the pXAC level, although they increased expression level of XSSH. Together with the result that ectopic expression of XSSH (CS) caused severe defects in gastrulation, it is strongly suggested that XSSH activity is regulated individually in cells during gastrulation. In mammalian cells, neuregulin-induced pathway of SSH activation has been demonstrated (Nagata-Ohashi *et al.*, 2004). Most recently, SSH and Limk have been demonstrated to form complex with other signal transducers and regulate ADF/cofilin activity in an interdependent manner (Soosairajah *et al.*, 2005). Regulatory pathway for the activation of XSSH during gastrulation awaits elucidation in future studies. Over-expression of XSSH also prevented gastrulation. One possible explanation for this effect is that active XAC increased by excessive amount of XSSH disturbs actin filament dynamics to inhibit cell migration, since total amount of pXAC was apparently decreased in the injected embryos. Or, insufficient amount of pXAC pool, induced by the excessive amount of XSSH, prevents cell

migration because of lack of dephosphorylated/reactivated XAC.

Injection of XSSH (CS) mRNA caused spina bifida and also inhibited thinning of animal roof (Fig. 5), in addition to formation of embryos with reduced head structures and shortened anteroposterior axis (Fig. 6). These results are likely to indicate that expression of XSSH (CS) prevents both epiboly and convergent extension during gastrulation. Experiments with Keller explants are required for elucidation of those points. In addition, it is necessary to observe changes in morphology and shape of living cells comparatively between control and XSSH (CS)-injected embryos. On the other hand, reduced head structures were also shown in mouse embryos in which the non-muscle type cofilin gene was targeted (Gurniak *et al.*, 2005). Mutant embryos (cof-/- embryos) at E10.5 showed smaller body size, failure of neural tube closure, and defects of eye development. All of these defects induced in the cof-/- embryos were also obvious in *Xenopus* embryos injected with XSSH (CS). However, cof-/- embryos developed normally by E9.5, suggesting that non-muscle cofilin is not essential for morphogenetic movements during gastrulation. Since there are three ADF/cofilin isoforms in mice, muscle-type or maternally expressed ADF/cofilin isoforms may function gastrulation movements. I currently assume that *Xenopus* gastrulation movement requires regulated phosphorylation and dephosphorylation of XAC in cells.

Finally, however, my results here could be interpreted in a quite different way. Ectopically expressed XSSH might bind to actin filaments in cells to disturb actin cytoskeletal architecture and prevent gastrulation movements, since XSSH tightly binds to actin filaments. Both wild type and CS mutant XSSHs also retain binding activity for actin filaments (unpublished results) as well as mammalian SSHs (Niwa *et al.*, 2002). This possibility can not be currently excluded but antagonized by several results. First, injection of much smaller amount of XSSH (WT) mRNA affected gastrulation than that of XSSH (CS) mRNA did (Table I). If the binding of XSSH to the actin filament were essential for the gastrulation defects, the dosage effects would show less difference between the two injections. Second, injection of mRNA of S3A-XAC, the constitutively active form of XAC, also caused gastrulation defects more effectively than that of wild type XAC (our unpublished results). This suggests that regulation of XAC activity by phosphorylation is necessary

for gastrulation. Exploration of regulatory mechanisms of XSSH activity, in addition to domain analysis of XSSH protein, will be important to understand the gastrulation movement mediated by phospho-regulation of XAC activity.

References

Abe, H., Nagaoka, R. and Obinata, T. (1993). Cytoplasmic localization and nuclear transport of cofilin in cultured myotubes. *Exp Cell Res* **206**, 1-10.

Abe, H., Obinata, T., Minamide, L. S. and Bamburg, J. R. (1996). Xenopus laevis actin-depolymerizing factor/cofilin: a phosphorylation-regulated protein essential for development. *J Cell Biol* **132**, 871-85.

Agnew, B. J., Minamide, L. S. and Bamburg, J. R. (1995). Reactivation of phosphorylated actin depolymerizing factor and identification of the regulatory site. *J Biol Chem* **270**, 17582-7.

Amano, T., Tanabe, K., Eto, T., Narumiya, S. and Mizuno, K. (2001). LIM-kinase 2 induces formation of stress fibres, focal adhesions and membrane blebs, dependent on its activation by Rho-associated kinase-catalysed phosphorylation at threonine-505. *Biochem J* **354**, 149-59.

Arber, S., Barbayannis, F. A., Hanser, H., Schneider, C., Stanyon, C. A., Bernard, O. and Caroni, P. (1998). Regulation of actin dynamics through phosphorylation of cofilin by LIM-kinase. *Nature* **393**, 805-9.

Bamburg, J. R. (1999). Proteins of the ADF/cofilin family: essential regulators of actin dynamics. *Annu Rev Cell Dev Biol* **15**, 185-230.

Bamburg, J. R., McGough, A. and Ono, S. (1999). Putting a new twist on actin: ADF/cofilins modulate actin dynamics. *Trends Cell Biol* **9**, 364-70.

Blin, N. and Stafford, D. W. (1976). A general method for isolation of high molecular weight DNA from eukaryotes. *Nucleic Acids Res* **3**, 2303-8.

Carlier, M. F., Ressad, F. and Pantaloni, D. (1999). Control of actin dynamics in cell motility. Role of ADF/cofilin. *J Biol Chem* **274**, 33827-30.

Cheng, A. K. and Robertson, E. J. (1995). The murine LIM-kinase gene (limk) encodes a novel serine threonine kinase expressed predominantly in trophoblast giant cells and the developing nervous system. *Mech Dev* **52**, 187-97.

Duncan, T. and Su, T. T. (2004). Embryogenesis: coordinating cell division with gastrulation. *Curr*

Biol **14**, R305-7.

Eaton, S., Wepf, R. and Simons, K. (1996). Roles for Rac1 and Cdc42 in planar polarization and hair outgrowth in the wing of Drosophila. *J Cell Biol* **135**, 1277-89.

Edwards, D. C., Sanders, L. C., Bokoch, G. M. and Gill, G. N. (1999). Activation of LIM-kinase by Pak1 couples Rac/Cdc42 GTPase signalling to actin cytoskeletal dynamics. *Nat Cell Biol* **1**, 253-9.

Fanto, M., Weber, U., Strutt, D. I. and Mlodzik, M. (2000). Nuclear signaling by Rac and Rho GTPases is required in the establishment of epithelial planar polarity in the Drosophila eye. *Curr Biol* **10**, 979-88.

Gurniak, C. B., Perlas, E. and Witke, W. (2005). The actin depolymerizing factor n-cofilin is essential for neural tube morphogenesis and neural crest cell migration. *Dev Biol* **278**, 231-41.

Habas, R., Kato, Y. and He, X. (2001). Wnt/Frizzled activation of Rho regulates vertebrate gastrulation and requires a novel Formin homology protein Daam1. *Cell* **107**, 843-54.

Habas, R., Dawid, I. B. and He, X. (2003). Coactivation of Rac and Rho by Wnt/Frizzled signaling is required for vertebrate gastrulation. *Genes Dev* **17**, 295-309.

Harland, R. M. (1991). In situ hybridization: an improved whole-mount method for Xenopus embryos. *Methods Cell Biol* **36**, 685-95.

Hayakawa, K., Ono, S., Nagaoka, R., Saitoh, O. and Obinata, T. (1996). Differential assembly of cytoskeletal and sarcomeric actins in developing skeletal muscle cells in vitro. *Zoolog Sci* **13**, 509-17.

Kaji, N., Ohashi, K., Shuin, M., Niwa, R., Uemura, T. and Mizuno, K. (2003). Cell cycle-associated changes in Slingshot phosphatase activity and roles in cytokinesis in animal cells. *J Biol Chem* **278**, 33450-5. Epub 2003 Jun 14.

Keller, R., Davidson, L. A. and Shook, D. R. (2003). How we are shaped: the biomechanics of gastrulation. *Differentiation* **71**, 171-205.

Koshimizu, U., Takahashi, H., Yoshida, M. C. and Nakamura, T. (1997). cDNA cloning, genomic organization, and chromosomal localization of the mouse LIM motif-containing kinase gene, Limk2. *Biochem Biophys Res Commun* **241**, 243-50.

Kuhl, M. (2002). Non-canonical Wnt signaling in Xenopus: regulation of axis formation and

gastrulation. *Semin Cell Dev Biol* **13**, 243-9.

Laemmli, U. K. (1970). Cleavage of structural proteins during the assembly of the head of bacteriophage T4. *Nature* **227**, 680-5.

Maciver, S. K. and Hussey, P. J. (2002). The ADF/cofilin family: actin-remodeling proteins. *Genome Biol* **3**, reviews3007. Epub 2002 Apr 26.

Maekawa, M., Ishizaki, T., Boku, S., Watanabe, N., Fujita, A., Iwamatsu, A., Obinata, T., Ohashi, K., Mizuno, K. and Narumiya, S. (1999). Signaling from Rho to the actin cytoskeleton through protein kinases ROCK and LIM-kinase. *Science* **285**, 895-8.

Marlow, F., Topczewski, J., Sepich, D. and Solnica-Krezel, L. (2002). Zebrafish Rho kinase 2 acts downstream of Wnt11 to mediate cell polarity and effective convergence and extension movements. *Curr Biol* **12**, 876-84.

Mizuno, K., Okano, I., Ohashi, K., Nunoue, K., Kuma, K., Miyata, T. and Nakamura, T. (1994). Identification of a human cDNA encoding a novel protein kinase with two repeats of the LIM/double zinc finger motif. *Oncogene* **9**, 1605-12.

Moon, A. and Drubin, D. G. (1995). The ADF/cofilin proteins: stimulus-responsive modulators of actin dynamics. *Mol Biol Cell* **6**, 1423-31.

Moriyama, K., Iida, K. and Yahara, I. (1996). Phosphorylation of Ser-3 of cofilin regulates its essential function on actin. *Genes Cells* **1**, 73-86.

Nagata-Ohashi, K., Ohta, Y., Goto, K., Chiba, S., Mori, R., Nishita, M., Ohashi, K., Kousaka, K., Iwamatsu, A., Niwa, R. et al. (2004). A pathway of neuregulin-induced activation of cofilin-phosphatase Slingshot and cofilin in lamellipodia. *J Cell Biol* **165**, 465-71.

Nakano, K., Kanai-Azuma, M., Kanai, Y., Moriyama, K., Yazaki, K., Hayashi, Y. and Kitamura, N. (2003). Cofilin phosphorylation and actin polymerization by NRK/NESK, a member of the germinal center kinase family. *Exp Cell Res* **287**, 219-27.

Niwa, R., Nagata-Ohashi, K., Takeichi, M., Mizuno, K. and Uemura, T. (2002). Control of actin reorganization by Slingshot, a family of phosphatases that dephosphorylate ADF/cofilin. *Cell* **108**, 233-46.

Nobes, C. D. and Hall, A. (1995). Rho, rac and cdc42 GTPases: regulators of actin structures, cell adhesion and motility. *Biochem Soc Trans* **23**, 456-9.

Nunoue, K., Ohashi, K., Okano, I. and Mizuno, K. (1995). LIMK-1 and LIMK-2, two members of a LIM motif-containing protein kinase family. *Oncogene* **11**, 701-10.

O'Farrell, P. Z., Goodman, H. M. and O'Farrell, P. H. (1977). High resolution two-dimensional electrophoresis of basic as well as acidic proteins. *Cell* **12**, 1133-41.

Ohashi, K., Nagata, K., Maekawa, M., Ishizaki, T., Narumiya, S. and Mizuno, K. (2000). Rho-associated kinase ROCK activates LIM-kinase 1 by phosphorylation at threonine 508 within the activation loop. *J Biol Chem* **275**, 3577-82.

Ohta, Y., Nishida, E., Sakai, H. and Miyamoto, E. (1989). Dephosphorylation of cofilin accompanies heat shock-induced nuclear accumulation of cofilin. *J Biol Chem* **264**, 16143-8.

Okada, K., Takano-Ohmuro, H., Obinata, T. and Abe, H. (1996). Dephosphorylation of cofilin in polymorphonuclear leukocytes derived from peripheral blood. *Exp Cell Res* **227**, 116-22.

Okada, K., Obinata, T. and Abe, H. (1999). XAIP1: a Xenopus homologue of yeast actin interacting protein 1 (AIP1), which induces disassembly of actin filaments cooperatively with ADF/cofilin family proteins. *J Cell Sci* **112**, 1553-65.

Okano, I., Hiraoka, J., Otera, H., Nunoue, K., Ohashi, K., Iwashita, S., Hirai, M. and Mizuno, K. (1995). Identification and characterization of a novel family of serine/threonine kinases containing two N-terminal LIM motifs. *J Biol Chem* **270**, 31321-30.

Osada, H., Hasada, K., Inazawa, J., Uchida, K., Ueda, R. and Takahashi, T. (1996). Subcellular localization and protein interaction of the human LIMK2 gene expressing alternative transcripts with tissue-specific regulation. *Biochem Biophys Res Commun* **229**, 582-9.

Soosairajah, J., Maiti, S., Wiggan, O., Sarmiere, P., Moussi, N., Sarcevic, B., Sampath, R., Bamburg, J. R. and Bernard, O. (2005). Interplay between components of a novel LIM kinase-slingshot phosphatase complex regulates cofilin. *Embo J* **24**, 473-86. Epub 2005 Jan 20.

Strutt, D. I., Weber, U. and Mlodzik, M. (1997). The role of RhoA in tissue polarity and Frizzled signalling. *Nature* **387**, 292-5.

Sumi, T., Matsumoto, K., Takai, Y. and Nakamura, T. (1999). Cofilin phosphorylation and actin cytoskeletal dynamics regulated by rho- and Cdc42-activated LIM-kinase 2. *J Cell Biol* **147**, 1519-32.

Suzuki, K., Yamaguchi, T., Tanaka, T., Kawanishi, T., Nishimaki-Mogami, T., Yamamoto, K., Tsuji, T., Irimura, T., Hayakawa, T. and Takahashi, A. (1995). Activation induces dephosphorylation of cofilin and its translocation to plasma membranes in neutrophil-like differentiated HL-60 cells. *J Biol Chem* **270**, 19551-6.

Tada, M., Concha, M. L. and Heisenberg, C. P. (2002). Non-canonical Wnt signalling and regulation of gastrulation movements. *Semin Cell Dev Biol* **13**, 251-60.

Tahinci, E. and Symes, K. (2003). Distinct functions of Rho and Rac are required for convergent extension during Xenopus gastrulation. *Dev Biol* **259**, 318-35.

Takahashi, T., Aoki, S., Nakamura, T., Koshimizu, U. and Matsumoto, K. (1997). Xenopus LIM motif-containing protein kinase, Xlimk1, is expressed in the developing head structure of the embryo. *Dev Dyn* **209**, 196-205.

Takahashi, T., Koshimizu, U., Abe, H., Obinata, T. and Nakamura, T. (2001a). Functional involvement of Xenopus LIM kinases in progression of oocyte maturation. *Dev Biol* **229**, 554-67.

Toshima, J., Toshima, J. Y., Amano, T., Yang, N., Narumiya, S. and Mizuno, K. (2001b). Cofilin phosphorylation by protein kinase testicular protein kinase 1 and its role in integrin-mediated actin reorganization and focal adhesion formation. *Mol Biol Cell* **12**, 1131-45.

Toshima, J., Toshima, J. Y., Takeuchi, K., Mori, R. and Mizuno, K. (2001). Cofilin phosphorylation and actin reorganization activities of testicular protein kinase 2 and its predominant expression in testicular Sertoli cells. *J Biol Chem* **276**, 31449-58. Epub 2001 Jun 19.

Towbin, H., Staehelin, T. and Gordon, J. (1979). Electrophoretic transfer of proteins from polyacrylamide gels to nitrocellulose sheets: procedure and some applications. *Proc Natl Acad Sci U S A* **76**, 4350-4.

Wang, Y., Shibasaki, F. and Mizuno, K. (2005). Calcium signal-induced cofilin dephosphorylation is mediated by Slingshot via calcineurin. *J Biol Chem* **280**, 12683-9. Epub 2005 Jan 24.

Winter, C. G., Wang, B., Ballew, A., Royou, A., Karess, R., Axelrod, J. D. and Luo, L. (2001). Drosophila Rho-associated kinase (Drok) links Frizzled-mediated planar cell polarity signaling to the actin cytoskeleton. *Cell* **105**, 81-91.

Yang, N., Higuchi, O., Ohashi, K., Nagata, K., Wada, A., Kangawa, K., Nishida, E., Mizuno, K., Arber, S., Barbayannis, F. A. et al. (1998). Cofilin phosphorylation by LIM-kinase 1 and its role in Rac-mediated actin reorganization

Regulation of actin dynamics through phosphorylation of cofilin by LIM-kinase. *Nature* **393**, 809-12.

Figure legends

Figure 1. (A) Specificity of anti-XSSH antibody. Whole protein lysates from Stage 35 embryos (lanes 1 and 1'), reticulocyte lysates expressing XSSH (lanes 2 and 2'), and reticulocyte lysates alone (lanes 3 and 3') were electrophoresed on SDS-polyacrylamide gels. Proteins were transferred to nitrocellulose membrane. Coomassie Blue-stained gels (lanes 1-3) and immunoblots with anti-XSSH antibody (lanes 1'-3') are shown. (B) Immunoblot analysis of the whole lysates of unfertilized eggs and developing embryos with anti-XSSH antibody. Embryonic stages are represented at the upper side of each lane. The same membrane was probed for α-tubulin to control for equal loading. The major bands, appeared in earlier and later stages, were represented by open and closed arrowheads, respectively. A small arrow indicates several bands showing lower mobility. A large arrow represent the band with the lowest mobility appeared in unfertilized eggs. (C) Expression of XSSH during embryonic development (stages 7 to 11) was examined by PCR. (D) Alkaline phosphatase treatment of egg extracts. 10 μl of CSF-extracts were treated with (+) or without (-) 3 U of calf intestine alkaline phosphatase (AP) for 60 min at 21 °C, and subjected to SDS-PAGE and immunoblotting with anti-XSSH antibody (lanes indicated by "egg"). The whole cell lysate of stage 35 embryos (st. 35) was also loaded.

Figure 2. *In situ* hybridization of *Xenopus* embryos with XSSH (A-E, and I), XAC (F), and α-cardiac actin (G and H) riboprobes. Developmental stages shown; stage 11 (A), 22 (B and F), 25 (C and E), 26 (G and H), and 32 (D and I). Control (I) used the sense RNA probe of XSSH. Ventral (A), lateral (B-D, G and I), and dorsal views (E, F and H) are shown. The small and large arrows in A represent the yolk plug and the dorsal side of embryo, respectively.

Figure 3. (A-F) Immunofluorescence localization of XSSH (A, E and F), XAC (B), and pXAC (C and D) in paraffin sections of stage 11 (A-D) and stage 33 embryos (E and F). Inserts at the right side of A and B indicate the enlarged images of blastomeres. The arrow and arrowhead in A and B show

ectodermal and mesodermal regions brightly stained, respectively. Two serial sections from a single embryo with an interval of six sections were stained with anti-pXAC antibody (C and D). Arrows represent cells scarcely stained by this antibody. Sections of anterior (E) and posterior (F) parts of the trunk of a single embryo were probed with XSSH. Arrows indicate bright staining around somites. Bars, 100 μm (A-F) or 10 μm (inserts). (G) Immunoblot analysis of whole lysates from stage 7 to 10.5 embryos subjected to 2D-PAGE. Arrows indicate phosphorylated XAC spots.

Figure 4. Effects of ectopically expressed XSSH on *Xenopus* embryos. (A) Purified GST-XSSH (lane 1), GST-XSSH (CS) (lane 2) and pXAC fraction (lane 3) used for in vitro phosphatase assay were subjected to SDS-PAGE. The arrow and asterisk indicate the position of GST-XSSH or GST-XSSH (CS) and that of pXAC, respectively. (B and C) In vitro phosphatase assay was examined by a combination of 2D-PAGE and immunoblotting (B) and summarized in C. The number in B is corresponding to that in C. 1, pXAC fraction alone; 2, pXAC fraction and GST; 3, pXAC fraction and GST-XSSH; 4, pXAC fraction and GST-XSSH (CS); 5, pXAC fraction and GST-XSSH in the presence of Na_3VO_4. (D) Inhibition of gastrulation by injection of XSSH mRNAs. β-gal (control), XSSH (wild type), or XSSH (CS mutant) mRNAs were injected into both blastomeres at the two cell stage, and embryos were incubated until control embryos developed at the stage 13. The arrow indicates endodermal cells. (E) Immunoblots of whole lysates from injected embryos, which developed at the stage 13. Embryos, injected with β-gal (control), XSSH (WT), or XSSH (CS) mRNAs, were lysed individually, and each sample was subjected to SDS-PAGE and immunoblotting with anti-XSSH antibody. Two examples of each injection are shown. 1 and 2, control injected embryos; 3 and 4, XSSH (WT)-injected embryos; 5 and 6, XSSH (CS)-injected embryos. (F and G) Phosphorylation states of XAC in embryos, injected with β-gal (control), XSSH (wild type), or XSSH (CS mutant) mRNAs, were examined by 2D-immunoblotting at the stage 12 (F), and the ratio of pXAC to XAC was quantified and summarized in G.

Figure 5. Time-lapse images of control (β-gal mRNA-injection, left) and XSSH (CS) mRNA-

injected (right) embryos. Injection was done into both blastomeres at the 2-cell stage and images were successively acquired from embryos that developed at stage 10.5 (time 0). Numbers indicate the time in min after the first frame, except for 24 hr passage (the last panel). Arrowheads show closing dorsal lip formed in the control embryo and the arrow represents the position of dorsal lip formation in the XSSH (CS)-injected embryo. Ventral images are shown until 150 min. XSSH (CS)-injected embryo alone is shown in the last panel. (B) Immunofluorescence micrographs of animal-vegetal sections of control (β-gal), XSSH (WT) and XSSH (CS) mRNAs. Animal cap regions, stained by anti-XSSH antibody, are shown. The arrow indicates the layer of animal cap roof.

Figure 6. (A) Two examples of β-gal (control), XSSH (WT), or XSSH (CS) mRNA-injected embryos with light phenotypes (escaped from the formation of spina bifida). Arrowheads represent reduced eyes in deformed embryos. (B) The head region of β-gal (control) or XSSH (CS) mRNA-injected embryos at stage 33 were vertically sectioned and examined by immunofluorescence microscopy using anti-XSSH antibody. The arrow in the control embryo and the XSSH (CS) injected embryo indicates the forebrain and notochord, respectively. The arrowhead represents the complete eye-defect. (C) Ventral views of stage 10.5 embryos examined by *in situ* hybridization with Xbra probes. *Left panel*, sense (upper two embryos) and antisense (lower two embryos) images of control (H_2O-injected) embryos; *middle panel*, control (upper two embryos), XSSH (WT) and XSSH (CS) mRNA-injected embryos; *right panel*, XSSH (CS) mRNA-injected embryos. The lateral view clearly shows the Xbra-staining is present at the equatorial region (indicated by an arrow). (D) Immunoblots of whole lysates from embryos injected with β-gal (control, lanes 1 and 2) or XSSH (CS, lanes 3 and 4) mRNAs using antibody specific for α-muscle actin (SKA-06). Lysates in the respective lanes were derived from distinct embryos.

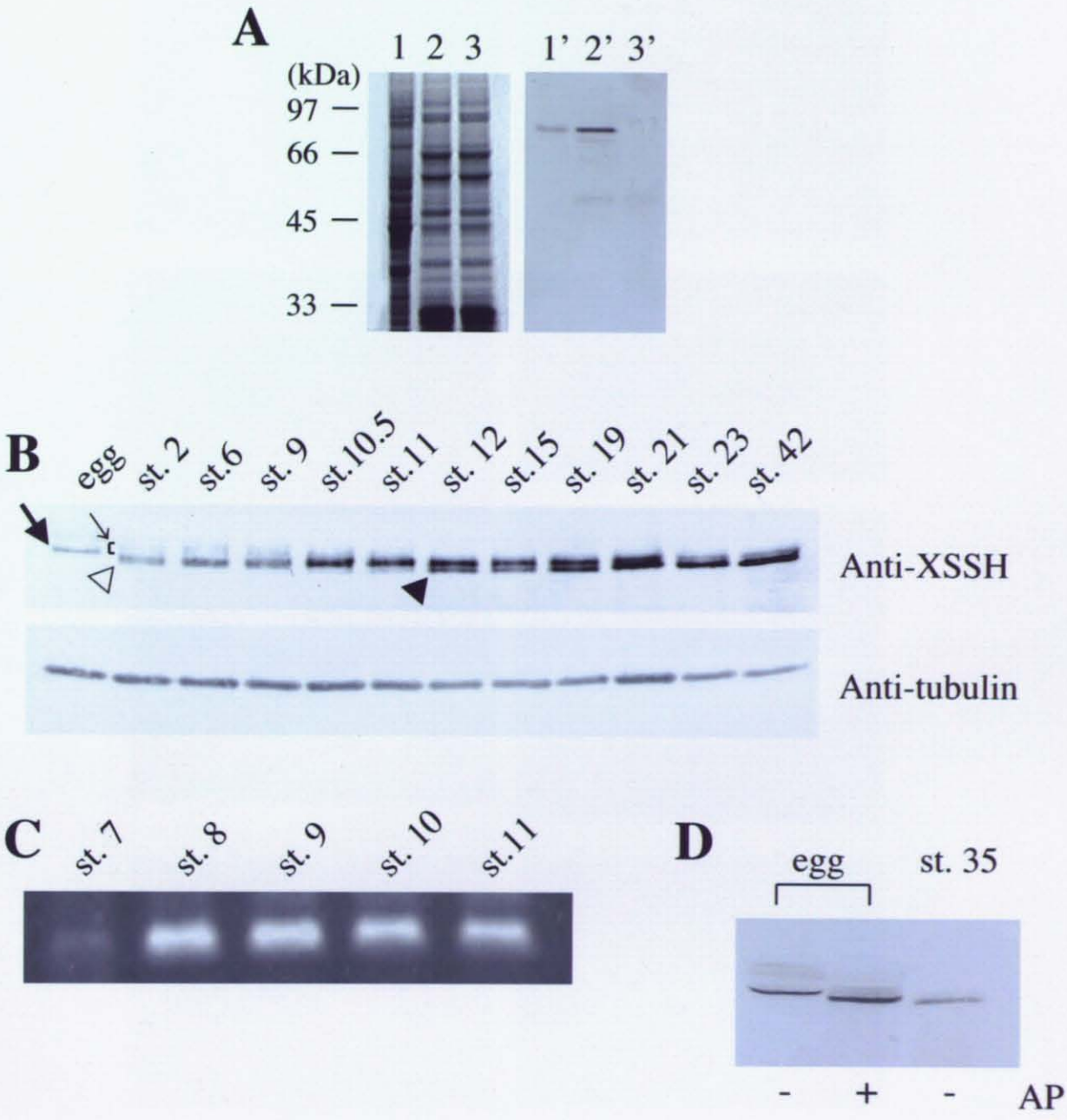
A
1 2 3
1' 2' 3'
(kDa)
97
66
45
33
B
egg
st. 2
st.6
st. 9
st.10.5
st.11
st. 12
st.15
st. 19
st. 21
st. 23
st. 42
Anti-XSSH
Anti-tubulin
C
st. 7
st. 8
st. 9
st. 10
st.11
D
egg
st. 35
- + - AP

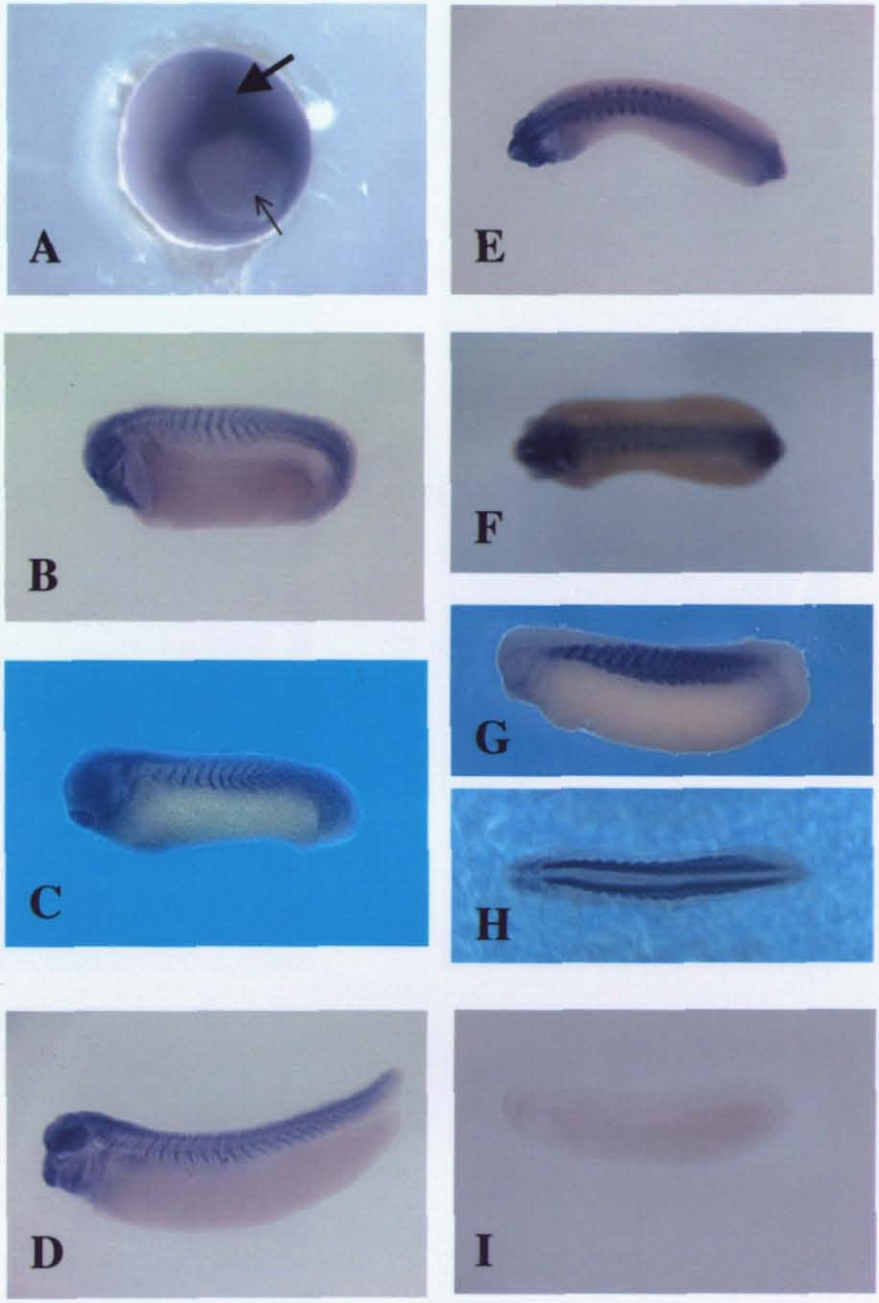
A
B
C
D
E
F
G
H
I

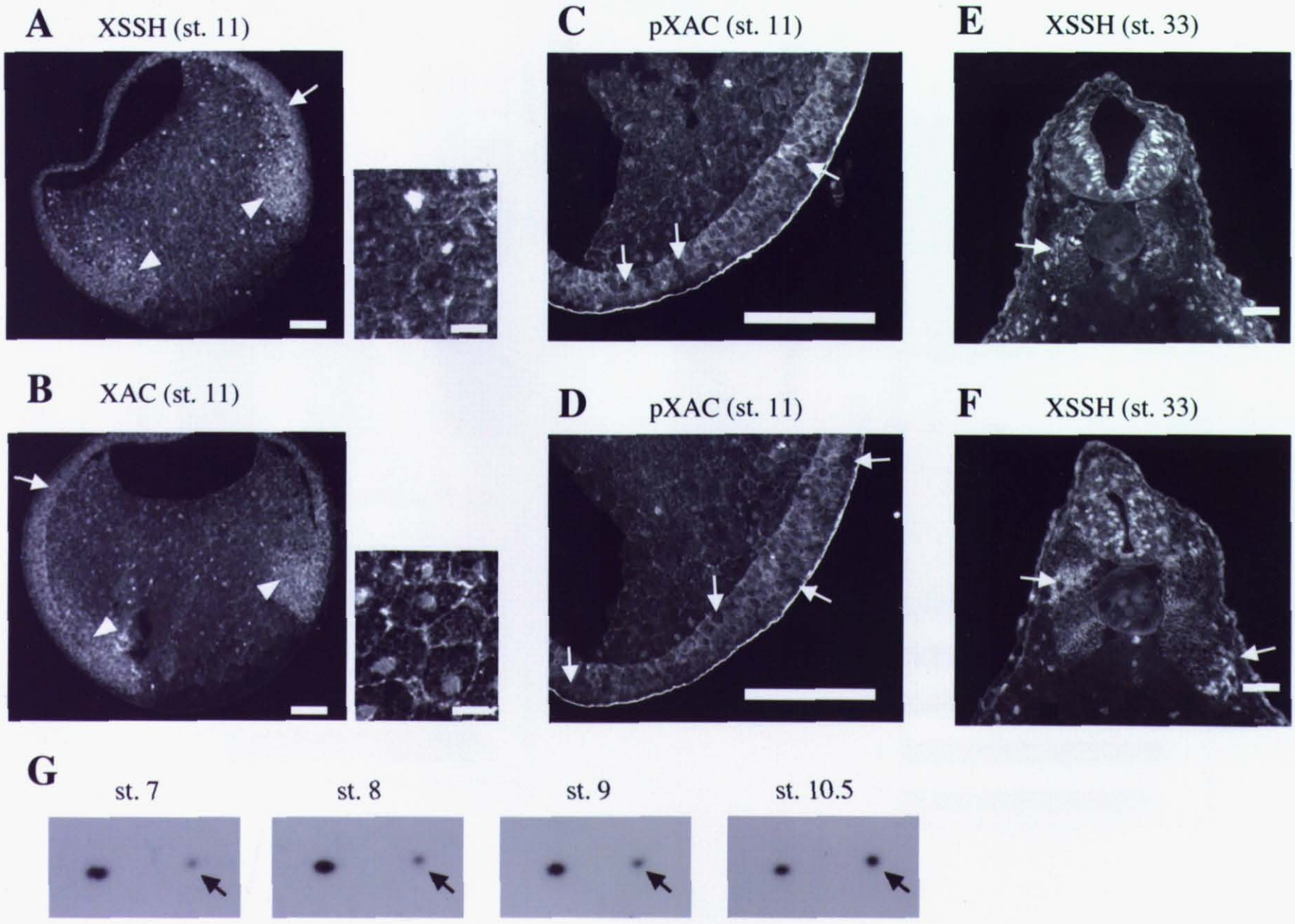
A
XSSH (st. 11)
B
XAC (st. 11)
C
pXAC (st. 11)
D
pXAC (st. 11)
E
XSSH (st. 33)
F
XSSH (st. 33)
G
st. 7
st. 8
st. 9
st. 10.5

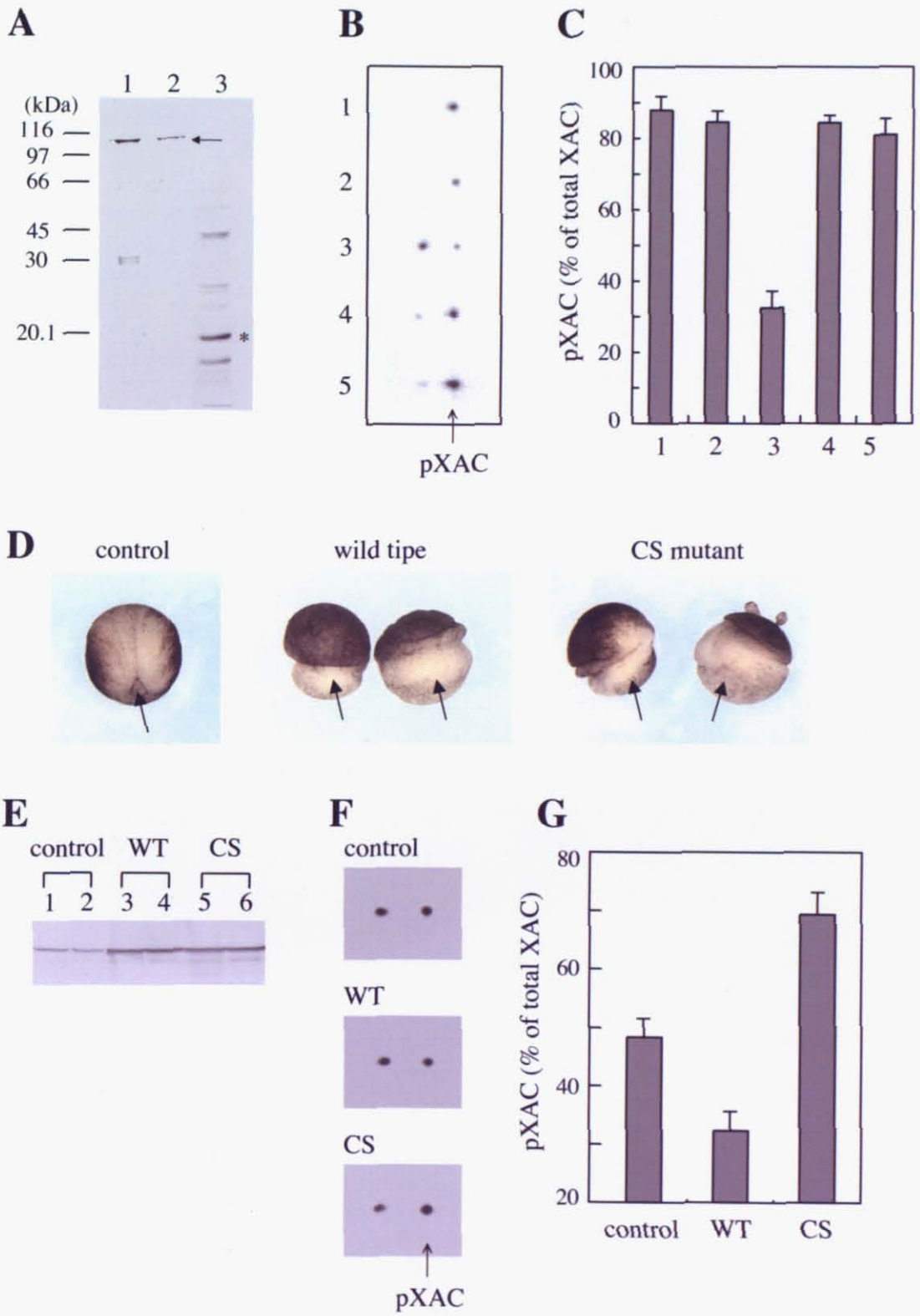
A
1 2 3
(kDa)
116
97
66
45
30
20.1
*
B
1
2
3
4
5
pXAC
C
pXAC (% of total XAC)
100
80
60
40
20
0
1 2 3 4 5
D
control
wild tipe
CS mutant
E
control WT CS
1 2 3 4 5 6
F
control
WT
CS
pXAC
G
pXAC (% of total XAC)
80
60
40
20
control WT CS

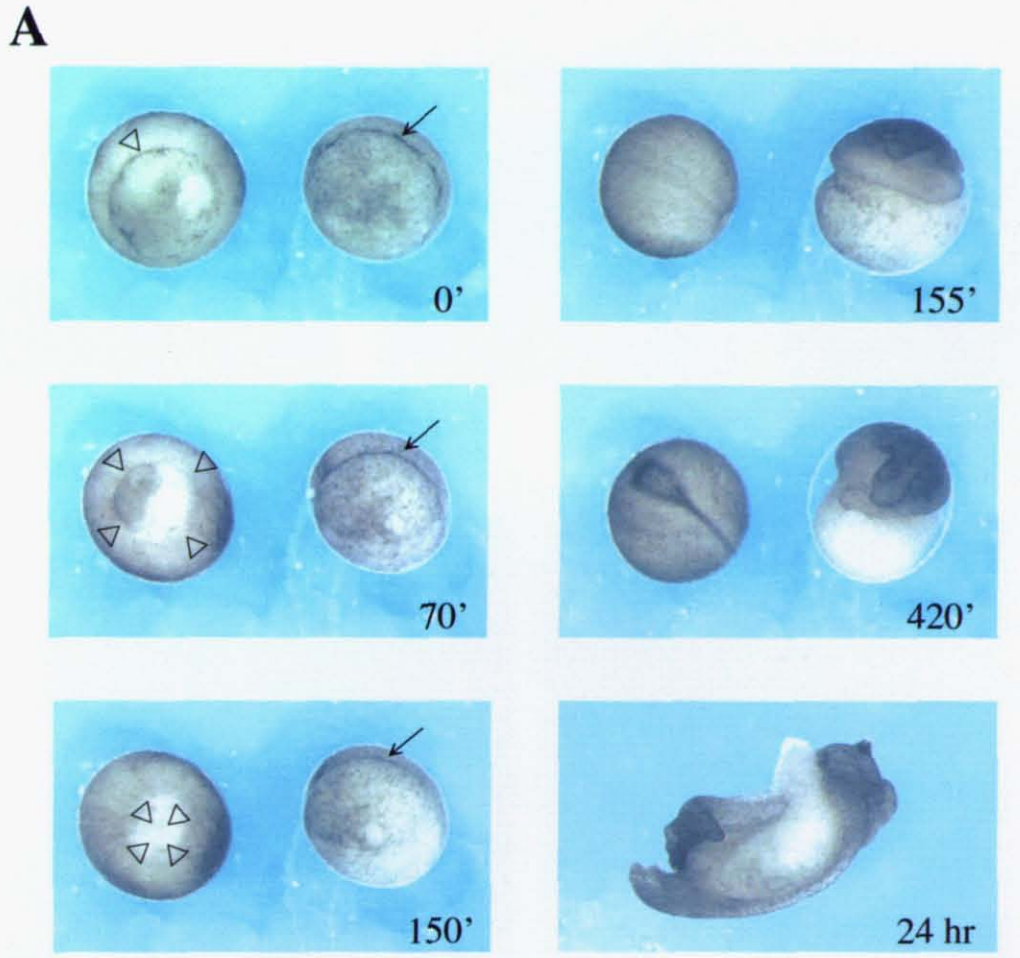
A
0'
155'
70'
420'
150'
24 hr
B
control
WT
CS

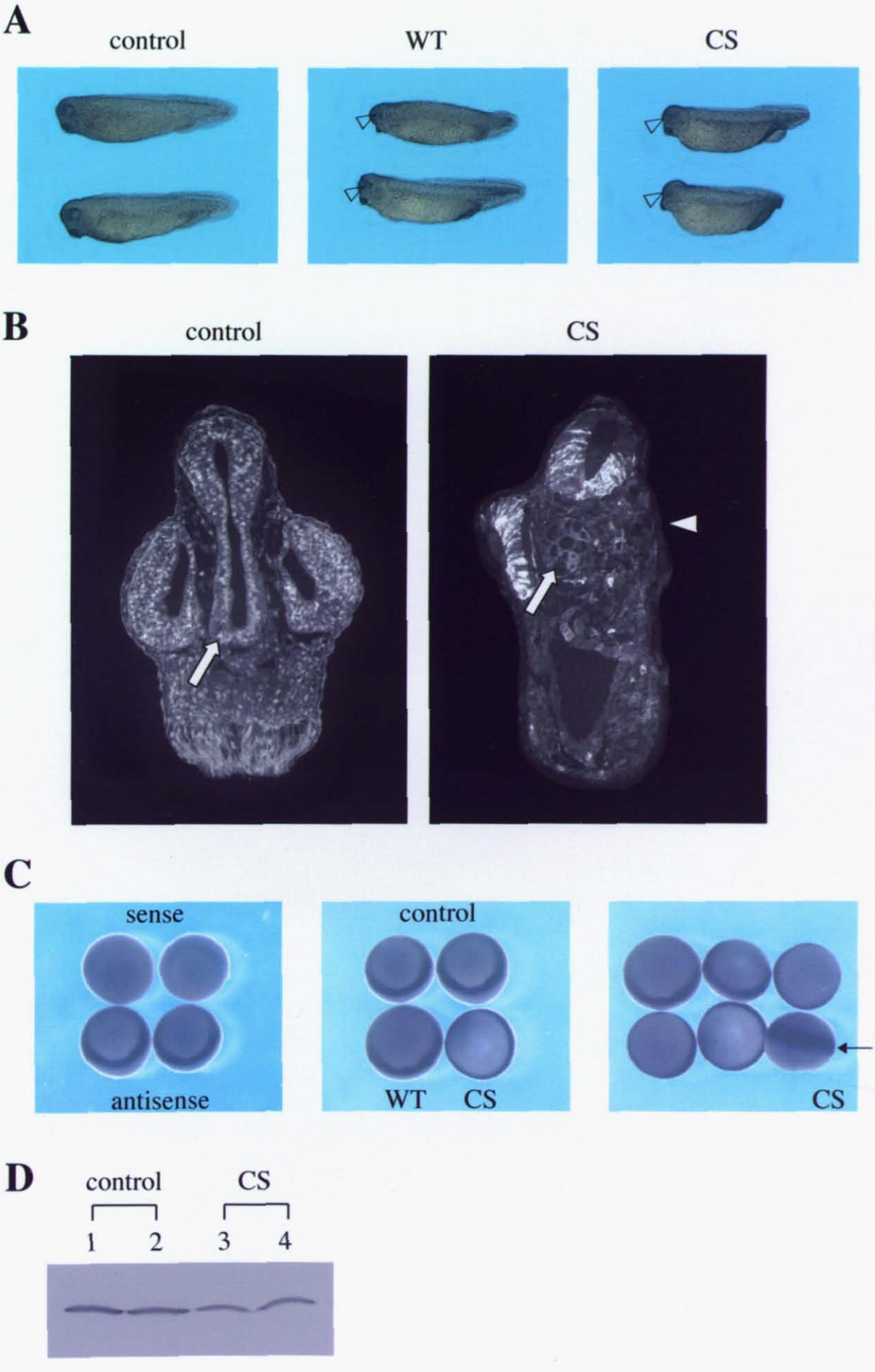
A
control
WT
CS
B
control
CS
C
sense
antisense
control
WT
CS
CS
D
control
CS
1
2
3
4

Table I. Gastrulation defects induced by ectopic expression of wild type and CS mutant XSSHs.

Sample RNA	Dose (ng)	Normal gastruration (%)	Defective gastrulation (%)	Total number of embryos
β-gal	0.5	92.9	7.1	28
	1	86.2	13.8	29
	2	84.0	16.0	25
XSSH (WT)	0.5	28.0	72.0	25
	1	18.2	81.8	22
	2	0	100	21
XSSH (CS)	0.5	66.7	33.3	27
	1	35.7	64.3	28
	2	20.8	79.2	24

Embryos were injected with β-gal (control), XSSH (WT), or XSSH (CS) mRNAs into the both blastomeres at the 2-cell stage. Phenotype of gastrulation was scored at stage 12.

Acknowledgments

I greatly thank Dr. Hiroshi Abe for directing my experiments and helpful suggestion. I thank Dr. Ono (Emory University) for critical reading of the manuscript, Dr. Bamburg (Colorado State University) for providing plasmids and anti-phospho-ADF/cofilin antibody, and for helpful advice, and Dr. Iida (Tokyo Metropolitan Institute of Medical Science) for providing anti-actin antibody.

I am grateful to Yoshiko Ohkubo and Reina Nishio for producing clear results in Chapter 1 Fig. 1-A and chapter 2 Fig. 3-E and F, respectively.

I also thank Professor Takashi Obinata and Dr. Naruki Sato for discussion and encouragement, all of the members of the Dr. Abe's and Dr. Obinata's labs for their encouragement during my study.

（既公表論文）

田中健之、大久保由子、阿部洋志：**Involvement of Slingshot in the Rho-mediated dephosphorylation of ADF/cofilin during *Xenopus* cleavage.**（７月現在、印刷公表はされていませんが、掲載は決定していますので、その通知と提出版を添付します）

田中健之、西尾玲奈、羽祢田核、阿部洋志：**Functional involvement of *Xenopus* homologue of ADF/cofilin phosphatase, Slingshot (XSSH), in the gastrulation movement.**（７月現在、印刷公表はされていませんが、掲載は決定していますので、その通知と提出版を添付します）

X-Original-To: habe@faculty.chiba-u.jp
Delivered-To: c6220014@chiba-u.jp
X-Sender: chiachia@mail.cdb.riken.go.jp
Date: Tue, 19 Jul 2005 16:11:30 +0900
To: habe@faculty.chiba-u.jp
From: Chiaki Nakayama <chiachia@cdb.riken.jp>
Subject: ZS-2005-094-2
Cc: zs-office@umin.ac.jp

Date:07/19/2005

MS number: ZS-2005-094

Dear Dr. Abe:

I am pleased to inform you that your revised manuscript, Involvement of Slingshot in the Rho-mediated dephosphorylation of ADF/cofilin during Xenopus cleavage, has been accepted for publication in Zoological Science.

Many thanks for sending your work to this journal.

Yours sincerely

Shigeru Kuratani
Editor

Shigeru Kuratani
Group Director
Laboratory for Evolutionary Morphology
Center for Developmental Biology, RIKEN
2-2-3 Minatojima-minami, Chuo-ku, Kobe
Hyogo 650-0047, JAPAN
e-mail: saizo@cdb.riken.jp
Tel: +81-78-306-3064
Fax: +81-78-306-3370

X-Original-To: habe@faculty.chiba-u.jp
Delivered-To: c6220014@chiba-u.jp
X-Sender: chiachia@mail.cdb.riken.go.jp
Date: Tue, 19 Jul 2005 16:11:27 +0900
To: habe@faculty.chiba-u.jp
From: Chiaki Nakayama <chiachia@cdb.riken.jp>
Subject: ZS-2005-093-2
Cc: zs-office@umin.ac.jp

Date:07/19/2005

MS number: ZS-2005-093

Dear Dr. Abe:

I am pleased to inform you that your revised manuscript,Functional involvement of Xenopus homologue of ADF/
cofilin phosphatase, Slingshot (XSSH), in the gastrulation movement, has been accepted for publication in Zoological Science.

Many thanks for sending your work to this journal.

Yours sincerely

Shigeru Kuratani
Editor

Shigeru Kuratani
Group Director
Laboratory for Evolutionary Morphology
Center for Developmental Biology, RIKEN
2-2-3 Minatojima-minami, Chuo-ku, Kobe
Hyogo 650-0047, JAPAN
e-mail: saizo@cdb.riken.jp
Tel: +81-78-306-3064
Fax: +81-78-306 -3370

（既公表論文１）

Involvement of Slingshot in the Rho-mediated dephosphorylation of ADF/cofilin during *Xenopus* cleavage

Kenji Tanaka, Yoshiko Okubo and Hiroshi Abe*

Department of Biology, Chiba University, Yayoi-cho, Inage-ku, Chiba 263-8522, Japan.

Running title: Dephosphorylation of ADF/cofilin by Slingshot

Section: Cell biology

*To whom correspondence should be addressed
Phone: 043-290-2805
E-mail: habe@faculty.chiba-u.jp

Abstract

ADF/cofilin is a key regulator for actin dynamics during cytokinesis. Its activity is suppressed by phosphorylation and reactivated by dephosphorylation. Little is known, however, about regulatory mechanisms of ADF/cofilin function during formation of contractile ring actin filaments. Using *Xenopus* cycling extracts, we found that ADF/cofilin was dephosphorylated at prophase and telophase. In addition, constitutively active Rho GTPase induced dephosphorylation of ADF/cofilin in the egg extracts. This dephosphorylation was inhibited by Na3VO4 but not by other conventional phosphatase-inhibitors. We cloned a *Xenopus* homologue of Slingshot phosphatase (XSSH), originally identified in *Drosophila* and human as an ADF/cofilin phosphatase, and raised antibody specific for the catalytic domain of XSSH. This inhibitory antibody significantly suppressed the Rho-induced dephosphorylation of ADF/cofilin in extracts, suggesting that the dephosphorylation at telophase is dependent on XSSH. XSSH bound to actin filaments with a dissociation constant of 0.4 μM, and the ADF/cofilin phosphatase activity was increased in the presence of F-actin. When latrunculin A, a G-actin-sequestering drug, was added to extracts, both Rho-induced actin polymerization and dephosphorylation of ADF/cofilin were markedly inhibited. Jasplakinolide, an actin-stabilizing drug, alone induced actin polymerization in the extracts and lead to dephosphorylation of ADF/cofilin. These results suggest that Rho-induced dephosphorylation of ADF/cofilin is dependent on the XSSH activation that is caused by increase in the amount of F-actin induced by Rho signaling. XSSH colocalized with both actin filaments and ADF/cofilin in the actin patches formed on the surface of the early cleavage furrow. Injection of inhibitory antibody blocked cleavage of blastomeres. Thus, XSSH may reorganize actin filaments through dephosphorylation and reactivation of ADF/cofilin at early stage of contractile ring formation.

Keywords: Slingshot, ADF/cofilin, actin filaments, cytokinesis, *Xenopus*

Introduction

Cytokinesis is the essential process to create two daughter cells. It begins at late anaphase to telophase and the contractile ring, the core components of which are actin filaments, is formed in the cortex of the cleavage furrow. Recent study demonstrated that actin dynamics in the contractile ring are critical for cytokinesis (Pelham and Chang, 2002). Actin filaments are dynamically regulated through interaction with various actin-binding proteins in cells. Among them, ADF/cofilin is the key regulator responsible for actin dynamics in cells (for reviews see Bamburg, 1999; Bamburg et al., 1999; Carlier et al., 1999; Maciver and Hussey, 2002).

ADF/cofilin is a ubiquitously expressed and highly conserved actin binding protein and also functions in cytokinesis (Gunsalus et al., 1995; Nagaoka et al., 1995; Abe *et al.*, 1996; Okada et al., 1999; Nakano et al., 2001; Ono et al., 2003). ADF/cofilin binds to actin in a 1:1 molar ratio, alters the twist of F-actin and causes both depolymerization and severing of actin filaments (Mabuchi, 1983; Nishida *et al.*, 1984; Carlier et al., 1997; MacGough et al., 1997). Acceleration of actin depolymerization by ADF/cofilin maintains the monomeric actin pool and thereby promotes actin filament turnover (for review see Pollard and Borisy, 2003). Severing of actin filaments by ADF/cofilin results in the generation of free barbed ends, which in turn is crucial for efficient enhancement of actin polymerization *in vivo* (Ghosh *et al.*, 2004). Both activities might be deeply involved in reorganization of actin filaments in cells.

These activities are suppressed by phosphorylation at Ser-3 (Agnew et al., 1995; Moriyama et al., 1996). LIM kinases (Limks) (Arber et al., 1998; Yang et al., 1998; Sumi et al., 1999), testicular protein kinases (TESKs) (Toshima et al., 2001a, 2001b), and Nck-interacting kinase (NIK)-related kinase (NRK)/NIK-like embryo-specific kinase (NESK) (Nakano et al., 2003) have been demonstrated to phosphorylate ADF/cofilin in vertebrates. Two types of Limks, designated by LIM kinase 1 and LIM kinase 2 are present in vertebrates (Mizuno et al., 1994; Okano et al., 1995; Nunoue et al., 1995; Cheng and Robertson, 1995; Osada et al., 1996; Koshimizu et al., 1997; Takahashi et al., 1997, 2001). Pioneering works (Arber et al., 1998; Yang et al., 1998) demonstrated that activation of Limk 1 is mediated by a small GTPase Rac1, and were followed by a study that activation of p21-activated kinase (Pak1) through Rac1 or Cdc42 directly increases Limk 1 activity (Edwards et al., 1999). Also, activation of Limks occurs downstream of Rho-Rho kinase (ROK/ROCK) signaling (Maekawa et al., 1999; Sumi et al., 1999; Ohashi et al., 2000; Amano et al., 2001). These studies all strongly suggest that phosphorylation, and thus inactivation, of ADF/cofilin proceeds through activation of Rho-GTPases. On the other hand, ADF/cofilin is also

dephosphorylated by extracellular stimuli (for review see Moon and Drubin, 1995). Recently, cofilin specific phosphatase, Slingshot (SSH), has been identified in *Drosophila*, human and mouse (Niwa *et al.*, 2002; Ohta *et al.*, 2003), which directly dephosphorylates and thus reactivates ADF/cofilin. This activity is also regulated downstream of PI3-kinase or Rac1 in lamellipodia of cultured mammalian cells and increased by binding to actin filaments (Nishita *et al.*, 2004; Nagata-Ohashi *et al.*, 2004).

During cytokinesis, ADF/cofilin is concentrated in the cleavage furrow in mammalian cells and *Xenopus* zygotes (Nagaoka et al., 1995; Abe et al., 1996). Injection of the antibody specific for *Xenopus* ADF/cofilin (XAC) inhibits cleavage of zygotes, suggesting that XAC is required for the progression of cytokinesis (Abe et al., 1996). Limk1 and SSH activities are differently regulated during cytokinesis of Hela cells: the activity of Limk1 is elevated at prometaphase to metaphase while the SSH activity increases at telophase to cytokinesis (Amano et al., 2002; Kaji et al., 2003). In addition, expression of dominantly negative form of SSH markedly increases multinucleated cells. These results strongly suggest that active ADF/cofilin is necessary for cytokinesis. On the other hand, the Rho GTPase is a key regulator for the contractile ring formation at cytokinesis (Mabuchi *et al.*, 1993; Kishi *et al.*, 1993; Drechsel *et al.*, 1997; Prokopenko *et al.*, 1999). GTP-bound Rho, which is the active form, increases at telophase, concentrated at the cleavage furrow and orchestrates various actin-binding proteins (Takaishi *et al.*, 1995; Kimura *et al.*, 2000; Yoshizaki *et al.*, 2003). Therefore, it is important to examine whether the ADF/cofilin activity is regulated under the Rho GTPase during cytokinesis.

In this study, we found that dephosphorylation of XAC was induced by addition of a constitutively active form of RhoA to the *Xenopus* egg extract which is able to reconstitute mitotic phases and cycles. Thus, we cloned a *Xenopus* homologue of SSH (XSSH) and investigated its involvement in dephosphorylation of XAC using *Xenopus* egg extracts. Finally, we conclude that Rho-induced XAC dephosphorylation is dependent on the XSSH activation that is caused by increase in the amount of F-actin induced by Rho signaling.

MATERIALS AND METHODS

Polyacrylamide gel electrophoresis and immunoblotting

SDS-polyacrylamide gel electrophoresis (SDS-PAGE) was carried out according to Laemmli (1970). Two-dimensional gel electrophoresis (2D-PAGE) was performed according to O'Farrell et al. (1977) using nonequilibrium-pH-gradient gel

electrophoresis (NEpHGE) for the first dimension. Samples were dissolved in 2D-PAGE buffer composed of 9 M urea, 2% ampholine pH 3.5-10, 5% 2-mercaptoethanol, 0.1% SDS, 1% NP-40, and 10 mM Tris-HCl, pH 7.5. For immunoblotting, proteins were electrophoretically transferred from the SDS-gel to nitrocellulose paper by the method of Towbin et al. (1979). The paper was treated with 5% skimmed milk in PBS for 1 hr, and then incubated with the primary antibody followed by treatment with alkaline phosphatase-conjugated secondary antibody. The paper was thoroughly washed with PBS after each immunoreaction and stained with nitroblue tetrazolium chloride (NBT) and 5-bromo-4-chloro-3-indolylphosphate p-toluidine salt (BCIP) in alkaline phosphatase buffer (0.1 M NaCl, 5 mM MgCl2, and 0.1 M Tris-HCl, pH 9.5), or detected by chemiluminescence with CDP-Star (Roche) using Light Capture (ATTO).

Preparation of egg extracts

Egg extracts (cycling extracts and cytostatic factor-arrested (CSF) extracts) were prepared from unfertilized eggs as described by Murray (1991) with some modifications. For cycling extracts, egg activation was carried out by treating eggs with 0.2 μg/ml calcium ionophore A23187 for 3 min at room temperature. Extracts were obtained by centrifugation in the absence of actin-depolymerizing drug such as cytochalasin B. Interphase extracts and re-entered mitotic extracts (prepared by adding ΔN85 cyclin B2 to interphase extracts; pGEX-ΔN85 cyclin B2 was kindly provided by Dr. Kishimoto, T of Tokyo Institute of Technology) were prepared according to Glotzer et al., 1991.

Cloning of XSSH and construction of expression vectors

A stage 30 *Xenopus* embryo cDNA library in λZAPII was screened by polymerase chain reaction (PCR) with a degenerated primer set of 5'-CTKGGWAGYGARTGGAAYGC and 5'-ACWCCCATYTTRCARTGTAC, corresponding to the nucleotide sequence of 1177-1415 in the *Drosophila* SSH catalytic domain that is highly homologous to human SSHs. A major band with about 240 bp was amplified and cloned into the EcoRV site of pBluescript II KS^+ vector. Sequencing of this PCR fragment exhibited about 70% identity with human SSH between their primary structures, suggesting a *Xenopus* homologue of SSH (XSSH). The PCR fragment was excised from pBluescript II KS^+ vector with EcoRI and XhoI and inserted into a pGEX-4T-1 vector digested with EcoRI and XhoI, and glutathione-S-transferase (GST)-fused catalytic domain was expressed. The anti-XSSH antibodies were obtained by immunizing the GST-catalytic domain to rabbits (see below). A full-length clone was isolated from a *Xenopus* ovary λZAPII cDNA library with anti-XSSH antibody (GenBank accession number AY 618876). A partial cDNA clone lacking N-terminus (pBluescript SK^--ΔN-XSSH) was also isolated from the stage 30 cDNA library, and

used for expression of His-tagged ΔN-XSSH protein.

To produce the full-length XSSH as GST-fusion protein (GST-XSSH), the XSSH cDNA in pBluescript SK⁻ was first digested with KpnI and blunted by T4 polymerase, and then excised with EcoRI. This fragment was inserted into EcoRI and SmaI sites of pGEX-4T-3 vector. For GST-SSH A and B domains (GST-AB), the XSSH cDNA was digested with EcoRI and XhoI, and cloned into the same sites of pGEX-4T-3 vector. To produce GST-Tail, a novel EcoRI site was generated by site-directed mutagenesis using complementary primers (5'-CAAACATATCAAGGAATTCTAGGA GCCAGTAAGC and 5'-GCTTACTGGCTCCTAGAATTCCTTGATATGTTTG), and checked by sequencing. The tail region of mutagenized cDNA was excised with EcoRI and inserted into the same site of pGEX-4T-2 vector. For expression of His-tagged ΔN-XSSH, ΔN-XSSH cDNA was excised with EcoRI and inserted into the same site of pRSET-A vector.

Preparation of proteins

pGEX expression plasmids carrying the XSSH full-length, SSH A and B domains and tail region were transformed into BL21 (DE3) pLysS and the expression of recombinant proteins was induced by adding 0.1 mM IPTG for overnight at 13 °C. Cells were harvested and lysed by sonication in PBS containing 0.1% Triton X-100, and soluble fractions were obtained by centrifugation at 15,000 g for 20 min at 4 °C. Supernatants were added to glutathione-Sepharose 4B (Pharmacia) prewashed with PBS. Mixtures were incubated for 1 hr at 4 °C with gentle, continuous stirring, and then resins were poured into columns and thoroughly washed with PBS containing 0.1% Triton X-100. Proteins were eluted with PBS containing 50 mM Tris-HCl, pH 8.0 and 10 mM glutathione, and dialyzed against F-buffer (0.1 M KCl, 2 mM $MgCl_2$, 0.1 mM DTT, 0.05% NaN_3, 20 mM HEPES-KOH, pH 7.2). BL21 (DE3) pLysS was also transformed by pRSET- ΔN-XSSH and the expression was induced by adding 0.5 mM IPTG for 3 hr at 37 °C. Inclusion bodies of ΔN-XSSH, washed with PBS containing 1% Triton X-100, was solubilized with 6 M urea containing 0.1 M $Na\text{-}PO_4$, pH 8.0, and applied to Ni-NTA column (QIAGEN). The column was washed with the same buffer, but at pH 6.5, and the same buffer containing 20 mM imidazole, pH 7.0. His-ΔN-XSSH was eluted by the same buffer containing 0.1 M imidazole, pH 7.0, dialyzed against coupling buffer (6M urea, 80 mM $CaCl_2$, 0.1 M HEPES-KOH, pH 7.4), and coupled to Affi-gel 10 (Bio-Rad).

GST-V14RhoA was prepared as described (Self and Hall, 1995). pGEX-human V14RhoA was a generous gift from Dr. Bamburg of Colorado States University. Purified GST-V14RhoA was concentrated to at least 4 mg/ml, dialyzed against 100 mM

KCl, 2 mM MgCl2, 50 mM sucrose, 10 mM HEPES-KOH, pH 7.7, and stored at –80 °C until use.

Actin was prepared from rabbit skeletal muscle by the method of Spudich and Watt (1971) and purified by gel filtration on a Sephadex G-200 column pre-equilibrated with G-buffer composed of 0.2 mM CaCl2, 0.1 mM DTT, 0.2 mM ATP, 0.01% NaN3, and 2.5 mM Tris-HCl, pH 8.0. 100 μl portions of G-actin were quick-frozen in liquid nitrogen and stored at –80 °C.

The phosphorylated XAC fraction was prepared from *Xenopus* ovaries. *Xenopus* ovaries were homogenized in 5 volumes of buffer A (0.1 M KCl, 2 mM EGTA, 2 mM DTT, 50 mM NaF, and 20 mM HEPES-KOH, pH 7.2) containing 40% saturation of ammonium sulfate, 20 μg/ml leupeptin, and 1 mM PMSF. After centrifugation at 15,000 g for 20 min at 4 °C, the supernatant was further fractionated by 60-90% saturation with ammonium sulfate. The precipitate was collected by centrifugation at 15,000 g for 30 min at 4 °C, and solubilized and dialyzed to buffer A. The dialysed sample was gel-filtrated on a Sephadex G-75 column, and fractions containing XAC were applied to a hydroxyapatite column pre-equilibrated with buffer A, followed by washing thoroughly with buffer A and buffer A containing 0.6 M KCl. XAC was eluted with buffer A containing 0.6 M KCl and 10 mM K-PO4, pH 7.5, and dialyzed against 20 mM NaCl, 2 mM DTT, and 20 mM Tris-HCl (pH 7.5). Finally, the flow-through fraction from a DE52 ion exchange column pre-equilibrated with the same buffer was concentrated, dialyzed against F-buffer, and stored at –80 °C until use.

Assays for dephosphorylation of XAC

Cycling extracts were incubated at 23 °C and 5 μl of the extract was removed and immediately added to 100 μl of 10% trichloroacetic acid (TCA) every 5 min to stop reaction and precipitate proteins. Samples were centrifuged at 15,000 g for 15 min at 4 °C, and pellets were once rinsed with 50% acetone and dried for 2D-PAGE. Progression of cell cycle was monitored by checking sperm morphology as described by Murray (1991).

1/20 volume of GST-V14RhoA or buffer alone was added to CSF extracts, interphase extracts or re-entered mitotic extracts at a final concentration of 4.2 μM, and incubated at 22 °C for 1 hr. When phosphatase inhibitors, latrunculin A, jasplakinolide, or 10 mg/ml of affinity-purified antibody were used, adding volume was fixed at 1/20 to the extract. Final concentrations of each drug are shown in figure legends. At the end of incubation, 10% TCA was added to the samples to stop reaction and proteins were precipitated, rinsed and dried as described above.

For in vitro phosphatase assay, 2 μM of GST-XSSH or GST was incubated with the

phosphorylated XAC (pXAC) fraction (the final concentration of pXAC was estimated to be 5.5 μM by densitometry) for 1 hr at room temperature in F-buffer. To examine the effect of F-actin, pXAC fraction was pre-incubated with F-actin in the absence or presence of latrunculin A (50 μM) for 30 min at room temperature in F-buffer, and then GST-XSSH or GST was added and incubated for additional 1 hr at room temperature. Reactions were stopped by addition of 10% TCA to samples and proteins were precipitated, rinsed and dried as described above.

Samples were solubilized in 2D-PAGE buffer and subjected to 2D-PAGE and immunoblotting. XAC spots were detected by chemiluminescence using Light Capture (ATTO) and analyzed by densitometry with a software of ATTO Lane Analyzer 10H.

Co-sedimentation assay of XSSH with F-actin

Binding of XSSH to actin filaments was examined by pelleting assay. Various amounts of GST-tagged full-length XSSH or truncated mutants were incubated with 3.0 μM F-actin, which had been polymerized in F-buffer for 1 hr at room temperature, for 3 hr at 4 °C. Samples were centrifuged at 400,000 g for 20 min and the supernatants and pellets were subjected to SDS-PAGE. Gels were stained with Coomassie Blue G-250 and destained in 7% acetic acid. Protein bands were quantified by densitometry using Light Capture (ATTO) and a software, ATTO Lane Analyzer 10H.

Antibodies

Inclusion bodies of GST-fused XSSH catalytic domain, as described above, was thoroughly washed with PBS containing 1% Triton X-100, and with 3M urea, and then solubilized with SDS-sample buffer (4% SDS, 5% 2-mercaptoethanol, 10% glycerol and 25 mM Tris-HCl, pH 6.8). After centrifugation at 15,000 g for 15 min, the supernatant was subjected to SDS-PAGE, stained with Coomassie Blue R-250 and the protein band corresponding to GST-catalytic domain was excised with a razor blade. GST-catalytic domain was electrophoretically eluted from gel slices, dialyzed to PBS, and used to immunize rabbits to produce polyclonal antibody. Antisera were purified by His-XSSH-coupled Affi-gel 10 column chromatography.

Anti-XAC monoclonal antibody was previously prepared (Okada et al., 1999). Anti-actin polyclonal and monoclonal (AC-40) antibodies were kindly provided by Dr. K. Iida of the Tokyo Metropolitan Institute of Medical Science and purchased from Sigma, respectively. Anti-phosphorylated ADF/cofilin-specific antibody was kindly provided by Dr. Bamburg of Colorado State University. Fluorescein or rhodamine-labeled goat anti-mouse or rabbit IgG was purchased from TAGO Inc. Alkaline phosphatase-conjugated goat anti-mouse or rabbit IgG was purchased from Bio-Rad.

Microinjection

Affinity-purified anti-XSSH IgG, concentrated to 10 mg/ml and dialyzed against the injection buffer consisting of 60 mM KCl, 2 mM $MgCl_2$, 5 mM HEPES-KOH, pH 7.2, was injected into one blastomere of two-cell stage embryos. Injection volumes from each pipette from a pressure injector (CIJ-1, Shimadzu, Kyoto) were calibrated by measuring the volume of an aqueous drop delivered into mineral oil. Control injections with injection buffer alone and the same amount of non-immune IgG were also done (Abe et al., 1996; Okada et al., 1999).

Immunofluorescence microscopy

Xenopus embryos were fixed in MEMFA (3.7% formaldehyde, 2 mM $MgSO_4$, 1 mM EGTA, and 0.1 M MOPS, pH 7.4) containing 1% TCA, embedded in paraffin, and sectioned as described elsewhere (Okada et al., 1999). *Xenopus* cleavage furrows were manually isolated and fixed according to Noguchi and Mabuchi (2000). After blocking with 20% goat serum in PBS for 1 hr at room temperature, specimens were incubated with primary antibodies or Alexa 488-wheatgerm agglutinin (WGA) for 1 hr at room temperature, and then with appropriate fluorochrome-conjugated secondary antibodies. After each immunoreaction step, specimens were rinsed and washed with PBS, and mounted in PBS containing 1 mg/ml p-phenylenediamine and 90 % glycerol.

RESULTS

XAC is dephosphorylated at prophase and telophase during cell cycle

In order to address whether the phosphorylation state of XAC is altered during mitosis of *Xenopus* zygotes, we first quantified changes of the ratio of phosphorylated XAC (pXAC) to unphosphorylated XAC using cycling extracts prepared from *Xenopus* unfertilized eggs. Progression of the cell cycle was monitored by morphological changes of added sperm nuclei. pXAC and unphosphorylated XAC were separated and detected by a combination of 2D-PAGE and immunoblotting using a monoclonal antibody specific for XAC. The signal intensity of each spots was quantified by densitometry. As shown in Fig. 1A, the amount of dephosphorylated XAC was clearly increased at prophase and telophase when actin filaments are thought to be drastically reorganized. Dephosphorylation of XAC (thus, reactivation of XAC) at telophase might exhibit necessity of XAC for contractile ring formation, since we have previously demonstrated that XAC is essential for the progression of cleavage of *Xenopus* zygotes. Therefore, we next examined effects of RhoA, a key regulator of the contractile ring formation, on the phosphorylation state of XAC using *Xenopus* CSF-extracts, instead of cycling extracts.

RhoA induces dephosphorylation of XAC in Xenopus egg extracts

Extracts, to which V14RhoA, a constitutively active form of RhoA, was added, were analyzed by 2D-PAGE and immunoblotting. As shown in Fig. 1B and C, although about 55% of endogenous XAC was phosphorylated in a control CSF extract, addition of V14 RhoA decreased pXAC to about 30%. Similar results were obtained by using either interphase extracts or mitotic extracts reentered to anaphase by addition of undegradable cyclin B (delta-N cyclin B) to the interphase extract (data not shown).

To determine which phosphatase is responsible for the dephosphorylation of XAC, effects of various phosphatase inhibitors were examined. V14RhoA was added to CSF extracts in the presence of okadaic acid (OA), a phosphatase inhibitor specific for phosphatase type 1 and type 2A (PP1 and PP2A), cypermethrin (specific for PP2B), or sodium orthovanadate (Na_3VO_4, specific for protein tyrosine phosphatases (PTP) and dual-specificity phosphatases (DSP)). Changes in the amount of pXAC were monitored chemiluminescently by immunoblotting using an antiserum that specifically recognizes the phosphorylated form of ADF/cofilin (Fig. 2A). Total amounts of XAC on each lane were confirmed by immunoblotting on the same membrane using a monoclonal antibody specific for XAC. Neither OA nor cypermethrin suppressed dephosphorylation of XAC induced by addition of V14RhoA (Fig. 2, Aand B), whereas Na_3VO_4 completely blocked it (Fig. 2, C and D). Thus, these results suggest that XAC phosphatase is a DSP but not a conventional Ser/Thr phosphatase.

XSSH is responsible for the dephosphorylation of XAC in the extracts

Slingshot (SSH) was recently identified as a cofilin-specific phosphatase and is a candidate for the XAC phosphatase, since it possesses a DSP-catalytic domain (DSPc). Therefore, we cloned a *Xenopus* homologue of SSH (XSSH, accession number AY618876) and raised a polyclonal antibody specific for the DSPc domain. This antibody, as shown in Fig. 3A, specifically reacted with bacterially expressed XSSH (His-ΔN–XSSH, see *Materials and Methods*) and a single band of an apparent molecular mass of 78 kDa in the egg extract, well corresponding to the calculated value from the deduced amino acid sequence of XSSH. In addition, this antibody also reacted the XSSH that was expressed in reticulocyte lysates. Thus, we concluded that this antibody specifically recognizes DSPc domain of XSSH. When V14RhoA was added to the CSF extract in the presence of this antibody, dephosphorylation of XAC was inhibited as shown in Fig. 3B and C. This inhibitory effect strongly suggests that XSSH is responsible for the dephosphorylation of XAC induced by RhoA.

XSSH is activated by actin polymerization induced by RhoA

Since purified SSH is shown to be activated by the presence of actin filaments

(Nagata-Ohashi et al., 2004), we hypothesized that RhoA-induced dephosphorylation of XAC in egg extracts may also be affected by the increasing amount of F-actin triggered by the active RhoA. In order to elucidate this point, we first quantified F-actin contents in extracts. As shown in Fig. 3D, addition of V14RhoA markedly decreased the amount of actin in the supernatant and hence increased that in the pellet, although a significant amount of actin was present in the supernatant in control extracts. Therefore, RhoA induces actin polymerization in this extract. When latrunculin A alone was added to extracts, the amount of F-actin was decreased. V14RhoA did not antagonize this effect of latrunculin A because of no increase in the amount of F-actin in the pellet. Next, as shown Fig. 3E, we examined phosphorylation states of XAC in the respective extracts and found that dephosphorylation of XAC by RhoA was suppressed in the presence of latrunculin A. In addition, the dephosphorylation effect of an exogenous GST-XSSH (see Fig. 4) was also inhibited to some extent by the presence of latrunculin A. It should be noted that addition of latrunculin A alone effectively increased the phosphorylation level of XAC in the extract, and staurosporine, a broad kinase inhibitor, did not repress this increase in the amount of pXAC (data not shown). Whether *Xenopus* LIM-kinases are involved in this phosphorylation remains to be elucidated.

Since repression of actin polymerization by latrunculin A prevented XAC dephosphorylation induced by RhoA, it is possible that increasing amount of F-actin directly causes dephosphorylation of XAC in the extract. To clarify this point, jasplakinolide, which promotes actin polymerization, was added to the extract. As shown in Fig. 3D and F, F-actin was increased in the high-speed precipitate and dephosphorylation of XAC was induced by addition of this drug. Na3VO4 completely inhibited this dephosphorylation.

XSSH tightly binds to actin filaments to increase dephosphorylation activity

In order to examine the binding property of XSSH to actin filaments, we prepared GST-tagged XSSH (full-length, GST-XSSH) and two truncate mutants of XSSH, the SSH domain (GST-AB) and the tail domain alone (GST-Tail) (Fig. 4, A and B). Pelleting assays revealed that both full-length and each truncate were cosedimented with F-actin (Fig. 4, C and D). Dissociation constants (Kd) of GST-XSSH and GST-AB for actin were calculated by Scatchard analyses to be 0.4 and 0.5 μM, respectively (Fig. 4E). In addition, their binding to actin was saturated at a molar ratio of 1:6.5 and 1:8.7, respectively. On the other hand, in vitro phosphatase activity of XSSH was examined with GST-XSSH and phosphorylated XAC fraction. As shown in Fig. 4F, the phosphorylated XAC fraction contained more than 85% of phosphorylated XAC, and no kinase, phosphatase, and proteinase activities were detected (data not shown). GST-

XSSH dephosphorylated XAC and its activity was markedly increased in the presence of F-actin, while the addition of F-actin preincubated with latrunculin A antagonized this effect (Fig. 4G). Taken all together, it is reasonable to conclude that XSSH activity increases by binding to F-actin, of which polymerization is induced by RhoA signaling.

Inhibition of cleavage by injection of an anti-XSSH antibody

We injected affinity-purified anti-XSSH antibody into one blastomere of 2-cell stage embryos. Injection of more than 100 ng of anti-XSSH IgG arrested the cleavage of blastomeres in about 70% of embryos injected (n=19/27) (Fig. 5B, arrows), but control injection of neither buffer alone nor non-immune IgG arrested development (Fig. 5A, arrowheads). Injection of less than 100 ng scarcely affected cleavage (9%, n=2/23). The process of the cleavage of antibody-injected blastomeres was monitored (Fig. 5C). De-vitellinized embryos were used to observe blastomeres clearly and the antibody was injected into one blastomere at the 2-cell stage. Buffer-injected control embryos normally divided and each blastomere separated (Fig. 5C, arrowhead). In contrast, the antibody-injected blastomere exhibited abnormal cleavage (Fig. 5C, arrow): the furrow ingress occurred partially, did not deepen, and sometimes regressed.

Distribution of XSSH in cleaving zygotes and its localization at the cleavage furrow

Cleaving zygotes were fixed, sectioned, and stained with anti-XSSH and anti-XAC antibodies. As shown in Fig. 6A and B, both proteins were diffusely distributed in the cytoplasm in addition to the localization at the cortex. XSSH also accumulated deeper in the cleavage furrow and its immunofluorescence was found in the midbody structure (Fig. 6, C and D). These distributions of XSSH were very similar to those of XAC (Abe et al., 1996).

The localization of XSSH at the cleavage furrow was further observed with isolated cleavage furrows. In the early stage of furrowing, as has been shown by Noguchi and Mabuchi (2000), bleb-like structures, which were detected by binding of wheatgerm agglutinin (WGA-bleb), were formed on the surface of the furrow region (Fig. 6E), and the F-actin patch was present underneath these structures (Fig. 6F). Immunofluorescent microscopy revealed that XAC is colocalized with WGA-bleb (Fig. 6, G and H) and F-actin patches (Fig. 6, I and J). While, XAC did not colocalize with long F-actin bundles formed in the cleavage furrow (Fig. 6J, arrowheads). As shown in Fig. 6K and L, colocalization of XAC with XSSH was also observed. These results suggest that XSSH localizes in F-actin patches to dephosphorylate XAC.

Discussion

Here we cloned a *Xenopus* homologue of slingshot ADF/cofilin phosphatase and

characterized its biochemical properties for dephosphorylation of XAC by using *Xenopus* egg extracts and demonstrated its biological significance for the cleavage of *Xenopus* zygotes. *Xenopus* egg extracts are primarily powerful materials for analyses of cell cycle progression and mitosis. In addition, recent studies provide the advantages of their usage in studies on the cytoskeletal organization, since extracts contains almost all materials, such as proteins, RNAs, and membranous vesicles, essential for reproduction of intracellular events without any novel gene expression. Therefore we chose the extract system to examine the dephosphorylation pathway of XAC.

XAC dephosphorylation downstream of RhoA in Xenopus egg extracts

Spikes in dephosphorylation (activation) of XAC were observed twice during mitotic phase, once in prophase and again in telophase. Generally in cultured animal cells, actin cytoskeleton that has been organized in interphase dramatically disassembles and cells round at prophase (for review see Glotzer 2001). At telophase, when cytokinesis begins, actin cytoskeleton is also reorganized to form contractile ring at the cleavage furrow. Since ADF/cofilin essentially possesses severing and depolymerizing activities for actin filaments, this protein could act in the opposite situation, i.e., disassemble actin filaments at prophase but function as a reorganizer to enhance turnover of actin filaments at telophase. It is necessary to confirm whether disassembly of actin filaments really arises at prophase in *Xenopus* zygotes. Rho protein is a key regulator of cytokinesis, since C3 exoenzyme, a Rho specific ADP-ribosyl transferase, blocks the cytokinesis and GTP-bound RhoA is increased at telophase and concentrated in the cleavage furrow (Kishi et al., 1993; Mabuchi et al., 1993; Takahashi et al., 1995; Drechsel et al., 1997; Prokopenko et al., 1999; Kimura et al., 2000; Yoshizaki et al., 2003). Thus, we focused our study on XAC dephosphorylation at telophase.

Interestingly, constitutively active RhoA induced XAC dephosphorylation, and this dephosphorylation was suppressed by addition of Na_3VO_4 (a PTP and DSP inhibitor), but not okadaic acid (a PP1 and PP2A inhibitor) and cypermethrin (a PP2B inhibitor). ADF/cofilin phosphatases were previously characterized by addition of phosphatase-type specific inhibitors, and suggested to be PP1 and PP2A in T lymphocytes, PP1 and PP2B in cultured neurons, and PP2C and/or other type phosphatase in neutrophils (Meberg et al., 1998; Ambach et al., 2000; Zhan et al., 2003). However, since conventional phosphatase inhibitors except Na_3VO_4 did not inhibit dephosphorylation of XAC in the extract, we assumed our phosphatase to be a novel one and began to explore it. Recently, however, SSH was identified as a cofilin specific phosphatase in *Drosophila*, human and mouse (Niwa et al., 2002; Ohta et al., 2003). SSH has DSPc domain in the central portion, and this activity is inhibited by addition of Na_3VO_4

(Niwa et al., 2002). Together, we predicted that XSSH might be involved in RhoA induced XAC dephosphorylation in the extracts. Therefore, we cloned a *Xenopus* homologue of SSH and raised an inhibitory antibody specific for XSSH DSPc domain. Finally, since addition of this antibody suppressed the RhoA-induced XAC dephosphorylation in extracts, we concluded that XSSH dephosphorylates and activates XAC downstream of Rho signaling at telophase.

Regulation of XSSH activity

SSH phosphatases consists of N-terminal SSH homology domain A and B, DSPc domain and tail region. Primary structures of N-terminal half, A, B, and catalytic domains, were well conserved in vertebrates, whereas the tail regions were less homologous between *Xenopus* and mammals. Previous work demonstrated that the tail region more tightly binds to F-actin than the N-terminal half without the tail region does (Ohta et al., 2003). Interestingly, however, the A and B domains of XSSH possessed much higher affinity for F-actin with Kd value of 0.5 μM than the tail region. The full length XSSH with Kd of 0.4 μM suggests that the tail region also participates in binding to F-actin. Several isoforms of mammalian SSH have S domain in the tail region. However, XSSH does not possess this domain in its tail region. This might be the reason for lower affinity of the tail region of XSSH for F-actin.

The phosphatase activity of purified XSSH markedly increased in the presence of F-actin (Fig. 4G). This result corresponds well to the case of mammalian SSH (Ohta et al., 2003). Mammalian SSH exhibited the same activity for ADF/cofilin dephosphorylation with or without tail region in the absence of F-actin. However, the truncated SSH without tail is scarcely activated by F-actin and decreased the affinity for F-actin. Tail region of human SSH (hSSH-1L) is phosphorylated and possesses two 14-3-3 binding motifs (Nagata-Ohashi et al., 2004). We have confirmed that tail region of XSSH is also phosphorylated and a single 14-3-3 binding motif (unpublished results). Tail region is likely to be more functional to control the XSSH activity and/or its localization. Studies along these lines are in progress.

V14RhoA induced both XAC dephosphorylation and actin polymerization in the egg extracts. Latrunculin A, an actin monomer sequestering drug, suppressed XAC dephosphorylation induced by V14RhoA in egg extracts. On the other hand, addition of jasplakinolide, an actin-stabilizing drug, into the egg extracts caused F-actin accumulation and XAC dephosphorylation, and this effect was blocked in the presence of Na_3VO_4. These results suggest that XSSH is activated by its binding to actin filaments which are induced to polymerize by RhoA signaling and dephosphorylates XAC. More of interest is that addition of latrunculin A alone caused increase in

phosphorylated XAC compared with addition of vehicle alone. The basal level of phosphorylated XAC in extracts was scarcely affected in the presence of phosphatase inhibitors or anti-XSSH antibody alone (Fig. 2 and 3). Therefore, we speculate that depolymerization of actin has driven the unknown machinery which leads to phosphorylation of XAC. This latrunculin A-induced XAC phosphorylation was not suppressed by staurosporine, a broad kinase inhibitor. Whether or not Limk is involved in this phosphorylation remains to be addressed.

Possible function of XSSH during cytokinesis

Immunofluorescence microscopy revealed that XSSH localizes to the midbody and actin patches on the surface of the furrow with XAC and actin. Noguchi and Mabuchi (2000) have shown that actin patches are fused with each other and with myosin spots and then simultaneously reorganized to form the contractile ring actin bundles. XSSH may dephosphorylate and activate XAC in these patches to reorganize actin filaments. Genetic studies using model animals demonstrated that ADF/cofilin mutants form unusual actin aggregates in cells and blockage of regular actin filament bundles (Gunsalus et al., 1995; Ono et al., 1999). In addition, inactivation of ADF/cofilin by expression of active Limk also induced to form actin aggregates (Sumi et al., 1999). Thus, ADF/cofilin may be required for the regular actin assembly in cells. The present result that injection of inhibitory antibody prevented cleavage of blastomeres suggests functional significance of XSSH for dephosphorylation of XAC at actin patches.

On the other hand, roles of ADF/cofilin in membrane protrusion and lamellipodia formation were reported (Chan et al., 2000; Zebda et al., 2000; Kempiak et al., 2003; DesMarais et al., 2004; Mounelimne et al., 2004;). A recent study using caged cofilin directly showed that cofilin activation induces actin polymerization, cell protrusion and determine the direction of cell migration (Ghosh et al., 2004). These reports suggest that cofilin generates free barbed ends, which in turn are necessary for polymerization of actin *in vivo*. In *Xenopus* zygotes, it was reported that exogenous G-actin was incorporated into contractile ring (Noguchi and Mabuchi 2000). It is possible that XAC, reactivated through dephosphorylation by XSSH, severs actin filaments to generate free barbed ends, sites for novel actin polymerization.

Together with previous works by Kaji et al. (2003), the present study provided evidence that dephosphorylation and hence reactivation of ADF/cofilin is critical for cytokinesis. Most recently, a novel ADF/cofilin-specific phosphatase, designated as chronophin (CIN), has been reported (Gohla et al., 2005). This phosphatase regulates ADF/cofilin dephosphorylation during mitosis and is activated differently from SSH. In our present study, XAC dephosphorylation occurred twice at prophase and telophase,

and we suggested the later dephosphorylation is Rho-dependent. Consistently with our results, mammalian SSH activity is also elevated at telophase to cytokinesis (Kaji et al., 2003). The first dephosphorylation peak at prophase is possibly dependent on *Xenopus* CIN, because it has been shown that CIN dephosphorylates ADF/cofilin prior to SSH activation. *Xenopus* egg extracts may offer an excellent experiment system in which to further examine their regulation and role during cytokinesis.

Acknowledgments

We thank Dr. Ono (Emory University) for critical reading of the manuscript, Dr. Bamburg (Colorado State University) for providing plasmids and anti-phospho-ADF/cofilin antibody, and for helpful advice, and Dr. Iida (Tokyo Metropolitan Institute of Medical Science) for providing anti-actin antibody.

This work was supported by research grants from the Ministry of Education, Culture, Sports, Science and Technology of Japan.

References

Abe, H., Obinata, T., Minamide, L. S., and Bamburg, J. R. (1996). *Xenopus laevis* actin-depolymerizing factor/cofilin: a phosphorylation-regulated protein essential for development. *J. Cell Biol.* 132, 871-885.

Agnew, B. J., Minamide, L. S., and Bamburg, J. R. (1995). Reactivation of phosphorylated actin depolymerizing factor and identification of the regulatory site. *J. Biol. Chem.* 270, 17582-17587.

Amano, T., Tanabe, K., Eto, T., Narumiya, S., and Mizuno, K. (2001). LIM-kinase 2 induces formation of stress fibers, focal adhesions and membrane blebs, dependent on its activation by Rho-associated kinase-catalysed phosphorylation at threonine-505. *Biochem. J.* 354, 149-159.

Amano, T., Kaji, N., Ohashi, K., and Mizuno, K. (2002). Mitosis-specific activation of LIM motif-containing protein kinase and roles of cofilin phosphorylation and dephosphorylation in mitosis. *J. Biol. Chem.* 277, 22093-22102

Ambach, A., Saunus, J., Konstandin, M., Wesselborg, S., Meuer, S. C., and Samstag, Y. (2000). The serine phosphatases PP1 and PP2A associate with and activate the actin-binding protein cofilin in human T lymphocytes. *Eur. J. Immunol.* 30, 3422-3431.

Arber, S., Barbayannis, F. A., Hanser, H., Schneider, C., Stanyon, C. A., Bernard, O., and Caroni, P. (1998). Regulation of actin dynamics through phosphorylation of cofilin by LIM-kinase. *Nature* 393, 805-809.

Bamburg, J. R. (1999). Proteins of the ADF/cofilin family: essential regulators of actin dynamics. *Annu. Rev. Cell. Dev. Biol.* 15, 185-230.

Bamburg J. R., McGough, A., and Ono, S. (1999). Putting a new twist on actin: ADF/cofilins modulate actin dynamics. *Trends Cell Biol.* 9, 364-370.

Carlier, M. F., Laurent, V., Santolini, J., Melki, R., Didry, D., Xia, G. X., Hong, Y., Chua, N. H., and Pantaloni, D. (1997). Actin depolymerizing factor (ADF/cofilin) enhances the rate of filament turnover: implication in actin-based motility. *J. Cell Biol.*

136, 1307-1322.

Carlier, M. F., Ressad, F., and Pantaloni, D. (1999). Control of actin dynamics in cell motility. Role of ADF/cofilin. *J. Biol. Chem.* 274, 33827-33830.

Chan, A. Y., Bailly, M., Zebda, N., Segall, J. E., and Condeelis, J. S. (2000). Role of cofilin in epidermal growth factor-stimulated actin polymerization and lamellipod protrusion. *J. Cell Biol.* 148, 531-542.

Cheng, A. K. and Robertson, E. J. (1995). The murine LIM-kinase gene (limk) encodes a novel serine threonine kinase expressed predominantly in trophoblast giant cells and the developing nervous system. *Mech. Dev.* 52, 187-197.

DesMarais, V., Macaluso, F., Condeelis, J., and Bailly, M. (2004). Synergistic interaction between the Arp2/3 complex and cofilin drives stimulated lamellipod extension. *J. Cell Sci.* 117, 3499-3510.

Drechsel, D. N., Hyman, A. A., Hall, A., and Glotzer, M. (1997). A requirement for Rho and Cdc42 during cytokinesis in *Xenopus* embryos. *Curr. Biol.* 7, 12-23.

Edwards, D. C., Sanders, L. C., Bokoch, G. M., and Gill, G. N. (1999). Activation of LIM-kinase by Pak1 couples Rac/Cdc42 GTPase signalling to actin cytoskeletal dynamics. *Nat. Cell Biol.* 1, 253-259.

Ghosh, M., Song, X., Mouneimne, G., Sidani, M., Lawrence, D. S., and Condeelis, J. S. (2004). Cofilin promotes actin polymerization and defines the direction of cell motility. *Science* 304, 743-746.

Glotzer, M., Murray, A. W., and Kirschner, M. W. (1991). Cyclin is degraded by the ubiquitin pathway. *Nature* 349, 132-138.

Glotzer, M. (2001). Animal cell cytokinesis. *Annu. Rev. Cell Dev. Biol.* 17, 351-86.

Gohla, A., Birkenfeld, J., and Bokoch, G. M. (2005). Chronophin, a novel HAD-type serine protein phosphatase, regulates cofilin-dependent actin dynamics. *Nat. Cell Biol.* 7, 21-29.

Gunsalus, K. C., Bonaccorsi, S., Williams, E., Verni, F., Gatti, M., and Goldberg, M. L. (1995). Mutations in twinstar, a Drosophila gene encoding a cofilin/ADF homologue, result in defects in centrosome migration and cytokinesis. *J. Cell Biol.* 131, 1243-1259.

Kaji, N., Ohashi, K., Shuin, M., Niwa, R., Uemura, T., and Mizuno, K. (2003) Cell cycle-associated changes in Slingshot phosphatase activity and roles in cytokinesis in animal cells. *J. Biol. Chem.* 278, 33450-33455.

Kempiak, S. J., Yip, S. C., Backer, J. M., and Segall, J. E. (2003). Local signaling by the EGF receptor. *J. Cell Biol.* 162, 781-787.

Kimura, K., Tsuji, T., Takada, Y., Miki, T., and Narumiya, S. (2000). Accumulation of GTP-bound RhoA during cytokinesis and a critical role of ECT2 in this accumulation. *J. Biol. Chem.* 275, 17233-17236.

Kishi, K., Sasaki, T., Kuroda, S., Itoh, T., and Takai, Y. (1993). Regulation of cytoplasmic division of Xenopus embryo by rho p21 and its inhibitory GDP/GTP exchange protein (rho GDI). *J. Cell Biol.* 120, 1187-1195.

Koshimizu, U., Takahashi, H., and Nakamura, T. (1997) cDNA cloning, genomic organization, and chromosomal localization of the mouse LIM-motif-containing kinase gene, Limk2. *Biochem. Biophys. Res. Commun.* 241, 243-250.

Laemmli, U. K. (1970). Cleavage of structural proteins during the assembly of the head of bacteriophage T4. *Nature* 227, 680-685.

Mabuchi, I. (1983) An actin-depolymerizing protein (Depactin) from starfish oocytes: properties and interaction with actin. *J. Cell Biol.* 97, 1612-1621.

Mabuchi, I., Hamaguchi, Y., Fujimoto, H., Morii, N., Mishima, M., and Narumiya, S. (1993) A rho-like protein is involved in the organisation of the contractile ring in dividing sand dollar eggs. *Zygote* 1, 325-331.

McGough, A., Pope, B., Chiu, W., and Weeds, A. (1997). Cofilin changes the twist of F-actin: implications for actin filament dynamics and cellular function. *J. Cell Biol.* 138,

771-781.

Maciver, S. K., and Hussey. P. J. (2002) The ADF/cofilin family: actin-remodeling proteins. *Genome Biol.* 3, 3007.3001-3007.3012

Maekawa, M., Ishizaki, T., Boku, S., Watanabe, N., Fujita, A., Iwamatsu, A., Obinata, T., Ohashi, K., Mizuno, K., and Narumiya, S. (1999). Signaling from Rho to the actin cytoskeleton through protein kinases ROCK and LIM-kinase. *Science* 285, 895-898.

Meberg, P. J., Ono, S., Minamide, L. S., Takahashi, M., and Bamburg, J. R. (1998). Actin depolymerizing factor and cofilin phosphorylation dynamics: response to signals that regulate neurite extension. *Cell Motil. Cytoskeleton* 39, 172-190.

Moon, A. L. and Drubin, D. G. (1995). The ADF/cofilin proteins. Stimulus-responsive modulators of actin dynamics. *Mol. Biol. Cell.* 6, 1423-1431.

Moriyama, K., Iida, K., and Yahara, I. (1996). Phosphorylation of Ser-3 of cofilin regulates its essential function on actin. *Genes Cells* 1, 73-86.

Mouneimne, G., Soon, L., DesMarais, V., Sidani, M., Song, X., Yip, S. C., Ghosh, M., Eddy, R., Backer, J. M., and Condeelis, J. (2004). Phospholipase C and cofilin are required for carcinoma cell directionality in response to EGF stimulation. *J. Cell Biol.* 166, 697-708.

Murray, A. W. (1991). Cell cycle extracts. Methods Cell Biol. 36, 581-605.

Nagaoka, R., Abe, H., Kusano, K., and Obinata, T. (1995). Concentration of cofilin, a small actin-binding protein, at the cleavage furrow during cytokinesis. *Cell Motil. Cytoskeleton* 30, 1-7.

Nagata-Ohashi, K., Ohta, Y., Goto, K., Chiba, S., Mori, R., Nishita, M., Ohashi, K., Kousaka, K., Iwamatsu, A., Niwa, R., Uemura, T., and Mizuno K. (2004). A pathway of neuregulin-induced activation of cofilin-phosphatase Slingshot and cofilin in lamellipodia. *J. Cell Biol.* 165, 465-471.

Nakano, K., Satoh, K., Morimatsu, A., Ohnuma, M. and Mabuchi, I. (2001).

Interactions among a fimbrin, a capping protein, and an actin-depolymerizing factor in organization of the fission yeast actin cytoskeleton. *Mol. Biol. Cell* 12, 3515-3526.

Nakano, K., Kanai-Azuma, M., Kanai, Y., Moriyama, K., Yazaki, K., Hayashi, Y., and Kitamura, N. (2003). Cofilin phosphorylation and actin polymerization by NRK/NESK, a member of the germinal center kinase family. *Exp. Cell Res.* 287, 219-227.

Nishida, E., Maekawa, S., and Sakai, H. (1984). Cofilin, a protein in porcine brain that binds to actin filaments and inhibits their interactions with myosin and tropomyosin. *Biochemistry* 23, 5307-5313.

Nishita, M., Wang, Y., Tomizawa, C., Suzuki, A., Niwa, R., Uemura, T., and Mizuno, K. (2004). Phosphoinositide 3-kinase-mediated activation of cofilin phosphatase Slingshot and its role for insulin-induced membrane protrusion. *J. Biol. Chem.* 279, 7193-7198.

Niwa, R., Nagata-Ohashi, K., Takeichi, M., Mizuno, K., and Uemura, T. (2002). Control of actin reorganization by Slingshot, a family of phosphatases that dephosphorylate ADF/cofilin. *Cell* 108, 233-246.

Noguchi, T. and Mabuchi, I. (2001). Reorganization of actin cytoskeleton at the growing end of the cleavage furrow of *Xenopus* egg during cytokinesis. *J. Cell Sci.* 114, 401-412.

Nunoue, K., Ohashi, K., Okano, I., and Mizuno, K. (1995) LIMK-1 and LIMK-2, two members of a LIM motif-containing protein kinase family. *Oncogene* 11, 701-710.

O'Farrell, P. Z., Goodman, H. M., and O'Farrell, P. H. (1977). High resolution two-dimensional electrophoresis of basic as well as acidic proteins. *Cell* 12, 1133-1141.

Ohashi, K., Nagata, K., Maekawa, M., Ishizaki, T., Narumiya, S., and Mizuno, K. (2000). Rho-associated kinase ROCK activates LIM-kinase 1 by phosphorylation at threonine 508 within the activation loop. *J. Biol. Chem.* 275, 3577-3582.

Ohta, Y., Kousaka, K., Nagata-Ohashi, K., Ohashi, K., Muramoto, A., Shima, Y., Niwa, R., Uemura, T., Mizuno, K., and Takeichi, M. (2003). Differential activities, subcellular

distribution and tissue expression patterns of three members of Slingshot family phosphatases that dephosphorylate cofilin. *Genes Cells* 8, 811-824.

Okada, K., Obinata, T., and Abe, H. (1999). XAIP1: a *Xenopus* homologue of yeast actin interacting protein 1 (AIP1), which induces disassembly of actin filaments cooperatively with ADF/cofilin family proteins. *J. Cell Sci.* 112, 1553-1565.

Okano, I., Hiraoka, J., Otera, H., Nunoue, K., Ohashi, K., Iwashita, S., Hirai, M., and Mizuno, K. (1995). Identification and characterization of a novel family of serine/threonine kinases containing two N-terminal LIM motifs. *J. Biol. Chem.* 270, 31321-31330.

Pantaloni, D., Le Clainche, C., and Carlier, M. F. (2001). Mechanism of actin-based motility. *Science* 292, 1502-1506.

Pelham, R. J. and Chang F. (2002). Actin dynamics in the contractile ring during cytokinesis in fission yeast. *Nature* 419, 82-86.

Pollard, T. D. and Borisy, G. G. (2003). Cellular motility driven by assembly and disassembly of actin filaments. *Cell* 112, 453-465.

Prokopenko, S. N., Brumby, A., O'Keefe, L., Prior, L., He, Y., Saint, R., and Bellen, H. J. (1999). A putative exchange factor for Rho1 GTPase is required for initiation of cytokinesis in Drosophila. *Genes Dev.* 13, 2301-2314.

Self, A. J. and Hall, A. (1995). Purification of recombinant Rho/Rac/G25K from *Escherichia coli*. *Methods Enzymol.* 256, 3-10.

Spudich, J. A. and Watt, S. (1971) The regulation of rabbit skeletal muscle contraction. I. Biochemical studies of the interaction of the tropomyosin-troponin complex with actin and the proteolytic fragments of myosin. *J. Biol. Chem.* 246, 4866-4871.

Sumi, T., Matsumoto, K., Takai, Y., and Nakamura, T. (1999). Cofilin phosphorylation and actin cytoskeletal dynamics regulated by rho- and Cdc42-activated LIM-kinase 2. *J. Cell Biol.* 147, 1519-1532.

Sumi, T., Matsumoto, K., and Nakamura, T. (2001a). Specific activation of LIM kinase 2 via phosphorylation of threonine 505 by ROCK, a Rho-dependent protein kinase. *J. Biol. Chem.* 276, 670-676.

Sumi, T., Matsumoto, K., Shibuya, A., and Nakamura, T. (2001b). Activation of LIM kinases by myotonic dystrophy kinase-related Cdc42-binding kinase alpha. *J. Biol. Chem.* 276, 23092-23096.

Takahashi, T., Aoki, S., Nakamura, T., Koshimizu, U., Matsumoto, K., and Nakamura, T. (1997). *Xenopus* LIM motif-containing protein kinase, Xlimk1, is expressed in the developing head structure of the embryo. *Dev. Dyn.* 209, 196-205.

Takahashi, T., Koshimizu, U., Abe, H., Obinata, T., and Nakamura, T. (2001). Functional involvement of *Xenopus* LIM kinases in progression of oocyte maturation. *Dev. Biol.* 229, 554-567.

Takaishi, K., Sasaki, T., Kameyama, T., Tsukita, S., and Takai, Y. (1995). Translocation of activated Rho from the cytoplasm to membrane ruffling area, cell-cell adhesion sites and cleavage furrows. *Oncogene* 11, 39-48.

Toshima, J., Toshima, J. Y., Amano, T., Yang, N., Narumiya, S., and Mizuno, K. (2001a) Cofilin phosphorylation by protein kinase testicular protein kinase 1 and its role in integrin-mediated actin reorganization and focal adhesion formation. *Mol. Biol. Cell* 12, 1131-1145.

Toshima, J., Toshima, J. Y., Takeuchi, K., Mori, R., and Mizuno, K. (2001b). Cofilin phosphorylation and actin reorganization activities of testicular protein kinase 2 and its predominant expression in testicular Sertoli cells. *J. Biol. Chem.* 276, 31449-31458.

Towbin, H., Staehelin, T., and Gordon, J. (1979). Electrophoretic transfer of proteins from polyacrylamide gels to nitrocellulose sheets: procedure and some applications. *Proc. Natl. Acad. Sci. USA* 76, 4350-4354.

Yang, N., Higuchi, O., Ohashi, K., Nagata, K., Wada, A., Kangawa, K., Nishida, E., and Mizuno, K. (1998). Cofilin phosphorylation by LIM-kinase 1 and its role in Rac-mediated actin reorganization. *Nature* 393, 809-12.

Yoshizaki, H., Ohba, Y., Kurokawa, K., Itoh, R. E., Nakamura, T., Mochizuki, N., Nagashima, K., and Matsuda, M. (2003). Activity of Rho-family GTPases during cell division as visualized with FRET-based probes. *J. Cell Biol.* 162, 223-232.

Zebda, N., Bernard, O., Bailly, M., Welti, S., Lawrence, D. S., and Condeelis, J. S. (2000). Phosphorylation of ADF/cofilin abolishes EGF-induced actin nucleation at the leading edge and subsequent lamellipod extension. *J. Cell Biol.* 151, 1119-1128.

Zhan, Q., Bamburg, J. R., and Badwey, J. A. (2003). Products of phosphoinositide specific phospholipase C can trigger dephosphorylation of cofilin in chemoattractant stimulated neutrophils. *Cell Motil. Cytoskeleton* 54, 1-15.

Figure legends

Figure 1. Dephosphorylation of XAC at prophase and telophase in cycling extracts (A) and induction of dephosphorylation of XAC by V14RhoA in CSF extracts (B and C). (A) Time course of changes in the amount of phosphorylated XAC is shown after incubation of cycling extracts at 23 °C. Samples were collected every 5 minutes. pXAC and XAC were separated and detected by a combination of 2D-PAGE and immunoblotting using anti-XAC antibody. Times from 30 to 60 min and from 85 to 130 min were in mitotic phase (M phase), and time points entered in prophase and telophase are shown, respectively. The results were obtained from at least three independent experiments. (B) CSF extracts were incubated in the presence of buffer alone or 4.2 μM V14RhoA for 1 hr at 22 °C, and XAC spots were detected by 2D-immunobloting. Right spots and left spots indicate phosphorylated XAC (pXAC) and dephosphorylated XAC (XAC), respectively. Control, addition of buffer alone; V14RhoA, addition of 4.2 μM V14RhoA. (C) Changes in the percentage of phosphorylated XAC were quantified after addition of buffer alone (-) or V14RhoA (+). The results were obtained from three independent experiments. Error bars represent S.E.M.

Figure 2. RhoA-induced XAC dephosphorylation was suppressed by addition of Na_3VO_4, but not okadaic acid (OA) and cypermethrin. (A) Effects of various concentration of okadaic acid (shown under the bottom panel) on RhoA-induced XAC dephosphorylation (+ indicates V14RhoA addition). *Top panel*, immunoblots using anti-phospho-cofilin antibody; *bottom panel*, immunoblots on the same membrane using anti-XAC antibody. The amount of pXAC is quantified and shown in the graph with the ratio of addition of buffer alone (OA 0 nM) without V14RhoA (-) taken as 1.0. (B) Effects of 1.0 nM cypermethrin on XAC dephosphorylation in the presence (+) or absence (-) of V14RhoA are shown as percentage of pXAC with the means ± S.E.M. of three independent experiments. (C and D) Effects of 1.0 mM Na_3VO_4 on XAC dephosphorylation in the presence (+) or absence (-) of V14RhoA were examined by 2D-immunoblotting (C) and shown as percentage of pXAC with the means ± S.E.M. of three independent experiments (D).

Figure 3. XSSH is involved in the XAC dephosphorylation induced by V14RhoA. (A) Specificity of the anti-XSSH antibody. Bacterially expressed XSSH (His-ΔN-XSSH, lanes 1 and 1'), CSF-extracts (lanes 2 and 2'), reticulocyte lysates expressing XSSH (lanes 3 and 3'), and reticulocyte lysates alone (lanes 4 and 4') were electrophoresed on

SDS-polyacrylamide gels. Proteins were transferred to nitrocellulose membrane. Coomassie Blue-stained gels (lanes 1-4) and immunoblots with anti-XSSH antibody (lanes 1'-4') are shown. (B) Typical patterns of immunoblot analysis of the RhoA-induced XAC dephosphorylation in the presence of affinity-purified anti-XSSH antibody. Addition of buffer alone (control), 4.2 μM V14RhoA, 200 ng of anti-XSSH antibody alone, or both anti-XSSH antibody and V14RhoA into CSF extracts were subjected to 2D-PAGE and immunoblotting using anti-XAC antibody. Arrows indicate phosphorylated XAC spots. (C) Quantification of the amounts of phosphorylated XAC in CSF extracts treated with (+) or without (-) V14RhoA in the presence (anti-XSSH) or absence of affinity-purified anti-XSSH antibody. All experimental conditions and procedures were the same as in B. (D) Polymerization of actin filaments in CSF extracts. CSF extracts were incubated with buffer alone (control), 4.2 μM V14RhoA (V14RhoA), 50 μM latrunculin A (LatA), both 50 μM latrunculin A and 4.2 μM V14RhoA (Lat A+V14RhoA), or 30 μM jasplakinolide (Jas), and then were ultracentrifuged. The supernatant (sup) and pellet (ppt) were subjected to SDS-PAGE and immnoblotting using anti-actin antibody. (E) Suppression of V14RhoA-induced XAC dephosphorylation by the presence of latrunculin A. Amounts of phosphorylated XAC in CSF extracts were quantified in the presence (+) or absence (-) of V14RhoA, latrunculin A (Lat A), or GST-XSSH. Concentrations of V14RhoA and latrunculin A added to the extract are the same as in D, and the concentration of GST-XSSH is 2 μM. (F) Effects of addition of jasplakinolide into CSF extracts on XAC dephosphorylation in the presence (+) or absence (-) of Na_3VO_4. Amounts of phosphorylated XAC were quantified in the presence (Jas, +) or absence (-) of 30 μM jasplakinolide. All error bars represent S.E.M.

Figure 4 Recombinant XSSH binds to F-actin and dephosphorylates pXAC. (A) Schematic representation of XSSH recombinant protein constructs. All constructs were GST-tagged at the N-terminus. XSSH possesses SSH homology domains A and B, catalytic domain (DSPc) and tail region. Numbers on the bars show amino acid residues flanking each domain in addition to N- and C-terminal residues. (B) Coomassie Blue staining of purified XSSH recombinant proteins. Numbers at left denote positions of molecular mass markers. (C) Co-sedimentation assay of the respective XSSH recombinant proteins with F-actin. 3.0 μM F-actin and various concentrations of recombinant proteins (as indicated at the top of the each panel) were mixed and incubated at 4°C for 3 hours and then ultracentrifuged. The supernatant (s) and pellet (p) were subjected to SDS-PAGE. *Top panel,* GST-XSSH; *middle panel,* GST-AB; *bottom*

panel, GST-Tail. Recombinant proteins and actin are indicated by arrowheads and arrows, respectively. (D) Direct plots of bound versus free for binding of different concentrations of the three recombinant proteins to fixed concentration of F-actin under the same condition as in C. *Top panel,* GST-XSSH (open squares); *middle panel,* GST-AB (closed triangles); *bottom panel,* GST-Tail (closed circles). (E) The affinity of GST-XSSH and GST-AB for actin filaments was analyzed by Scatchard plots, respectively. (F) The phosphorylated XAC (pXAC) fraction prepared from *Xenopus* oocytes was subjected to SDS-PAGE (upper panel). pXAC is shown by an asterisk. This fraction was subjected to 2D-immunoblot (lower panel). Since more than 85% of XAC is phosphorylated in this fraction (arrow), dephosphorylated XAC is scarcely detected (arrowhead). (G) Increase in XSSH activity in the presence of F-actin. Phosphatase assays were carried out using pXAC fraction and purified GST-XSSH in the presence (+) or absence (-) of F-actin or latrunculin A. Addition of buffer alone (buffer) or GST alone (GST) into pXAC fraction was also performed as control experiments. The results were obtained from at least three independent experiments. Error bars represent S.E.M.

Figure 5. The significance of XSSH activity for complete cytokinesis. Control IgG (A) or affinity purified anti-XSSH antibody (B; 140 ng) was injected into one blastomere of *Xenopus* embryo at the 2-cell stage. Four representative examples are shown with allowheads or allows pointing to the injected blastomere. (C) Time course of the cleavage after injection. *Xenopus* eggs were fertilized, dejellied, and then vitelline membranes were removed manually with watchmaker's forceps. After the first cleavage, 20 nl of affinity purified anti-XSSH antibody (allows) or same volume of buffer (allowheads) was injected into one blastomere. Times after injection are shown at the upper right.

Figure 6. Distribution and localization of XSSH in *Xenopus* zygotes and isolated cleavage furrows. Paraffin sections of the first cleaving embryos were immunostained dually with anti-XSSH antibody (A and C) and anti-XAC monoclonal antibody (B and D), respectively. The midbody region was amplified in C and D. Bar, 100 μm. (E-L) Isolated cleavage furrows were dually stained with Alexa-488-WGA (E and G) and anti-actin antibody (F) or anti-XAC antibody (H), anti-XAC antibody (I) and anti-actin antibody (J), or anti-XAC antibody (K) and anti-XSSH antibody (L). The inserts show the enlarged image of actin patches surrounded by white squares in each panels. Arrowheads in J show long F-actin bundles, and large arrowheads in K and L represent colocalization of XAC and XSSH. Bar, 20 μm.

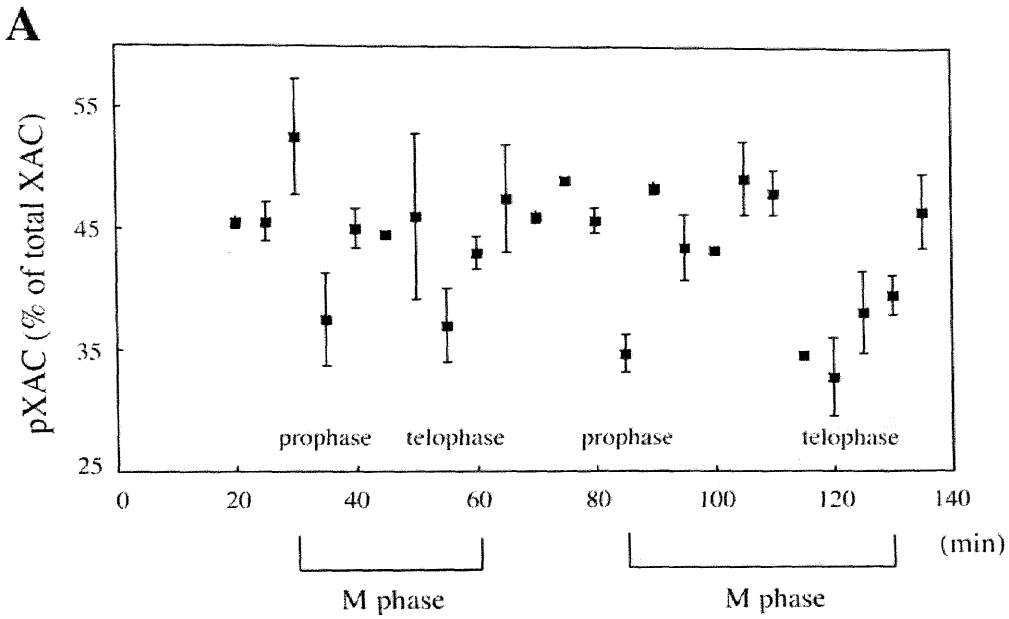
A
pXAC (% of total XAC)
55
45
35
25
prophase
telophase
prophase
telophase
0
20
40
60
80
100
120
140
(min)
M phase
M phase

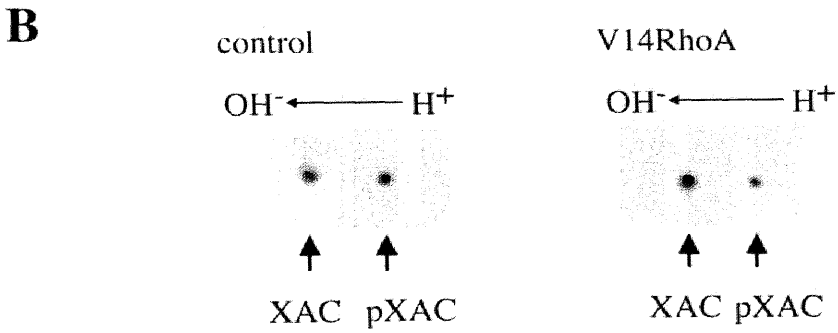
B
control
V14RhoA
OH⁻
H⁺
OH⁻
H⁺
XAC
pXAC
XAC
pXAC

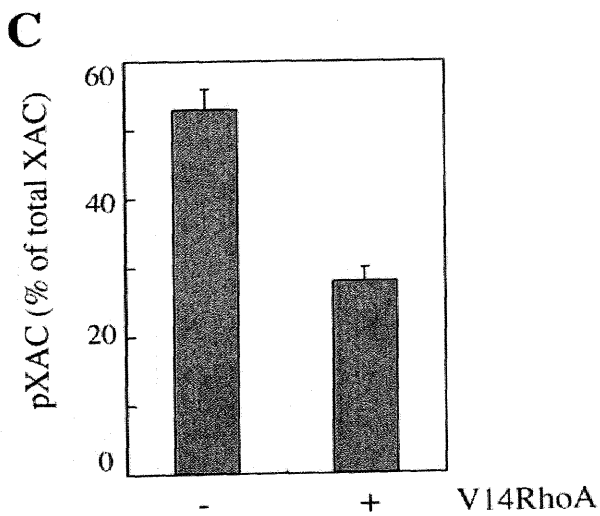
C
pXAC (% of total XAC)
60
40
20
0
-
+
V14RhoA

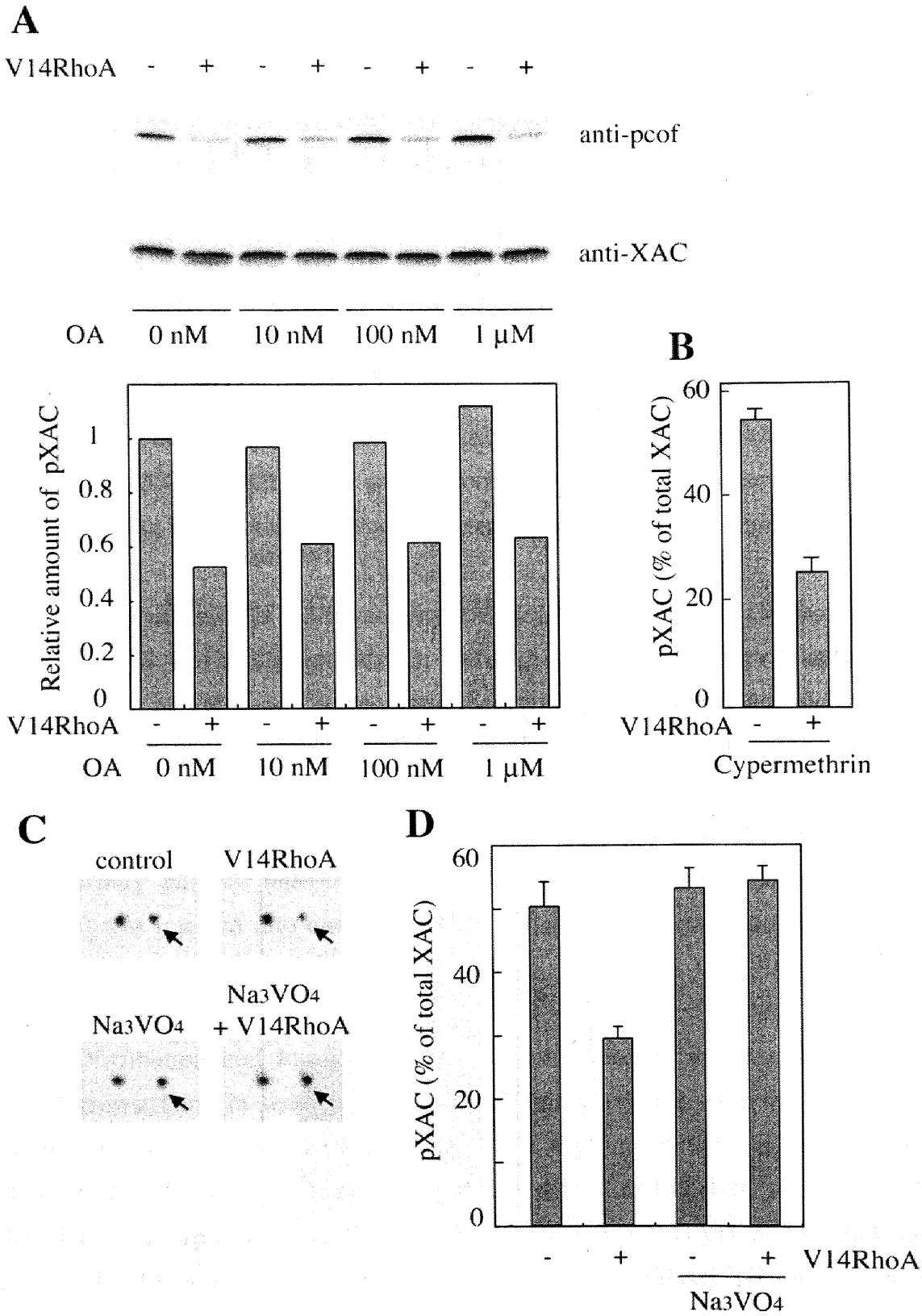
A
V14RhoA - + - + - + - +
anti-pcof
anti-XAC
OA 0 nM 10 nM 100 nM 1 μM
Relative amount of pXAC
1
0.8
0.6
0.4
0.2
0
V14RhoA - + - + - + - +
OA 0 nM 10 nM 100 nM 1 μM
B
pXAC (% of total XAC)
60
40
20
0
V14RhoA - +
Cypermethrin
C
control
V14RhoA
Na3VO4
Na3VO4 + V14RhoA
D
pXAC (% of total XAC)
60
40
20
0
- + - + V14RhoA
Na3VO4

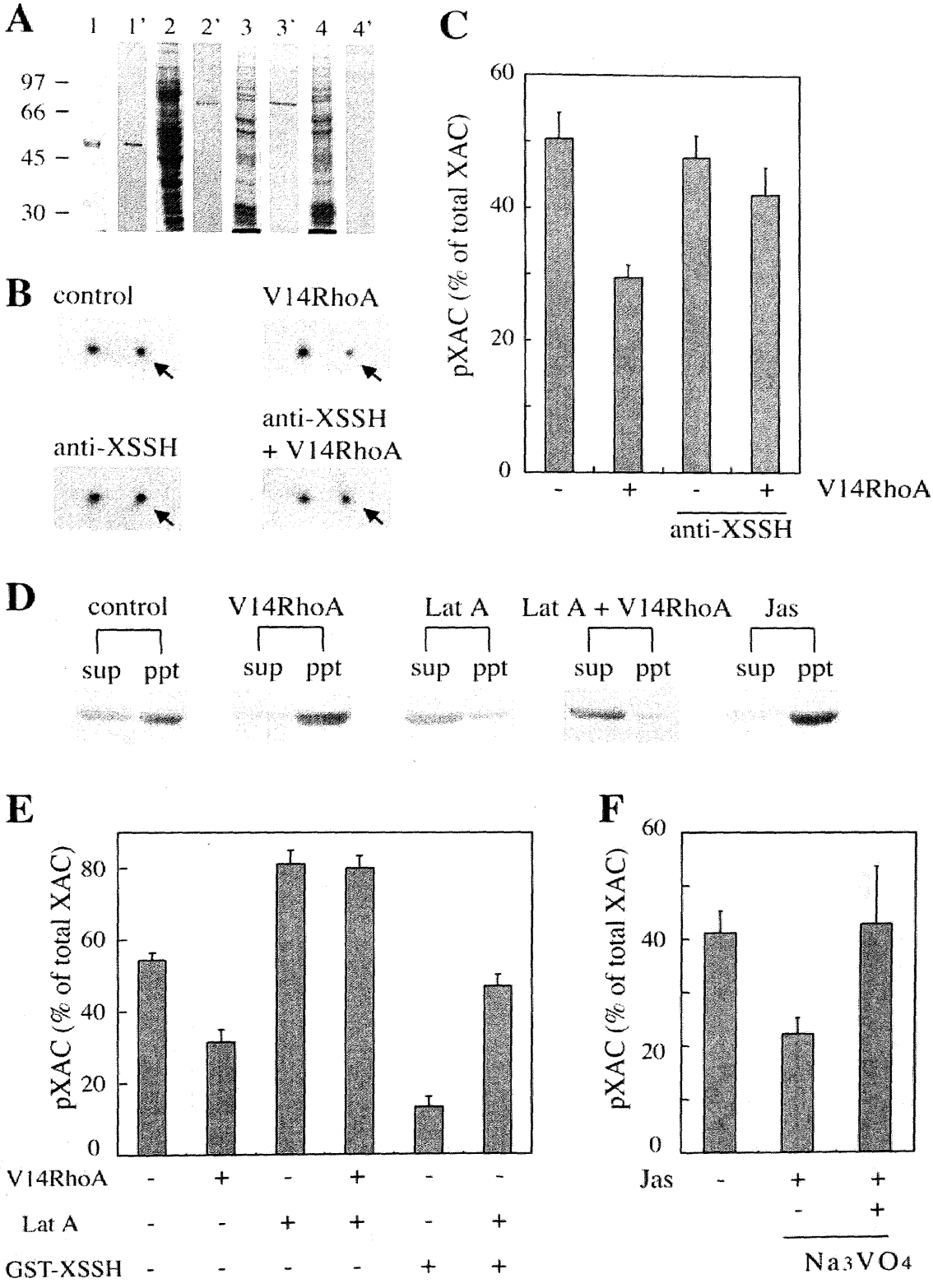
A
1 1' 2 2' 3 3' 4 4'
97 –
66 –
45 –
30 –
B
control
V14RhoA
anti-XSSH
anti-XSSH
+ V14RhoA
C
pXAC (% of total XAC)
60
40
20
0
- + - +
V14RhoA
anti-XSSH
D
control
V14RhoA
Lat A
Lat A + V14RhoA
Jas
sup ppt sup ppt sup ppt sup ppt sup ppt
E
pXAC (% of total XAC)
80
60
40
20
0
V14RhoA - + - + - -
Lat A - - + + - +
GST-XSSH - - - - + +
F
pXAC (% of total XAC)
60
40
20
0
Jas - + +
- +
Na3VO4

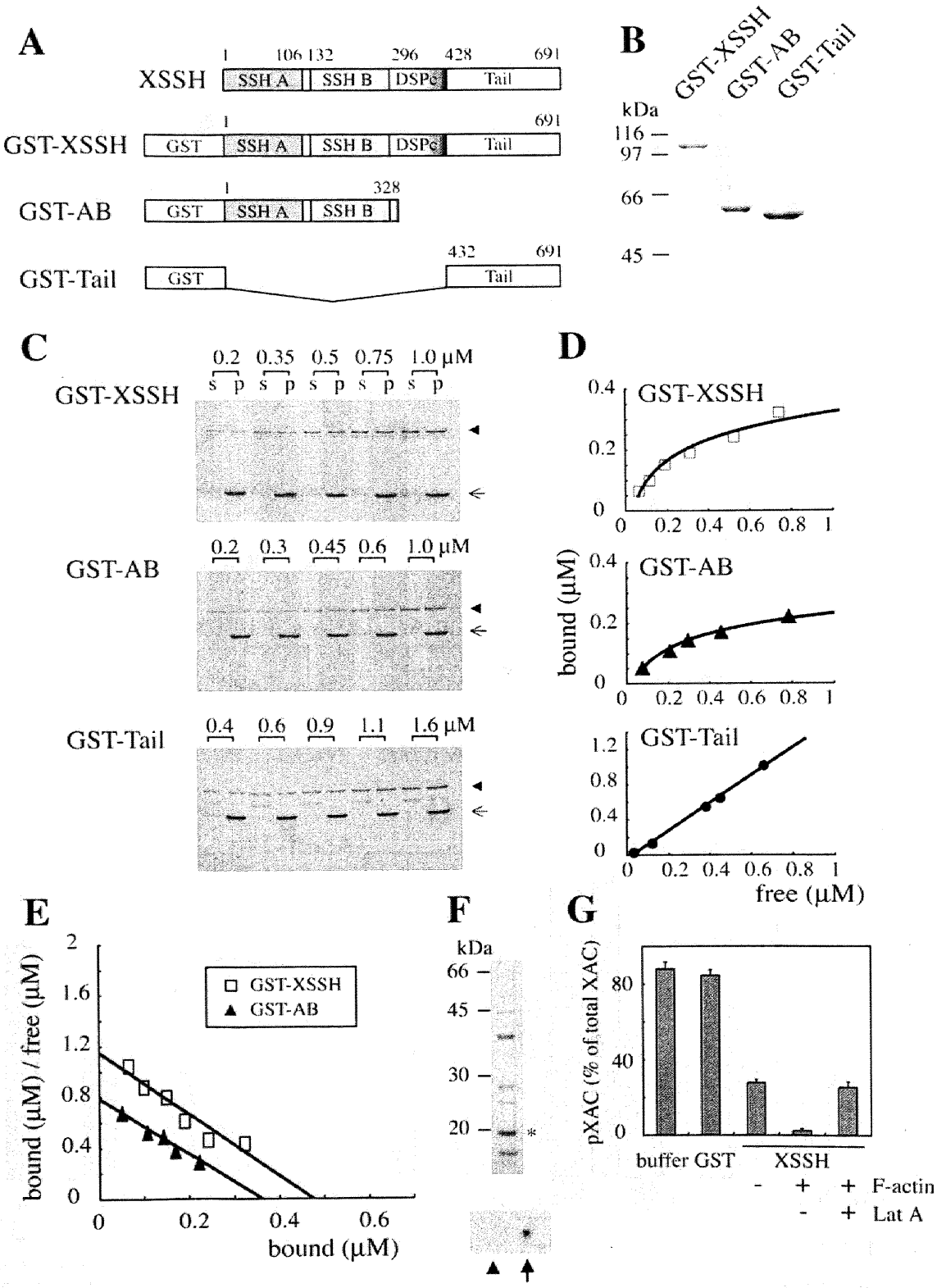
A
XSSH
SSH A
SSH B
DSPc
Tail
GST-XSSH
GST
GST-AB
GST-Tail
B
GST-XSSH
GST-AB
GST-Tail
kDa
116
97
66
45
C
GST-XSSH
GST-AB
GST-Tail
s p
D
GST-XSSH
GST-AB
GST-Tail
bound (μM)
free (μM)
E
GST-XSSH
GST-AB
bound (μM) / free (μM)
bound (μM)
F
kDa
66
45
30
20
G
pXAC (% of total XAC)
buffer
GST
XSSH
F-actin
Lat A

A control IgG

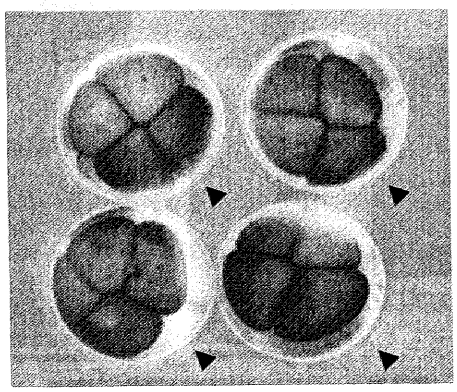

B anti-XSSH antibody

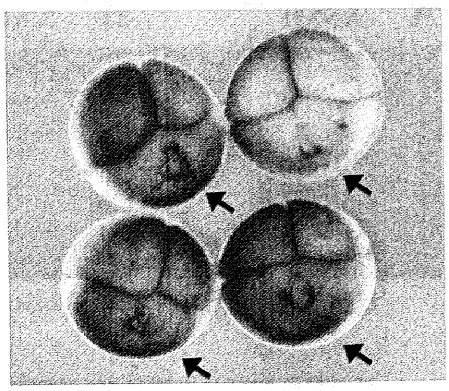

C

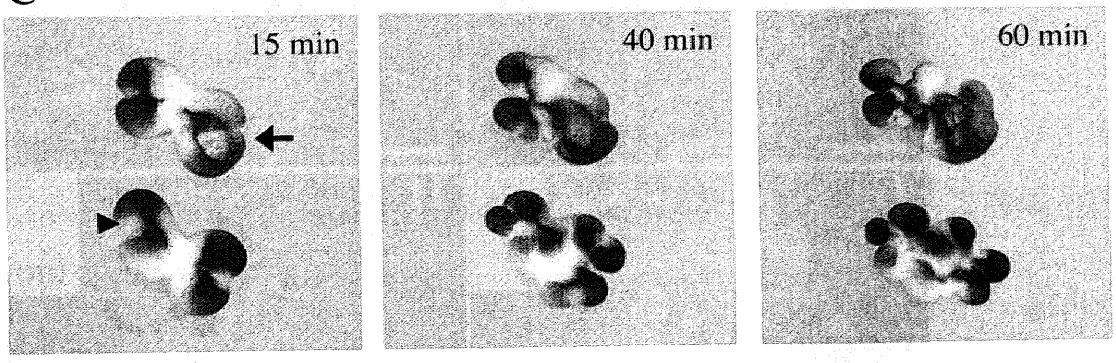

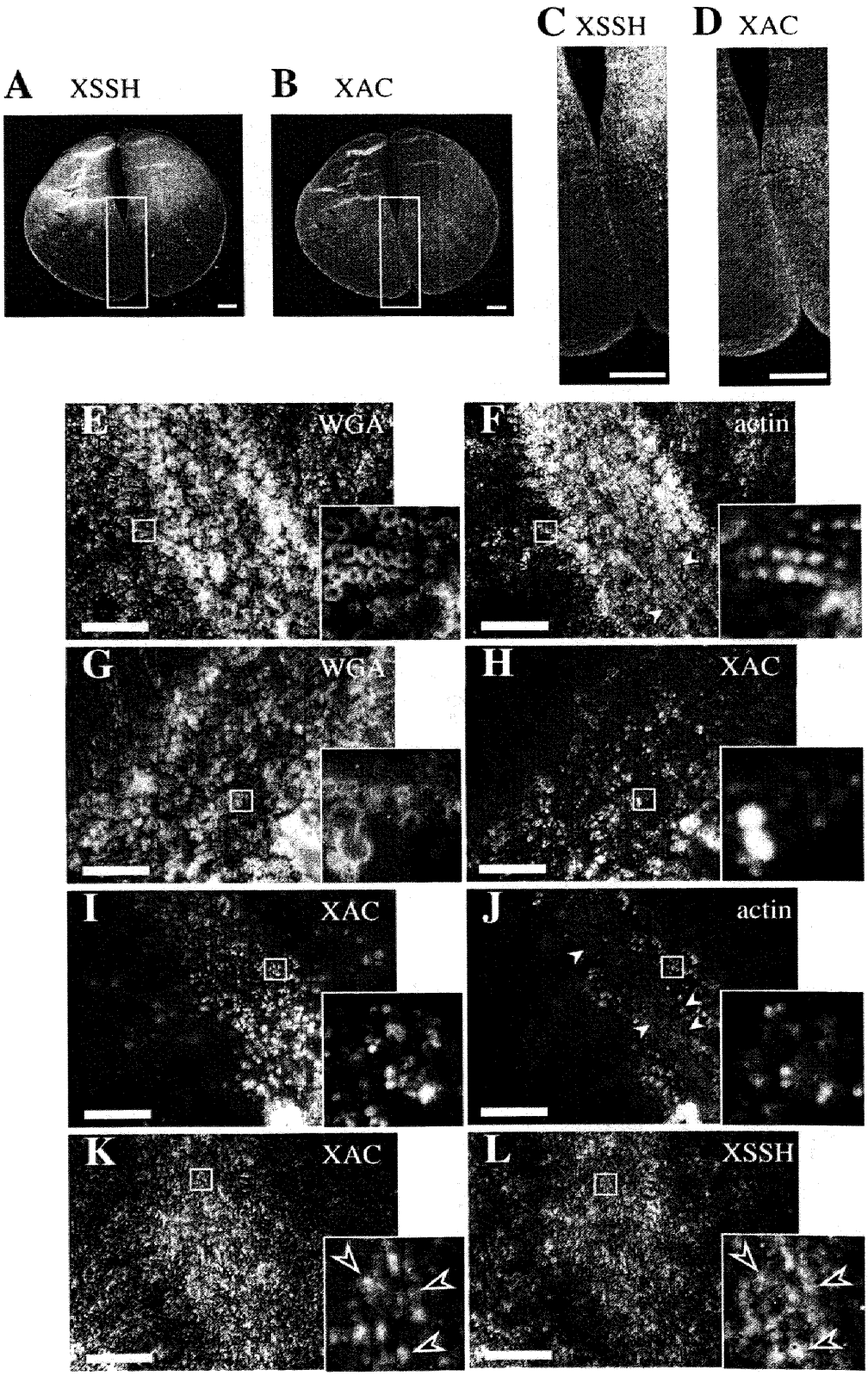
A XSSH
B XAC
C XSSH
D XAC
E WGA
F actin
G WGA
H XAC
I XAC
J actin
K XAC
L XSSH

（既公表論文２）

Functional involvement of *Xenopus* homologue of ADF/cofilin phosphatase, Slingshot (XSSH), in the gastrulation movement

Kenji Tanaka, Reina Nishio, Kaku Haneda and Hiroshi Abe*

Department of Biology, Chiba University, Yayoi-cho, Inage-ku, Chiba 263-8522, Japan.

Running title: Slingshot function in Xenopus gastrulation

Section: Cell biology

*To whom correspondence should be addressed
Phone: 043-290-2805
E-mail: habe@faculty.chiba-u.jp

ABSTRACT

ADF/cofilin is a phosphorylation-regulated protein essential for actin filament dynamics in cells. Here, we cloned two cDNAs encoding *Xenopus* ADF/cofilin (XAC)-specific phosphatase, slingshot (XSSH), one of which contains an extra 15 nucleotides in a coding sequence of the other, possibly generated by alternative splicing. Whole mount *in situ* hybridization showed XSSH transcripts in the blastopore lip and sensorial ectoderm at stage 11, and subsequently localized to developing brain, branchial arches, developing retina, otic vesicle, cement gland, and spinal chord in neurula to tailbud embryos. Immunostaining of animal-vegetal sections of gastrula embryos demonstrated that both XAC and XSSH proteins are predominant in ectodermal and involuting mesodermal cells. Microinjection of either a wild type (thus induces overexpression) or a phosphatase-defective mutant (functions as dominantly negative form) resulted in defects in gastrulation, and often generated the spina bifida phenotype with reduced head structures. Interestingly, the ratio of phosphorylated XAC to dephosphorylated XAC markedly increased from the early gastrula stage (stage 10.5), although the amount of XSSH protein markedly increased from this stage. These results suggest that gastrulation movement requires ADF/cofilin activity through dynamic regulation of its phosphorylation state.
Keywords: Slingshot, ADF/cofilin, actin filaments, gastrulation, Xenopus

INTRODUCTION

Gastrulation, a complex process essential for the development of most animals to establish their body plans, comprises coordinated regulation of several distinct types of cell movements. In *Xenopus*, the morphogenetic cell behavior during gastrulation, such as epiboly of the ectoderm, rotation of the endoderm, involution of the mesoderm, and convergent extension of the dorsal mesoderm, is well defined by extensive studies (for reviews see Keller et al., 2003; Duncan and Su, 2004). The molecular basis for these movements remains to be fully understood, while recent studies have considerably shed light on the molecular mechanism that underlies the convergent extension; non-canonical Wnt signaling is shown to play a central role in this process (Kuhl, 2002; Tada et al., 2002)

Dynamic changes in cell polarity, adhesion, morphology and motility are well known to be directly dependent on the actin cytoskeleton, and remodeling and reorganization of actin filaments in cells are regulated by Rho family small GTPases, Rho, Rac, and Cdc42 (Nobes and Hall, 1995). It has been shown that Rho and Rac participate in several developmental processes, including planar cell polarity pathway in *Drosophila* (Eaton et al., 1996; Strutt et al., 1997; Fanto et al., 2000; Winter et al., 2001) and convergent extension in *Xenopus* (Habas et al., 2001, 2003; Tahinci and Symes, 2003). Dishevelled (Dvl), a scaffold protein possessing multi-functional domains, mediates coactivation of Rho and Rac but the respective activities are differently regulated; Rho but not Rac activation requires the Formin-homology protein Daam1 which binds to both Rho and Dvl. (Habas et al., 2003). In addition, Rho and Rac coordinately control dynamic properties and polarity of lamellipodia formation in axial mesodermal cells to promote convergent extension (Tahinci and Symes, 2003). Several downstream effectors for Rho-GTPases are also reported to be involved in vertebrate gastrulation. Rac activation that proceeds from Dvl resulted in the activation of the JUN N-terminal kinase (JNK) (Kuhl, 2002; Habas et al., 2003). Rho kinase 2, one of downstream effectors of Rho, is shown to be involved in the cell polarity and motility during convergent extension movements of Zebrafish (Marlow et al., 2002).

The actin depolymerizing factor (ADF)/cofilin family of proteins, which has been shown to be essential in eukaryotes, enhances actin filament dynamics by depolymerizing and severing actin filaments (Bamburg, 1999; Bamburg et al., 1999; Carlier et al., 1999; Maciver and Hussey, 2002). The activity of this protein is inhibited by phosphorylation of an N-terminal serine residue (Agnew et al., 1995; Moriyama et al., 1996). In a wide variety of cells, ADF/cofilin exhibits rapid dephosphorylation in response to certain exogenous stimuli, for example, such as heat shock in cultured cells (Ohta et al., 1989; Abe et al., 1993) and formyl-methionyl-leucyl-phenylalanine (fMLP) in polymorphonuclear leukocytes (Suzuki et al., 1995; Okada et al., 1996), and the dephosphorylation accompanies dramatic changes in actin organization that are required for cellular function (Moon and Drubin, 1995). LIM kinases (Limks) (Arber et al., 1998; Sumi et al., 1999; Yang et al., 1998), testicular protein kinases (TESKs)

(Toshima et al., 2001a, 2001b), and Nck-interacting kinase (NIK)-related kinase (NRK)/NIK-like embryo-specific kinase (NESK) (Nakano et al., 2003) are responsible for phosphorylation of ADF/cofilin in vertebrates. Two types of LIM kinases, designated by LIM kinase 1 and LIM kinase 2 are present in vertebrates (Mizuno et al., 1994; Okano et al., 1995; Nunoue et al., 1995; Osada et al., 1996; Cheng et al., 1995; Koshimizu et al., 1997; Takahashi et al., 1997, 2001). Pioneering works (Arber et al., 1998; Yang et al., 1998) demonstrated that activation of Limk 1 is mediated by Rac1, and were followed by a study that activation of Pak1 through Rac1 or Cdc42 directly increases Limk 1 activity (Edwards et al., 1999). Also, Limks activation occur downstream of Rho-Rho kinase (ROK/ROCK) signaling (Maekawa et al., 1999; Sumi et al., 1999; Ohashi et al., 2000; Amano et al., 2001). These studies all strongly suggest that phosphorylation, and thus inactivation, of ADF/cofilin proceeds through activation of Rho-GTPases. On the other hand, Slingshot (SSH) has been identified as an ADF/cofilin-specific phosphatase in *Drosophila* and human (Niwa et al., 2002). SSH genetically interacts with the LIMK gene in *Drosophila*, and over-expression of SSH with Limk1 or Tesk1 suppresses actin-rich structures induced by these kinases. Therefore, SSH might reactivate ADF/cofilin, phosphorylated by Limks, to increase actin filament dynamics and/or to reorganize pre-existing actin cytoskeleton.

In *Xenopus*, ADF/cofilin is highly phosphorylated in oocytes and unfertilized eggs, and undergoes rapid dephosphorylation in response to the fertilization. Both overexpression and down-regulation of ADF/cofilin cause a defect in cytokinesis (Abe et al., 1996). *Xenopus* Limk1 and 2 (Xlimk1 and 2) are shown to be functionally responsible for the completion of oocyte maturation (Takahashi et al., 2001). These results suggest that phosphorylation-regulation of ADF/cofilin is tightly regulated during actin-dependent cellular processes. To understand the biological significance of regulation of the ADF/cofilin activity, we cloned *Xenopus* SSH (XSSH) and examined its functions during *Xenopus* early development. Here we report that XSSH is functionally involved in the gastrulation. This finding provides novel insights into the regulatory mechanism of gastrulation movements from a cell biological aspect.

MATERIALS AND METHODS

Polyacrylamide gel electrophoresis and immunoblotting

SDS-polyacrylamide gel electrophoresis (SDS-PAGE) was carried out according to Laemmli (1970). Two-dimensional gel electrophoresis (2D-PAGE) was performed according to O'Farrell et al. (1977) using nonequilibrium-pH-gradient gel electrophoresis (NEpHGE) for the first dimension. Samples were dissolved in 2D-PAGE buffer composed of 9 M urea, 2% ampholine pH 3.5-10, 5% 2-mercaptoethanol, 0.1% SDS, 1% NP-40, and 10 mM Tris-HCl, pH 7.5. For immunoblotting, proteins were electrophoretically transferred from the SDS-gel to nitrocellulose paper by the method of Towbin et al. (1979). The paper was treated with 5% skimmed milk in PBS for 1 hr, and then incubated with the primary antibody followed by treatment with alkaline phosphatase-conjugated secondary antibody. The paper was thoroughly washed with PBS after each immunoreaction and stained with nitroblue tetrazolium

chloride (NBT) and 5-bromo-4-chloro-3-indolylphosphate p-toluidine salt (BCIP) in alkaline phosphatase buffer (0.1 M NaCl, 5 mM MgCl2, and 0.1 M Tris-HCl, pH 9.5), or detected by chemiluminescence with CDP-Star (Roche) using Light Capture (ATTO).

Cloning of cDNA and genomic DNA and construction of expression vectors

A stage 30 *Xenopus* embryo cDNA library in λZAPII was screened by polymerase chain reaction (PCR) with a degenerated primer set of 5'-CTKGGWAGYGARTGGAAYGC and 5'-ACWCCCATYTTRCARTGTAC, corresponding to the nucleotide sequence of 1177-1415 in the *Drosophila* SSH catalytic domain that is highly homologous to human SSHs. A major band with about 240 bp was amplified and cloned into the EcoRV site of pBluescript II KS^+ vector. Sequencing of this PCR fragment exhibited about 70% identity with human SSH between their primary structures, suggesting a *Xenopus* homologue of SSH (XSSH). A full-length clone of XSSH (XSSH (+)) was isolated from the stage 30 cDNA library by hybridization screening using the PCR fragment as a probe. The PCR fragment was excised from pBluescript II KS^+ vector with EcoRI and XhoI and inserted into a pGEX-4T-1 vector digested with EcoRI and XhoI, and glutathione-S-transferase (GST)-fused catalytic domain was expressed in *E. coli*. The anti-XSSH antibodies were obtained by immunizing the GST-catalytic domain to rabbits (see below). A full-length clone (XSSH (-)) was isolated from a *Xenopus* ovary λZAPII cDNA library with anti-XSSH antibody (GenBank accession number AY 618876). In addition, a partial cDNA clone lacking N-terminus (pBluescript SK^--ΔN-XSSH) was also isolated from the stage 30 cDNA library, and used for expression of His-tagged ΔN-XSSH protein.

To isolate the XSSH gene fragment, *Xenopus* genomic DNA was purified from female liver according to Blin and Stafford (1976). By a PCR reaction with a primer set of 5'-GGATGATGAAAAAGCAGAAGAAAGCGAATGCAGAG and 5'-CTATAGGTTCCCCTTCATCCTGCAGAAGAAGTGCTG, the genomic DNA fragment was isolated and sequenced.

Xenopus brachyury (Xbra) and α-cardiac actin cDNA fragments were obtained by PCR using *Xenopus* stage 30 cDNA library and primer sets of 5'-GAGTCACTACCTGCCGATCA and 5'-TCTCCAGTGGGCTCCAAAG for Xbra and 5'-GATCTGGCACCACACCTTCT and 5'-CATAGCTCTTCTCCAGGG for actin. The amplified 533 bp fragment of Xbra and 470 bp fragment of actin were cloned into EcoRV site of pBluescript II KS^+ vector, respectively and confirmed by sequencing.

To produce the full-length XSSH (-) as GST-fusion protein (GST-XSSH), the XSSH (-) cDNA in pBluescript SK^- was first digested with KpnI and blunted by T4 polymerase, and then excised with EcoRI. This fragment was inserted into EcoRI and SmaI sites of pGEX-4T-3 vector. To produce catalytically inactive mutant (GST-XSSH (CS)), the catalytically essential Cys^{380} of pBluescript SK^--XSSH was changed to Ser by site-directed mutagenesis using complementary primers (5'-GTGTACTTGTGCACTCCAAGATGGGAGTCTCTC and 5'-GAGAGACTCCCATCTTGGAGTGCACAAGTACAC), and checked by sequencing.

Expression plasmid carrying GST-XSSH (CS) was constructed according to the same procedure of GST-XSSH (-). For expression of His-tagged ΔN-XSSH, ΔN-XSSH cDNA was excised out with EcoRI and inserted into the same site of pRSET-A vector.

RT-PCR samples and primers

mRNAs were extracted from *Xenopus* embryos using a QuickPrep MicromRNA purification kit (Amersham Bioscience, UK) and were reverse-transcripted with oligo-dT primers. PCR was carried out using a primer set of 5'-ATATCGCTTGGAGTCCCTGTGACATGG and 5'-CCCCTTCATCCTGCAGAAGAAGTGCTG.

Preparation of mRNA and proteins

For mRNA production, the XSSH (-) and XSSH (CS) cDNA in pBluescript SK$^-$ were digested with KpnI and EcoRI, blunted with T4 DNA polymerase, and inserted into the EcoRV site of pBluescript KS$^+$ vector, respectively. Each constract was linearized with SalI, and mRNA was generated by T7 RNA polymerase using an mMESSAGE mMachine T7 kit (Ambion Inc.).

pGEX expression plasmids carrying the full-length XSSH or XSSH (CS) were transformed into BL21 (DE3) pLysS and the expression of recombinant proteins was induced by adding 0.1 mM IPTG for overnight at 13 °C. Cells were harvested and lysed by sonication in PBS containing 0.1% Triton X-100, and soluble fractions were obtained by centrifugation at 15,000 g for 20 min at 4 °C. Supernatants were added to glutathione-Sepharose 4B (Pharmacia) prewashed with PBS. Mixtures were incubated for 1 hr at 4 °C with gentle, continuous stirring, and then resins were poured into columns and thoroughly washed with PBS containing 0.1% Triton X-100. Proteins were eluted with PBS containing 50 mM Tris-HCl, pH 8.0 and 10 mM glutathione, and dialyzed against F-buffer (0.1 M KCl, 2 mM $MgCl_2$, 0.1 mM DTT, 0.05% NaN_3, 20 mM HEPES-KOH, pH 7.2).

BL21 (DE3) pLysS was also transformed by pRSET- ΔN-XSSH and the expression was induced by adding 0.5 mM IPTG for 3 hr at 37 °C. Inclusion bodies of ΔN-XSSH, washed with PBS containing 1% Triton X-100, was solubilized with 6 M urea containing 0.1 M Na-PO_4, pH 8.0, and applied to Ni-NTA column (QIAGEN). The column was washed with the same buffer, but at pH 6.5, and the same buffer containing 20 mM imidazole, pH 7.0. His-ΔN-XSSH was eluted by the same buffer containing 0.1 M imidazole, pH 7.0, dialyzed against coupling buffer (6M urea, 80 mM $CaCl_2$, 0.1 M HEPES-KOH, pH 7.4), and coupled to Affi-gel 10 (Bio-Rad).

Egg extracts (cytostatic factor-arrested (CSF) extracts) were prepared from unfertilized eggs as described by Murray (1991).

The phosphorylated XAC fraction was prepared from *Xenopus* ovaries. *Xenopus* ovaries were homogenized in 5 volumes of buffer A (0.1 M KCl, 2 mM EGTA, 2 mM DTT, 50 mM NaF, and 20 mM HEPES-KOH, pH 7.2) containing 40% saturation of ammonium sulfate, 20 μg/ml leupeptin, and 1 mM PMSF. After centrifugation at 15,000 g for 20 min at 4 °C, the supernatant was further fractionated by 60-90% saturation with ammonium sulfate. The precipitate was collected by centrifugation at 15,000 g for 30 min at 4 °C, and solubilized and dialyzed to buffer A. The dialyzed

sample was gel-filtrated on a Sephadex G-75 column, and fractions containing XAC were applied to a hydroxyapatite column pre-equilibrated with buffer A, followed by washing thoroughly with buffer A and buffer A containing 0.6 M KCl. XAC was eluted with buffer A containing 0.6 M KCl and 10 mM K-PO4, pH 7.5, and dialyzed against 20 mM NaCl, 2 mM DTT, and 20 mM Tris-HCl, pH 7.5. Finally, the flow-through fraction from a DE52 ion exchange column pre-equilibrated with the same buffer was concentrated, dialyzed against F-buffer, and stored at –80 °C until use.

In vitro phosphatase assay

2 μM of GST-XSSH or GST was incubated with the phosphorylated XAC (pXAC) fraction (the final concentration of pXAC was estimated to be 5.5 μM by densitometry) for 1 hr at room temperature in F-buffer. Reactions were stopped by addition of 10% TCA to samples and proteins were precipitated, rinsed and dried. Samples were solubilized in 2D-PAGE buffer and subjected to 2D-PAGE and immunoblotting. XAC spots were detected by chemiluminescence using Light Capture (ATTO) and analyzed by densitometry with a software of ATTO Lane Analyzer 10H.

Antibodies

Inclusion bodies of GST-fused XSSH catalytic domain, as described above, was thoroughly washed with PBS containing 1% Triton X-100, and with 3M urea, and then solubilized with SDS-sample buffer (4% SDS, 5% 2-mercaptoethanol, 10% glycerol and 25 mM Tris-HCl, pH 6.8). After centrifugation at 15,000 g for 15 min, the supernatant was subjected to SDS-PAGE, stained with Coomassie Blue R-250 and the protein band corresponding to GST-catalytic domain was excised with a razor blade. GST-catalytic domain was electrophoretically eluted from gel slices, dialyzed to PBS, and used to immunize rabbits for producing polyclonal antibody. Antisera were purified by His-XSSH-coupled Affi-gel 10 column chromatography.

Anti-XAC monoclonal antibody was previously prepared (Okada et al., 1999). Anti-phosphorylated ADF/cofilin-specific antibody was kindly provided by Dr. Bamburg of Colorado State University. The monoclonal antibody specific for both α-cardiac and α-skeletal muscle actin (SKA-06) was used as described in elsewhere (Hayakawa et al., 1996). anti-tubulin monoclonal antibody (DM1A) was purchased from Sigma. Fluorescein or rhodamine-labeled goat anti-mouse or rabbit IgG was purchased from TAGO Inc. Alkaline phosphatase-conjugated goat anti-mouse or rabbit IgG was purchased from Bio-Rad.

Microinjection

0.05 or 0.1 μg/μl mRNA was injected into each blastomere of two-cell stage embryos. Injection volumes from each pipette from a pressure injector (CIJ-1, Shimadzu, Kyoto) were calibrated by measuring the volume of an aqueous drop delivered into mineral oil. Control injections with H_2O alone or the same amount of β-galactosidase mRNA was also done.

***In situ* hybridization and immunofluorescence microscopy**

For *in situ* hybridization, digoxigenin-labeled single strand RNA probes were prepared using the DIG RNA Labeling Kit (Roche). 420 bp of 3'-sequence of XSSH was amplified by PCR using 3'-primer (GCTATGCATGCCAGAAGATAC) and T7

primer with λZAPII-XSSH (-) as a template. Amplified fragments were digested with XhoI and inserted into EcoRV and XhoI sites of pBluescript II KS$^+$ vector. To generate RNA probes, this construct was linearized either with EcoRI for the antisense probe or with XhoI for the sense probe. For Xbra RNA probe production, pBluescript II KS$^+$-Xbra was linearized by XhoI for the antisense probe or with EcoRI for the sense probe. *In situ* hybridization was done according to Harland (1991).

For immunofluorescence microscopy, *Xenopus* embryos were fixed in MEMFA (3.7% formaldehyde, 2 mM MgSO4, 1 mM EGTA, and 0.1 M MOPS, pH 7.4) containing 1% TCA, embedded in paraffin, and sectioned as described elsewhere (Okada et al., 1999). After blocking with 20% goat serum in PBS for 1 hr at room temperature, specimens were incubated with primary antibodies for 1 hr at room temperature, and then with appropriate fluorochrome-conjugated secondary antibodies. After each immunoreaction step, specimens were rinsed and washed with PBS, and mounted in PBS containing 1 mg/ml p-phenylenediamine and 90 % glycerol. Samples were examined with an Axioskop (Carl Zeiss, Germany) with a cooled charge-coupled devise camera, CoolSNAP (Nippon ROPER, Japan).

Results

Two embryonic cDNAs encode *Xenopus* SSH homologue

We first isolated about a 240 bp cDNA fragment from *Xenopus* stage 30 cDNA library by PCR using degenerated primer, corresponding to catalytic domain of *Drosophila* SSH, and confirmed it to be a *Xenopus* homologue of SSH by sequencing. By using this cDNA fragment, we isolated two positive clones and partial sequencing showed that one clone encoded a full-length protein with the first methionine but the other encoded a partial sequence lacking the N-terminus. The full-length clone (GenBank accession number AY233266) was restriction-mapped and completely sequenced. On the other hand, we generated antisera specific for XSSH as described in *Materials and Methods* and shown in Fig. 2, and carried out expression screening for *Xenopus* ovary cDNA library using antisera. Two full-length clones among five positive clones were obtained and the longest one (GenBank accession number AY618876) was completely sequenced. As shown in Fig. 1, the respective full-length clones derived from the distinct libraries exhibited almost identical nucleotide sequences except for an additional 15 bases insertion located at position 142-156 bases of the AY233266 sequence. Open reading frame of AY618876 starts at position 76 and the deduced amino acid sequence of the N-terminus is well correspondent with that of mammalian and *Drosophila* SSH. In AY233266 sequence, however, the initiation codon ATG is placed at position 170-172 to yield an unexpectedly long 5'-noncoding region, since in-frame stop codon TAA arises at position 149-151 in the insertion. Thus XSSH with the insertion (XSSH (+)) lacks N-terminal 38 amino acids in comparison with XSSH without the insertion (XSSH (-)).

To clarify the origin of this insertion sequence, we examined the genomic DNA sequence of XSSH. The composition of the exon and intron in human three SSH genes

was helpful for deducing that in the *Xenopus* SSH gene. The PCR could amplify a 212 bp fragment which contained putative exon 2, intron and 5' half of exon 3 of the XSSH gene. Sequencing of this fragment (Fig 1) revealed that the 15 bp insertion in XSSH (+) is coded in intron region of XSSH (-), that is, the putative exon 3 of XSSH (+) starts 15 nucleotides upstream of that of XSSH (-). The splice acceptor sequence CAG was located next to the 5' ends of the respective exon 3 with a consensus 5' splice donor sequence GTAAG located at the 5' end of the intron. Therefore, we conclude that these two mRNAs of XSSH (+) and XSSH (-) are generated by a different selection of cryptic splice acceptor sites, respectively.

To investigate which isoform is predominantly expressed in eggs and embryos during early development, the two cDNA libraries were screened by PCR (Fig. 1C). A 167 bp product of XSSH (-) was amplified in both libraries, while a 182 bp product of XSSH (+) was detected only in the stage 30 cDNA library. Next, we purified mRNA from oocytes, stage 10.5, and stage 30 embryos respectively, and carried out RT-PCR with the same primer set. Through developmental stages, a 167 bp product predominated and a 182 bp product was scarcely detected. These results indicate that XSSH (-) is the major isoform in eggs and early embryos.

Expression and phosphorylation of XSSH during development

We raised antibodies specific for XSSH by immunizing rabbits with GST-tagged XSSH catalytic domain. The specificity of the antibody was examined by immunoblotting (Fig. 2A). The antibody specifically recognized the protein with expected mobility in the whole lysates from stage 35 embryos. In addition, XSSH (-) protein translated in rabbit reticulocyte lysates was specifically reacted with the antibody. Thus, this antibody is specific for the XSSH protein.

As shown in Fig. 2B, immunoblotting of whole lysates from unfertilized eggs and different stages of embryos showed that XSSH was present as a maternal protein and remained unchanged in amount during cleavage. The amount of the XSSH protein markedly increased from stage 10.5 when the gastrulation movement dynamically occurs, and persisted hereafter. On the other hand, as shown in Fig. 2C, RT-PCR revealed that XSSH transcripts are markedly increased from stage 8 when the mid-blastula transition occurs. Although this time lag of expression between the transcript and the protein is unknown, XSSH function is assumed to be required for the gastrulation movements.

The mobility sift on an SDS-gel was a remarkable feature of this protein (Fig. 2B). In addition to a major band (shown by an open arrowhead), faint bands showing lower mobility (shown by a small arrow) were detected during cleavage, while those faint bands disappeared from the gastrula stage (stage 10.5) and a novel band with higher mobility (shown by a closed arrowhead) gradually increased and became a major form from late neurula stage (stage 23). In unfertilized eggs (lane 1), however, the major band showed the mobility much lower than that of 2 cell stage embryos. As shown in Fig. 2D, the faint bands were disappeared and shifted to the position of the major band of the cleaving stage embryos when cell lysates of unfertilized eggs were treated with

an alkaline phosphatase. Therefore, the faint bands with the lower mobility are suggested to be the phosphorylated form of XSSH. However, this mobility sift by alkaline phsphatase did not change any more to the position of that of tail-bud stage embryos (stage 35, Fig. 2D, lane 2 and 3). In addition, it should be noted that phosphorylation of XSSH is prominent during cleavage, but not during morphogenetic movements.

Spatial expression of XSSH in embryos

Whole mount *in situ* hybridization showed that XSSH transcripts are concentrated at blastopore lips and the dorsal side of stage 11 embryos (Fig. 3A). In the neurula stage, XSSH was present in the head structures and the dorsal part of trunk, and these patterns became clear in the tailbud stage (Fig 3, B, C and D). XSSH mRNA was predominantly expressed in brain, optic and otic vesicles, hyoid and branchial arch, and spinal cords. The striped pattern in the dorsal part of trunk was also obvious and was well correspondent with that of XAC (Fig. 3, E and F). When these stripes of XSSH were compared to the staining pattern of somites by cardiac actin probe (Fig. 3, G and H), stripes of XSSH were more narrow and appeared to position at the regions between somites, or at the restricted region in somites (compare C with G, and E with H)

We next examined expression patterns of both XSSH and XAC proteins by immunofluorescence microscopy of animal-vegetal sections of early gastrula stage embryos. As shown in Fig. 4, A and B, both proteins predominantly expressed in the involuting mesodermal cells and ectodermal cells. XAC accumulated to the cortical region of cells, while XSSH showed rather diffuse in cells. When distribution of phosphorylated XAC (pXAC) in embryos was examined by the antiserum specific for pXAC, both mesodermal and ectodermal cells were also stained diffusely by this antiserum and it is characteristic of pXAC staining to show that cells scarcely stained by the pXAC antiserum were scattered among staining-positive cells (Fig. 4, C and D; two serial sections with an interval of six sections). Therefore, cells with faint staining might be promoting dephosphorylation of pXAC. The circumferential strong staining by this antiserum is non-specific binding of antibody to the vitellin membrane surrounding embryos, since a non-specific serum also stained this membrane (data not shown). Since the amount of XSSH increased from the early gastrula stage, changes in ratio of pXAC to XAC from blastula to gastrula were examined by a combination of 2D-PAGE and immunoblotting. Unexpectedly, the amount of pXAC was drastically increased at stage 10.5 when gastrulation movements have just begun (Fig. 4G). We assume that activation of both phosphorylation and dephosphorylation might require for the gastrulation movements.

On the other hand, additional immunofluorescence staining for XSSH was done on sections from embryos at stage 33. Anterior and posterior dorsal parts of the trunk of a single embryo were shown in Fig. 4, E and F. Cells within the neural tube, notochord, and epidermis were brightly stained, and bright patches were often observed in the somite regions (shown by arrows). These patches are likely to be correspondent to the

striped pattern shown by *in situ* hybridization.

XSSH is required for the gastrulation movements

In order to clarify the significance of XSSH activity during gastrulation, we constructed a phosphatase-inactive mutant of XSSH (XSSH (CS)). The wild type XSSH (XSSH (WT)) and XSSH (CS) were expressed in *E. coli* and purified, and their phosphatase activities were assayed using partially purified pXAC fraction. As shown in Fig. 5A, partially purified pXAC fraction contained many other proteins, but any phosphatase or kinase activities, or 14-3-3 family proteins were never detected (data not shown). A combination of 2D-PAGE and immunoblotting (Fig. 5, B and C) showed that XSSH dephosphorylates pXAC, whereas XSSH (CS) completely lacks phosphatase activity. Sodium orthovanadate also inhibited XSSH phosphatase activity.

Effects of ectopic expression of XSSH on gastrulation movements were then examined. Injection of either wild type XSSH or XSSH (CS) mRNA impaired gastrulation movements (Fig. 5D). As summarized in Table I, these effects were dependent on the concentration of injected mRNA and significant amounts of embryos injected with 1 ng mRNAs showed the defective phenotypes. We confirmed the protein expression from ectopic mRNAs by immunoblotting of whole lysates of 1 ng mRNA-injected embryos. Fig. 5E clearly demonstrated about two- to three-fold increase in amount of ectopically expressed proteins. The phosphorylation state of XAC in injected embryos was also examined by 2D-PAGE when control embryos developed to reach stage 12. The amount of pXAC was decreased by injection of wild type XSSH mRNA, and was markedly increased when XSSH (CS) mRNA was injected (Fig. 5, F and G). These results strongly suggest that XSSH (CS) functions as a dominantly negative form in embryos as reported in mammalian cultured cells transfected by SSH (CS) (see *discussion*). Time-lapse images of XSSH (CS) injected embryos were shown in Fig. 6A. At the onset of gastrulation, the blastopore lip formed more equatorially in XSSH (CS) injected embryos, suggesting that pregastrula epiboly is inhibited. Although the gastrulation of control embryos progressed, XSSH (CS) injected embryos showed neither involution nor epiboly and finally formed spina bifida which resulted from the inability of the blastopore to close. Animal-vegetal sections of control (stage 11), XSSH (WT)- and XSSH (CS)-injected embryos were shown in Fig. 6B. The control embryo formed two cell layers at the animal cap, the epithelial and sensorial layers of cells. In XSSH (WT)- and XSSH (CS)-injected embryos, however, animal cap cells might be defective in epiboly, since the animal cap region constituted five to six layers of cells. In addition, injected embryos often showed expanded blastocoels and incomplete involution without any formation of archenterons (data not shown). These results strongly suggest that intracellular perturbation of phosphorylation state of XAC entirely disrupts the gastrulation movement.

28.0% (n=7/25) and 35.7% (n=10/28) of embryos injected with 0.5 ng XSSH (WT) and 1 ng XSSH (CS) underwent normal gastrulation, respectively (Table I), but 60-70% of these embryos (n=5/7 in XSSH (WT) injection and n=6/10 in XSSH (CS) injection) showed shortening of the anteroposterior axis and reduction of head

structures including a defect in the eye development (Fig. 7A). Immunofluorescence staining of XSSH in vertical sections of control and XSSH (CS)-injected embryos (Fig. 7B) showed that the forebrain, formed in the control embryo (indicated by an arrow), completely disappeared in the XSSH (CS)-injected embryo and instead, notochord was still observed (indicated by an arrowhead). Eyes abnormally developed with reduced size. These phenotypes were observed in all embryos examined (n=4/4) and also in XSSH (WT)-injected embryos (data not shown). In addition, in this embryo, one of eyes (the right side in this case) failed to form.

Finally, to exclude the possibility that the gastrulation-defective phenotypes resulted from indirect effects by suppression of the mesoderm induction but not inhibition of a normal cell migration, we examined the expression of the mesoderm marker *Xenopus* brachyury (Xbra) by whole mount *in situ* hybridization and of the muscle-specific α-actin by immunoblotting in control and XSSH (CS) injected embryos. As shown in Fig. 7C, whole mount *in situ* hybridization clearly demonstrated that Xbra expression was obvious surrounding blastopores in both control and injected stage 10.5 embryos, while the staining in XSSH (CS) injected embryos localized to more equatorial region compared with that in control embryos, according to the position of blastopore lip formation (Fig. 6A). Expression of the muscle specific α-actin was also confirmed in XSSH (CS) injected embryos (Fig. 7D). Together, these results suggest that mesoderm induction and differentiation are not influenced by XSSH (CS)-injection and that cell migration itself is disrupted in XSSH (CS)-injected embryos.

Discussion

In the present study, we confirmed that a *Xenopus* homologue of SSH possesses an activity to dephosphorylate *Xenopus* ADF/cofilin. Thus, XSSH is both structurally and functionally identical to *Drosophila* and mammalian SSHs. By injection of XSSH mRNAs, we found that ectopic expression of XSSH (CS), the phosphatase-inactive mutant, caused severe defects in gastrulation. Over-expression of XSSH also inhibited gastrulation movements. These results suggest that gastrulation movement requires proper regulation of XAC activity in cells. We cloned two splicing variants of XSSH, one of which has an additional 15 nucleotide sequence, generating the in-frame stop codon. This XSSH (+) was significantly amplified from stage 30 cDNA library, whereas RT-PCR with stage 30 embryos showed only a slight amplification of XSSH (+). This discrepancy might be due to an additional amplification step in construction of cDNA library, and XSSH (-) is the major isoform present in cleaving embryos. On the other hand, after the gastrula stage, a novel XSSH band, exhibiting the highest mobility on an SDS gel, appeared and gradually became the major band. Since the mobility of XSSH (-) in egg extracts did not sift to the position of this novel band after treatment by alkaline phosphatase, it is possible that the XSSH showing highest mobility is an isoform distinct from either XSSH (-) or XSSH (+), or XSSH (-) at cleaving stage is likely to be modified by phosphorylation at a specific residue where

the alkaline phosphatase can not associate. Furthermore, we can not deny that the other modification could regulate the XSSH activity until early neurula stage.

The expression pattern of XSSH was well correspondent to that of XAC during early embryogenesis (Abe et al, 1996). Both were predominantly expressed in neural tissues. The striped pattern at dorsal side of trunk was also characteristic to both staining by *in situ* hybridization. These stripes were apparently narrow in width in comparison with somites stained by alpha-cardiac actin probe and seemed to position between somites. Supporting these *in situ* hybridization images, immunofluorescence microscopy of vertical sections revealed that somites were patched with fluorescence, but never stained entirely with anti-XSSH antibody. Recently, knock out study demonstrated that non-muscle type cofilin is essential for neural crest cell migration as well as other cell types in the paraxial mesoderm in mice (Gurniak et al, 2005). Together, we assume that the striped region might contain neural crest cells. Experiments with probes specific for each type of mesodermal cells may confirm cell types in these striped regions.

The full-length XSSH (-) tagged with GST was successfully purified from *E. coli*, and possessed XAC dephosphorylation activity that was inhibited by Na_3VO_4. And the mutant (GST-XSSH (CS)), the essential Cys residue of which was substituted by Ser, completely lost dephosphorylation activity. These results were well corresponding to studies with *Drosophila* and mammalian SSH (Niwa et al., 2002). Previous studies demonstrated that SSH (CS) functions as a dominantly negative form to prevent cofilin dephosphorylation when expressed in cultured cells (Kaji et al., 2003; Nagata-Ohashi et al., 2004; Wang et al., 2005). In this study, ectopic expression of XSSH (CS) also increased the level of XAC phosphorylation and over-expression of wild type XSSH decreased the total amount of phosphorylated XAC (pXAC). Therefore, we conclude that XSSH (CS) also functions as a dominantly negative form in embryos.

pXAC level was kept lower in the blastula stage, while, in the gastrula stage, its level was markedly increased. Since the amount of XAC did not alter during these stages (Okada et al., 1999), it is suggested that XAC phosphorylation activity is elevated at the gastrula stage. On the other hand, the amount of XSSH protein apparently increased from the gastrula stage. *In situ* hybridization and immunofluorescence microscopy indicate that this increased expression of XSSH occur in ectodermal and mesodermal cells in gastrula embryos. In these cells, however, staining by anti-pXAC antibody was not uniform and not weak, and cells with faint staining by anti-pXAC antibody were scattered in ectodermal and mesodermal cells with clear staining. These results suggest that respective cells may independently regulate pXAC level, although they increase expression level of XSSH. Together with the result that ectopic expression of XSSH (CS) caused severe defects in gastrulation, it is strongly suggested that XSSH activity is regulated individually in cells during gastrulation by unknown upstream signaling. In mammalian cells, neuregulin-induced pathway of SSH activation has been demonstrated (Nagata-Ohashi et al., 2004). Most recently, SSH and Limk have been demonstrated to form complex with other signal transducers and regulate ADF/cofilin activity in an interdependent manner (Soosairajah

et al., 2005). Regulatory pathway for the activation of XSSH during gastrulation awaits elucidation in future studies. Over-expression of XSSH also prevented gastrulation. One possible explanation for this effect is that active XAC increased by excessive amount of XSSH disturbs actin filament dynamics to inhibit cell migration, since total amount of pXAC was apparently decreased in the injected embryos. Or, insufficient amount of pXAC pool, induced by the excessive amount of XSSH, prevents cell migration because of lack of dephosphorylated/reactivated XAC.

Injection of XSSH (CS) mRNA caused spina bifida and also inhibited thinning of animal roof (Fig. 6), in addition to formation of embryos with reduced head structures and shortened anteroposterior axis (Fig. 7). These results are likely to indicate that expression of XSSH (CS) prevents both epiboly and convergent extension during gastrulation. Experiments with Keller explants are required for elucidation of those points. In addition, it is necessary to observe changes in morphology and shape of living cells comparatively between control and XSSH (CS)-injected embryos. On the other hand, reduced head structures were also shown in mouse embryos in which the non-muscle type cofilin gene was targeted (Gurniak et al., 2005). Mutant embryos (cof-/- embryos) at E10.5 showed smaller body size, failure of neural tube closure, and defects of eye development. All of these defects induced in the cof-/- embryos were also obvious in *Xenopus* embryos injected with XSSH (CS). However, cof-/- embryos developed normally by E9.5, suggesting that non-muscle cofilin is not essential for morphogenetic movements during gastrulation. Since there are three ADF/cofilin isoforms in mice, muscle-type or maternally expressed ADF/cofilin isoforms may function gastrulation movements. We currently assume that *Xenopus* gastrulation movement requires regulated phosphorylation and dephosphorylation of XAC in cells.

Finally, however, our results here could be interpreted in a quite different way. Ectopically expressed XSSH might bind to actin filaments in cells to disturb actin cytoskeletal architecture and prevent gastrulation movements, since XSSH tightly binds to actin filaments. Both wild type and CS mutant XSSHs also retain binding activity for actin filaments (unpublished results) as well as mammalian SSHs (Niwa et al., 2002). This possibility can not be currently excluded but antagonized by several results. First, injection of much smaller amount of XSSH (WT) mRNA affected gastrulation than that of XSSH (CS) mRNA did (Table I). If the binding of XSSH to the actin filament were essential for the gastrulation defects, the dosage effects would show less difference between the two injections. Second, injection of mRNA of S3A-XAC, the constitutively active form of XAC, also caused gastrulation defects more effectively than that of wild type XAC (our unpublished results). This suggests that regulation of XAC activity by phosphorylation is necessary for gastrulation. Exploration of regulatory mechanisms of XSSH activity, in addition to domain analysis of XSSH protein, will be important to understand the gastrulation movement mediated by phospho-regulation of XAC activity.

References

Abe, H., Nagaoka, R. and Obinata, T. (1993). Cytoplasmic localization and nuclear transport of cofilin in cultured myotubes. *Exp Cell Res* 206, 1-10.

Abe, H., Obinata, T., Minamide, L. S. and Bamburg, J. R. (1996). Xenopus laevis actin-depolymerizing factor/cofilin: a phosphorylation-regulated protein essential for development. *J Cell Biol* 132, 871-85.

Agnew, B. J., Minamide, L. S. and Bamburg, J. R. (1995). Reactivation of phosphorylated actin depolymerizing factor and identification of the regulatory site. *J Biol Chem* 270, 17582-7.

Amano, T., Tanabe, K., Eto, T., Narumiya, S. and Mizuno, K. (2001). LIM-kinase 2 induces formation of stress fibres, focal adhesions and membrane blebs, dependent on its activation by Rho-associated kinase-catalysed phosphorylation at threonine-505. *Biochem J* 354, 149-59.

Arber, S., Barbayannis, F. A., Hanser, H., Schneider, C., Stanyon, C. A., Bernard, O. and Caroni, P. (1998). Regulation of actin dynamics through phosphorylation of cofilin by LIM-kinase. *Nature* 393, 805-9.

Bamburg, J. R. (1999). Proteins of the ADF/cofilin family: essential regulators of actin dynamics. *Annu Rev Cell Dev Biol* 15, 185-230.

Bamburg, J. R., McGough, A. and Ono, S. (1999). Putting a new twist on actin: ADF/cofilins modulate actin dynamics. *Trends Cell Biol* 9, 364-70.

Blin, N. and Stafford, D. W. (1976). A general method for isolation of high molecular weight DNA from eukaryotes. *Nucleic Acids Res* 3, 2303-8.

Carlier, M. F., Ressad, F. and Pantaloni, D. (1999). Control of actin dynamics in cell motility. Role of ADF/cofilin. *J Biol Chem* 274, 33827-30.

Cheng, A. K. and Robertson, E. J. (1995). The murine LIM-kinase gene (limk) encodes a novel serine threonine kinase expressed predominantly in trophoblast giant cells and the developing nervous system. *Mech Dev* 52, 187-97.

Duncan, T. and Su, T. T. (2004). Embryogenesis: coordinating cell division with gastrulation. *Curr Biol* 14, R305-7.

Eaton, S., Wepf, R. and Simons, K. (1996). Roles for Rac1 and Cdc42 in planar polarization and hair outgrowth in the wing of Drosophila. *J Cell Biol* 135, 1277-89.

Edwards, D. C., Sanders, L. C., Bokoch, G. M. and Gill, G. N. (1999). Activation of LIM-kinase by Pak1 couples Rac/Cdc42 GTPase signalling to actin cytoskeletal dynamics. *Nat Cell Biol* 1, 253-9.

Fanto, M., Weber, U., Strutt, D. I. and Mlodzik, M. (2000). Nuclear signaling by Rac and Rho GTPases is required in the establishment of epithelial planar polarity in the Drosophila eye. *Curr Biol* 10, 979-88.

Gurniak, C. B., Perlas, E. and Witke, W. (2005). The actin depolymerizing factor n-cofilin is essential for neural tube morphogenesis and neural crest cell migration. *Dev Biol* 278, 231-41.

Habas, R., Kato, Y. and He, X. (2001). Wnt/Frizzled activation of Rho regulates vertebrate gastrulation and requires a novel Formin homology protein Daam1. *Cell* 107, 843-54.

Habas, R., Dawid, I. B. and He, X. (2003). Coactivation of Rac and Rho by Wnt/Frizzled signaling is required for vertebrate gastrulation. *Genes Dev* 17, 295-309.

Harland, R. M. (1991). In situ hybridization: an improved whole-mount method for Xenopus embryos. *Methods Cell Biol* 36, 685-95.

Hayakawa, K., Ono, S., Nagaoka, R., Saitoh, O. and Obinata, T. (1996). Differential assembly of cytoskeletal and sarcomeric actins in developing skeletal muscle cells in vitro. *Zoolog Sci* 13, 509-17.

Kaji, N., Ohashi, K., Shuin, M., Niwa, R., Uemura, T. and Mizuno, K. (2003). Cell cycle-associated changes in Slingshot phosphatase activity and roles in cytokinesis in animal cells. *J Biol Chem* 278, 33450-5. Epub 2003 Jun 14.

Keller, R., Davidson, L. A. and Shook, D. R. (2003). How we are shaped: the biomechanics of gastrulation. *Differentiation* 71, 171-205.

Koshimizu, U., Takahashi, H., Yoshida, M. C. and Nakamura, T. (1997). cDNA cloning, genomic organization, and chromosomal localization of the mouse LIM motif-containing kinase gene, Limk2. *Biochem Biophys Res Commun* 241, 243-50.

Kuhl, M. (2002). Non-canonical Wnt signaling in Xenopus: regulation of axis formation and gastrulation. *Semin Cell Dev Biol* 13, 243-9.

Laemmli, U. K. (1970). Cleavage of structural proteins during the assembly of the head of bacteriophage T4. *Nature* 227, 680-5.

Maciver, S. K. and Hussey, P. J. (2002). The ADF/cofilin family: actin-remodeling proteins. *Genome Biol* 3, reviews3007. Epub 2002 Apr 26.

Maekawa, M., Ishizaki, T., Boku, S., Watanabe, N., Fujita, A., Iwamatsu, A., Obinata, T., Ohashi, K., Mizuno, K. and Narumiya, S. (1999). Signaling from Rho to the actin cytoskeleton through protein kinases ROCK and LIM-kinase. *Science* 285, 895-8.

Marlow, F., Topczewski, J., Sepich, D. and Solnica-Krezel, L. (2002). Zebrafish Rho kinase 2 acts downstream of Wnt11 to mediate cell polarity and effective convergence and extension movements. *Curr Biol* 12, 876-84.

Mizuno, K., Okano, I., Ohashi, K., Nunoue, K., Kuma, K., Miyata, T. and Nakamura, T. (1994). Identification of a human cDNA encoding a novel protein kinase with two repeats of the LIM/double zinc finger motif. *Oncogene* 9, 1605-12.

Moon, A. and Drubin, D. G. (1995). The ADF/cofilin proteins: stimulus-responsive modulators of actin dynamics. *Mol Biol Cell* 6, 1423-31.

Moriyama, K., Iida, K. and Yahara, I. (1996). Phosphorylation of Ser-3 of cofilin regulates its essential function on actin. *Genes Cells* 1, 73-86.

Nagata-Ohashi, K., Ohta, Y., Goto, K., Chiba, S., Mori, R., Nishita, M., Ohashi, K., Kousaka, K., Iwamatsu, A., Niwa, R. et al. (2004). A pathway of neuregulin-induced activation of cofilin-phosphatase Slingshot and cofilin in lamellipodia. *J Cell Biol* 165, 465-71.

Nakano, K., Kanai-Azuma, M., Kanai, Y., Moriyama, K., Yazaki, K., Hayashi, Y. and Kitamura, N. (2003). Cofilin phosphorylation and actin polymerization by NRK/NESK, a member of the germinal center kinase family. *Exp Cell Res* 287, 219-27.

Niwa, R., Nagata-Ohashi, K., Takeichi, M., Mizuno, K. and Uemura, T. (2002). Control of actin reorganization by Slingshot, a family of phosphatases that dephosphorylate ADF/cofilin. *Cell* 108, 233-46.

Nobes, C. D. and Hall, A. (1995). Rho, rac and cdc42 GTPases: regulators of actin structures, cell adhesion and motility. *Biochem Soc Trans* 23, 456-9.

Nunoue, K., Ohashi, K., Okano, I. and Mizuno, K. (1995). LIMK-1 and LIMK-2, two members of a LIM motif-containing protein kinase family. *Oncogene* 11, 701-10.

O'Farrell, P. Z., Goodman, H. M. and O'Farrell, P. H. (1977). High resolution two-dimensional electrophoresis of basic as well as acidic proteins. *Cell* 12, 1133-41.

Ohashi, K., Nagata, K., Maekawa, M., Ishizaki, T., Narumiya, S. and Mizuno, K. (2000). Rho-associated kinase ROCK activates LIM-kinase 1 by phosphorylation at threonine 508 within the activation loop. *J Biol Chem* 275, 3577-82.

Ohta, Y., Nishida, E., Sakai, H. and Miyamoto, E. (1989). Dephosphorylation of cofilin accompanies heat shock-induced nuclear accumulation of cofilin. *J Biol Chem* 264, 16143-8.

Okada, K., Takano-Ohmuro, H., Obinata, T. and Abe, H. (1996). Dephosphorylation of cofilin in polymorphonuclear leukocytes derived from peripheral blood. *Exp Cell Res* 227, 116-22.

Okada, K., Obinata, T. and Abe, H. (1999). XAIP1: a Xenopus homologue of yeast actin interacting protein 1 (AIP1), which induces disassembly of actin filaments cooperatively with ADF/cofilin family proteins. *J Cell Sci* 112, 1553-65.

Okano, I., Hiraoka, J., Otera, H., Nunoue, K., Ohashi, K., Iwashita, S., Hirai, M. and Mizuno, K. (1995). Identification and characterization of a novel family of serine/threonine kinases containing two N-terminal LIM motifs. *J Biol Chem* 270, 31321-30.

Osada, H., Hasada, K., Inazawa, J., Uchida, K., Ueda, R. and Takahashi, T. (1996). Subcellular localization and protein interaction of the human LIMK2 gene expressing alternative transcripts with tissue-specific regulation. *Biochem Biophys Res Commun* 229, 582-9.

Soosairajah, J., Maiti, S., Wiggan, O., Sarmiere, P., Moussi, N., Sarcevic, B., Sampath, R., Bamburg, J. R. and Bernard, O. (2005). Interplay between components of a novel LIM kinase-slingshot phosphatase complex regulates cofilin. *Embo J* 24, 473-86. Epub 2005 Jan 20.

Strutt, D. I., Weber, U. and Mlodzik, M. (1997). The role of RhoA in tissue polarity and Frizzled signalling. *Nature* 387, 292-5.

Sumi, T., Matsumoto, K., Takai, Y. and Nakamura, T. (1999). Cofilin phosphorylation and actin cytoskeletal dynamics regulated by rho- and Cdc42-activated LIM-kinase 2. *J Cell Biol* 147, 1519-32.

Suzuki, K., Yamaguchi, T., Tanaka, T., Kawanishi, T., Nishimaki-Mogami, T., Yamamoto, K., Tsuji, T., Irimura, T., Hayakawa, T. and Takahashi, A. (1995). Activation induces dephosphorylation of cofilin and its translocation to plasma membranes in neutrophil-like differentiated HL-60 cells. *J Biol Chem* 270, 19551-6.

Tada, M., Concha, M. L. and Heisenberg, C. P. (2002). Non-canonical Wnt signalling and regulation of gastrulation movements. *Semin Cell Dev Biol* 13, 251-60.

Tahinci, E. and Symes, K. (2003). Distinct functions of Rho and Rac are required for convergent extension during Xenopus gastrulation. *Dev Biol* 259, 318-35.

Takahashi, T., Aoki, S., Nakamura, T., Koshimizu, U. and Matsumoto, K. (1997). Xenopus LIM motif-containing protein kinase, Xlimk1, is expressed in the developing head structure of the embryo. *Dev Dyn* 209, 196-205.

Takahashi, T., Koshimizu, U., Abe, H., Obinata, T. and Nakamura, T. (2001). Functional involvement of Xenopus LIM kinases in progression of oocyte maturation. *Dev Biol* 229, 554-67.

Toshima, J., Toshima, J. Y., Amano, T., Yang, N., Narumiya, S. and Mizuno, K. (2001a). Cofilin phosphorylation by protein kinase testicular protein kinase 1 and its role in integrin-mediated actin reorganization and focal adhesion formation. *Mol Biol Cell* 12, 1131-45.

Toshima, J., Toshima, J. Y., Takeuchi, K., Mori, R. and Mizuno, K. (2001b). Cofilin phosphorylation and actin reorganization activities of testicular protein kinase 2 and its predominant expression in testicular Sertoli cells. *J Biol Chem* 276, 31449-58. Epub 2001 Jun 19.

Towbin, H., Staehelin, T. and Gordon, J. (1979). Electrophoretic transfer of proteins from polyacrylamide gels to nitrocellulose sheets: procedure and some applications. *Proc Natl Acad Sci U S A* 76, 4350-4.

Wang, Y., Shibasaki, F. and Mizuno, K. (2005). Calcium signal-induced cofilin dephosphorylation is mediated by Slingshot via calcineurin. *J Biol Chem* 280, 12683-9. Epub 2005 Jan 24.

Winter, C. G., Wang, B., Ballew, A., Royou, A., Karess, R., Axelrod, J. D. and Luo, L. (2001). Drosophila Rho-associated kinase (Drok) links Frizzled-mediated planar cell polarity signaling to the actin cytoskeleton. *Cell* 105, 81-91.

Yang, N., Higuchi, O., Ohashi, K., Nagata, K., Wada, A., Kangawa, K., Nishida, E., Mizuno, K., Arber, S., Barbayannis, F. A. et al. (1998). Cofilin phosphorylation by LIM-kinase 1 and its role in Rac-mediated actin reorganization. *Nature* 393, 809-12

Figure legends

Figure 1. (A) Comparison of 5'-nucleotide sequences between XSSH (-) and XSSH (+) cDNAs. Boxes and a double underline indicate the initiation codon and the in-frame stop codon, respectively. Asterisks indicate identical nucleotides. (B) Alignment of genomic and cDNA sequences encoding XSSH. The nucleotide sequence corresponding to the intron is represented in small letters. Conserved 5'-splice donor and 3'-splice acceptor sequences are surrounded by boxes. Sequences used for PCR primers are indicated by arrows. (C) Identification of the expression of the two XSSH. mRNAs purified from unfertilized eggs (lane 1), stage 10.5 embryos (lane 2) and stage 30 embryos (lane 3) were subjected to RT-PCR. And cDNA libraries prepared from *Xenopus* ovary (lane 4) or from stage 30 embryos (lane 5) were also examined by PCR. PCR products corresponding to XSSH (+) and XSSH (-) are represented by arrows, respectively.

Figure 2. (A) Specificity of anti-XSSH antibody. Whole protein lysates from Stage 35 embryos (lanes 1 and 1'), reticulocyte lysates expressing XSSH (+) (lanes 2 and 2'), and reticulocyte lysates alone (lanes 3 and 3') were electrophoresed on SDS-polyacrylamide gels. Proteins were transferred to nitrocellulose membrane. Coomassie Blue-stained gels (lanes 1-3) and immunoblots with anti-XSSH antibody (lanes 1'-3') are shown. (B) Immunoblot analysis of the whole lysates of unfertilized eggs and developing embryos with anti-XSSH antibody. Embryonic stages are represented at the upper side of each lane. The same membrane was probed for α-tubulin to control for equal loading. The major bands, appeared in earlier and later stages, were represented by open and closed arrowheads, respectively. A small arrow indicates several bands showing lower mobility. A large arrow represent the band with the lowest mobility appeared in unfertilized eggs. (C) Expression of XSSH during embryonic development (stages 7 to 11) was examined by PCR. (D) Alkaline phosphatase treatment of egg extracts. 10 μl of CSF-extracts were treated with (+) or without (-) 3 U of calf intestine alkaline phosphatase (AP) for 60 min at 21 °C, and subjected to SDS-PAGE and immunoblotting with anti-XSSH antibody (lanes indicated by "egg"). The whole cell lysate of stage 35 embryos (st. 35) was also loaded.

Figure 3. *In situ* hybridization of *Xenopus* embryos with XSSH (A-E, and I), XAC (F), and α-cardiac actin (G and H) riboprobes. Developmental stages shown; stage 11 (A), 22 (B and F), 25 (C and E), 26 (G and H), and 32 (D and I). Control (I) used the sense RNA probe of XSSH. Ventral (A), lateral (B-D, G and I), and dorsal views (E, F and H) are shown. The small and large arrows in A represent the yolk plug and the dorsal side of embryo, respectively.

Figure 4. (A-F) Immunofluorescence localization of XSSH (A, E and F), XAC (B), and pXAC (C and D) in paraffin sections of stage 11 (A-D) and stage 33 embryos (E and F). Inserts at the right side of A and B indicate the enlarged images of blastomeres.

The arrow and arrowhead in A and B show ectodermal and mesodermal regions brightly stained, respectively. Two serial sections from a single embryo with an interval of six sections were stained with anti-pXAC antibody (C and D). Arrows represent cells scarcely stained by this antibody. Sections of anterior (E) and posterior (F) parts of the trunk of a single embryo were probed with XSSH. Arrows indicate bright staining around somites. Bars, 100 μm (A-F) or 10 μm (inserts). (G) Immunoblot analysis of whole lysates from stage 7 to 10.5 embryos subjected to 2D-PAGE. Arrows indicate phosphorylated XAC spots.

Figure 5. Effects of ectopically expressed XSSH on *Xenopus* embryos. (A) Purified GST-XSSH (lane 1), GST-XSSH (CS) (lane 2) and pXAC fraction (lane 3) used for in vitro phosphatase assay were subjected to SDS-PAGE. The arrow and asterisk indicate the position of GST-XSSH or GST-XSSH (CS) and that of pXAC, respectively. (B and C) In vitro phosphatase assay was examined by a combination of 2D-PAGE and immunoblotting (B) and summarized in C. The number in B is corresponding to that in C. 1, pXAC fraction alone; 2, pXAC fraction and GST; 3, pXAC fraction and GST-XSSH; 4, pXAC fraction and GST-XSSH (CS); 5, pXAC fraction and GST-XSSH in the presence of Na_3VO_4. (D) Inhibition of gastrulation by injection of XSSH mRNAs. β-gal (control), XSSH (wild type), or XSSH (CS mutant) mRNAs were injected into both blastomeres at the two cell stage, and embryos were incubated until control embryos developed at the stage 13. The arrow indicates endodermal cells. (E) Immunoblots of whole lysates from injected embryos, which developed at the stage 13. Embryos, injected with β-gal (control), XSSH (WT), or XSSH (CS) mRNAs, were lysed individually, and each sample was subjected to SDS-PAGE and immunoblotting with anti-XSSH antibody. Two examples of each injection are shown. 1 and 2, control injected embryos; 3 and 4, XSSH (WT)-injected embryos; 5 and 6, XSSH (CS)-injected embryos. (F and G) Phosphorylation states of XAC in embryos, injected with β-gal (control), XSSH (wild type), or XSSH (CS mutant) mRNAs, were examined by 2D-immunoblotting at the stage 12 (F), and the ratio of pXAC to XAC was quantified and summarized in G.

Figure 6. Time-lapse images of control (β-gal mRNA-injection, left) and XSSH (CS) mRNA-injected (right) embryos. Injection was done into both blastomeres at the 2-cell stage and images were successively acquired from embryos that developed at stage 10.5 (time 0). Numbers indicate the time in min after the first frame, except for 24 hr passage (the last panel). Arrowheads show closing dorsal lip formed in the control embryo and the arrow represents the position of dorsal lip formation in the XSSH (CS)-injected embryo. Ventral images are shown until 150 min. XSSH (CS)-injected embryo alone is shown in the last panel. (B) Immunofluorescence micrographs of animal-vegetal sections of control (β-gal), XSSH (WT) and XSSH (CS) mRNAs. Animal cap regions, stained by anti-XSSH antibody, are shown. The arrow indicates the layer of animal cap roof.

Figure 7. (A) Two examples of β-gal (control), XSSH (WT), or XSSH (CS) mRNA-injected embryos with light phenotypes (escaped from the defect in gastrulation). The head region surrounded by boxes is enlarged in lower panels. Arrowheads represent the position of eyes in control and eyes with reduced size in deformed embryos (WT and CS), respectively. (B) The head region of β-gal (control) or XSSH (CS) mRNA-injected embryos at stage 33 were vertically sectioned and examined by immunofluorescence microscopy using anti-XSSH antibody. The arrow in the control embryo and the XSSH (CS) injected embryo indicates the forebrain and notochord, respectively. The arrowhead represents the complete eye-defect. (C) Ventral views of stage 10.5 embryos examined by *in situ* hybridization with Xbra probes. *Left panel*, sense (upper two embryos) and antisense (lower two embryos) images of control (H_2O-injected) embryos; *middle panel*, control (upper two embryos), XSSH (WT) and XSSH (CS) mRNA-injected embryos; *right panel*, XSSH (CS) mRNA-injected embryos. The lateral view clearly shows the Xbra-staining is present at the equatorial region (indicated by an arrow). (D) Immunoblots of whole lysates from embryos injected with β-gal (control, lanes 1 and 2) or XSSH (CS, lanes 3 and 4) mRNAs using antibody specific for α-muscle actin (SKA-06). Lysates in the respective lanes were derived from distinct embryos.

A

```
XSSH (-)   1'  CCTGATTTTGCAGGAAAAGTTTTCATCAACTAATAAAAGAAGCTACATTTAAATATCGCT
AY618876                                                **************************
XSSH (+)   1"                                           AAAGAAGCTACATTTAAATATCGCT
AY233266

           61' TGGAGTCCCTGTGACATGGCTCTAGTAACTCTTCAGGTCTCTTCGCTCGATGTGGGTTCG
               ************************************************************
           26" TGGAGTCCCTGTGACATGGCTCTAGTAACTCTTCAGGTCTCTTCGCTCGATGTGGGTTCG

          121' AATATTACACCTGTCCAGGATGATGAAAAAAGCAGAAGAAAGCGAATGCAGAGACG----
               ************************************************************
           86" AATATTACACCTGTCCAGGATGATGAAAAAAGCAGAAGAAAGCGAATGCAGAGACGTTTA

          177' -----------GCAGAGCTTTGTCATGGTGAAGGGAGCAGCACTTCTTCTGCAGGATGAA
                          ************************************************
          146" CTCTAATTCAGGCAGAGCTTTGTCATGGTGAAGGGAGCAGCACTTCTTCTGCAGGATGAA
```

B

```
Genomic XSSH   1 GGATGATGAAAAAAGCAGAAGAAAGCGAATGCAGAGACGgtaagggagatcattttcctg
XSSH (-)       1 GGATGATGAAAAAAGCAGAAGAAAGCGAATGCAGAGACG--------------------
XSSH (+)       1 GGATGATGAAAAAAGCAGAAGAAAGCGAATGCAGAGACG--------------------

              61 aacacttctcttttaatctagttttagttcatgcttttatcagatcaaatatccctgttt
              40 ------------------------------------------------------------
              40 ------------------------------------------------------------

             121 ctgatcttgcccagTTTACTCTAATTCAGGCAGAGCTTTGTCATGGTGAAGGGAGCAGCA
              40 --------------TTTACTCTAATTCAGGCAGAGCTTTGTCATGGTGAAGGGAGCAGCA
              40 ------------------------------GCAGAGCTTTGTCATGGTGAAGGGAGCAGCA

             181 CTTCTTCTGCAGGATGAAGGGGAACCTATAG
              86 CTTCTTCTGCAGGATGAAGGGGAACCTATAG
              71 CTTCTTCTGCAGGATGAAGGGGAACCTATAG
```

C

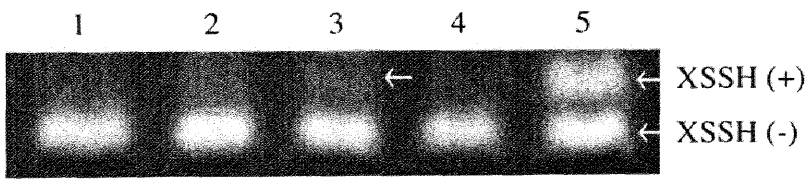

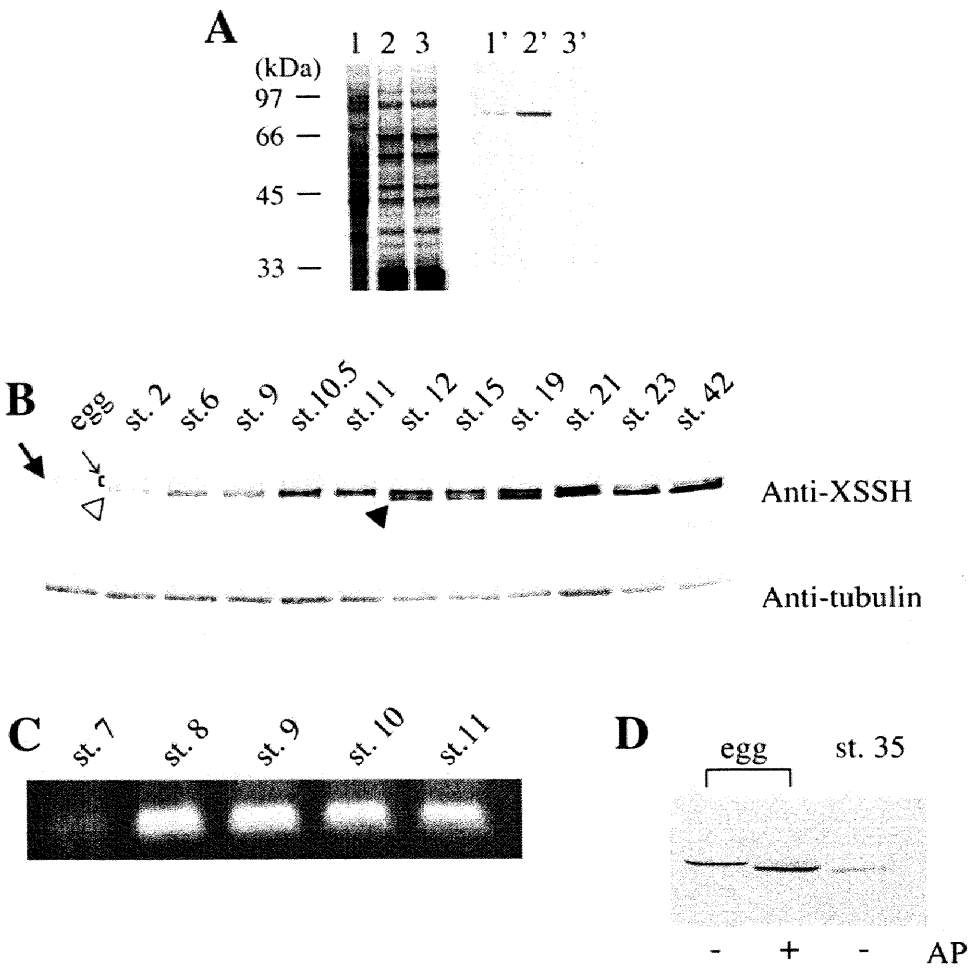
A
1 2 3 1' 2' 3'
(kDa)
97
66
45
33
B
egg
st. 2
st.6
st. 9
st.10.5
st.11
st. 12
st.15
st. 19
st. 21
st. 23
st. 42
Anti-XSSH
Anti-tubulin
C
st. 7
st. 8
st. 9
st. 10
st.11
D
egg
st. 35
-
+
-
AP

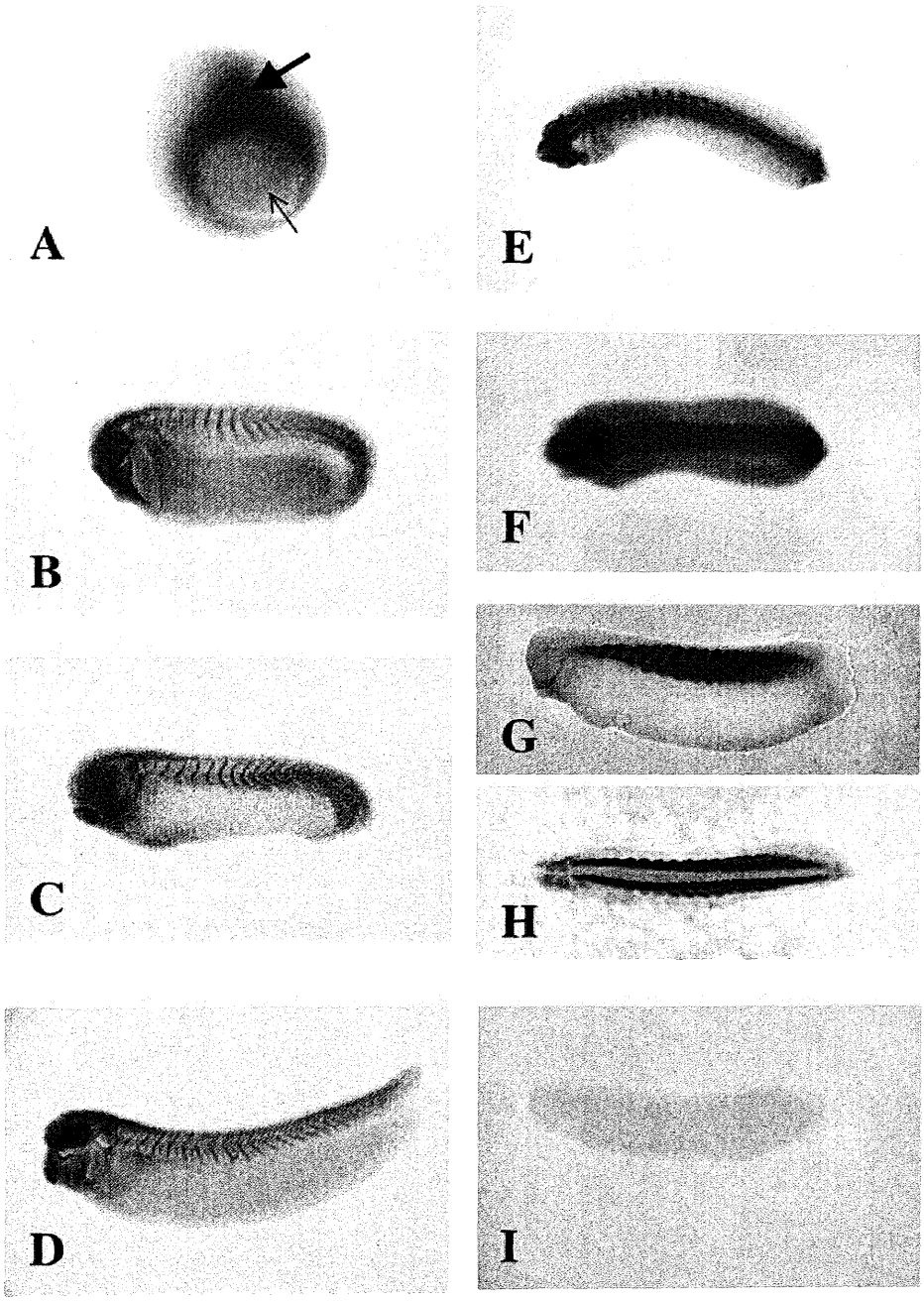
A
B
C
D
E
F
G
H
I

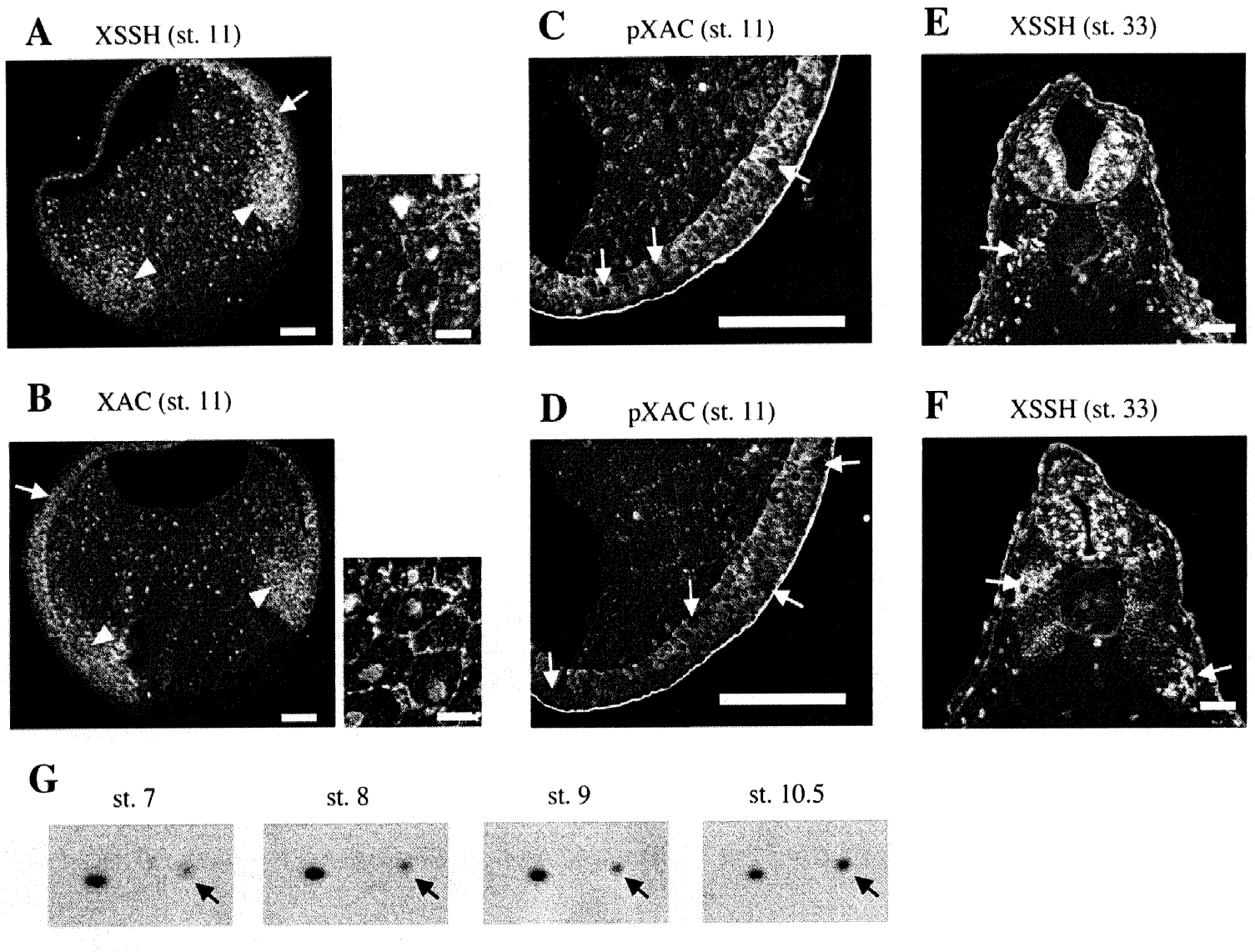
A
XSSH (st. 11)
B
XAC (st. 11)
C
pXAC (st. 11)
D
pXAC (st. 11)
E
XSSH (st. 33)
F
XSSH (st. 33)
G
st. 7
st. 8
st. 9
st. 10.5

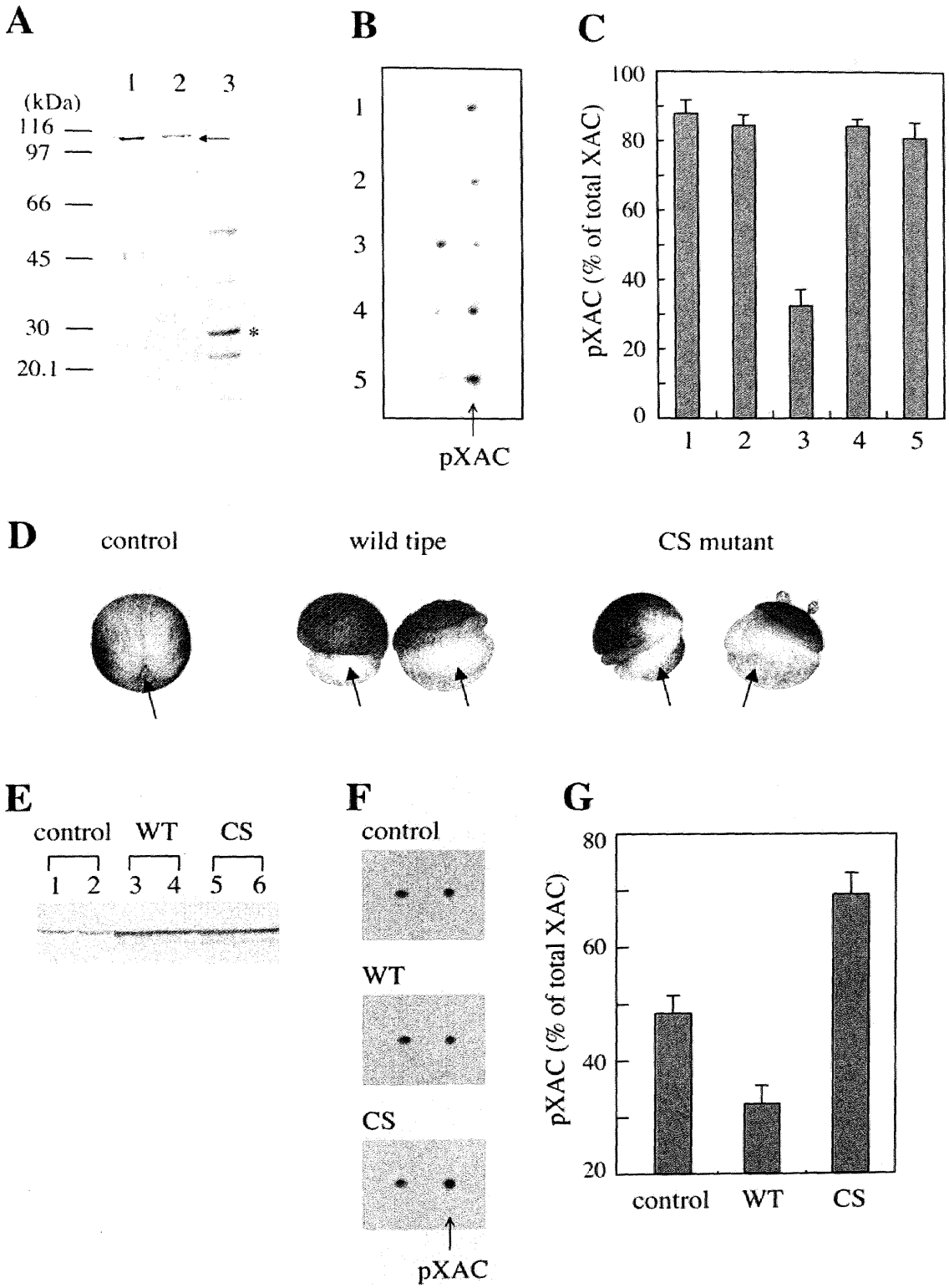
A
1 2 3
(kDa)
116
97
66
45
30
20.1
*
B
1
2
3
4
5
pXAC
C
pXAC (% of total XAC)
100
80
60
40
20
0
1 2 3 4 5
D
control
wild tipe
CS mutant
E
control WT CS
1 2 3 4 5 6
F
control
WT
CS
pXAC
G
pXAC (% of total XAC)
80
60
40
20
control WT CS

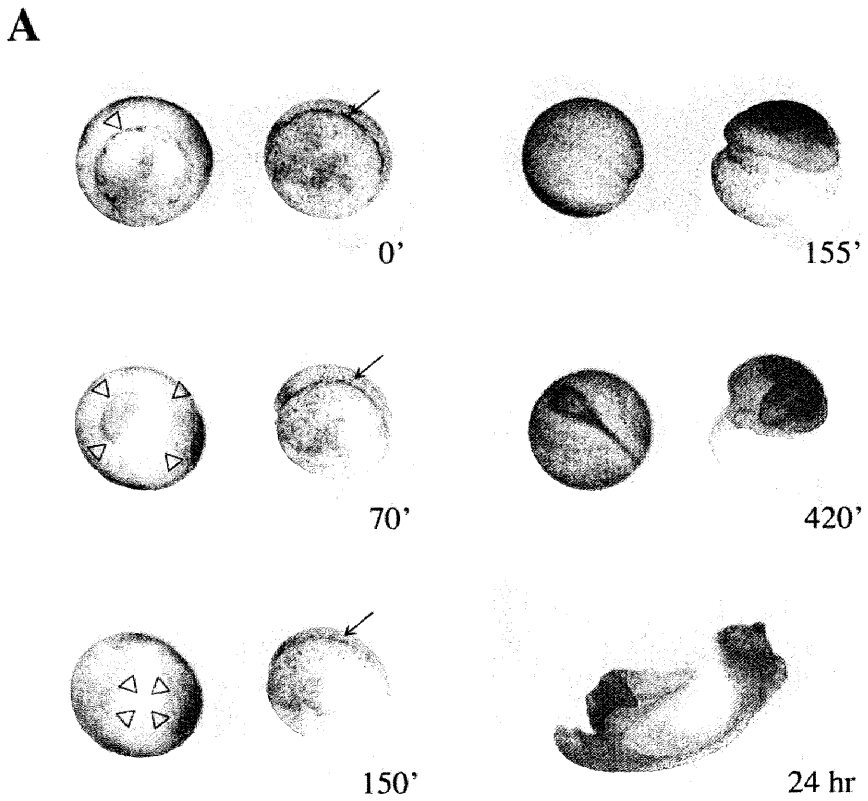
A
0'
155'
70'
420'
150'
24 hr
B
control
WT
CS

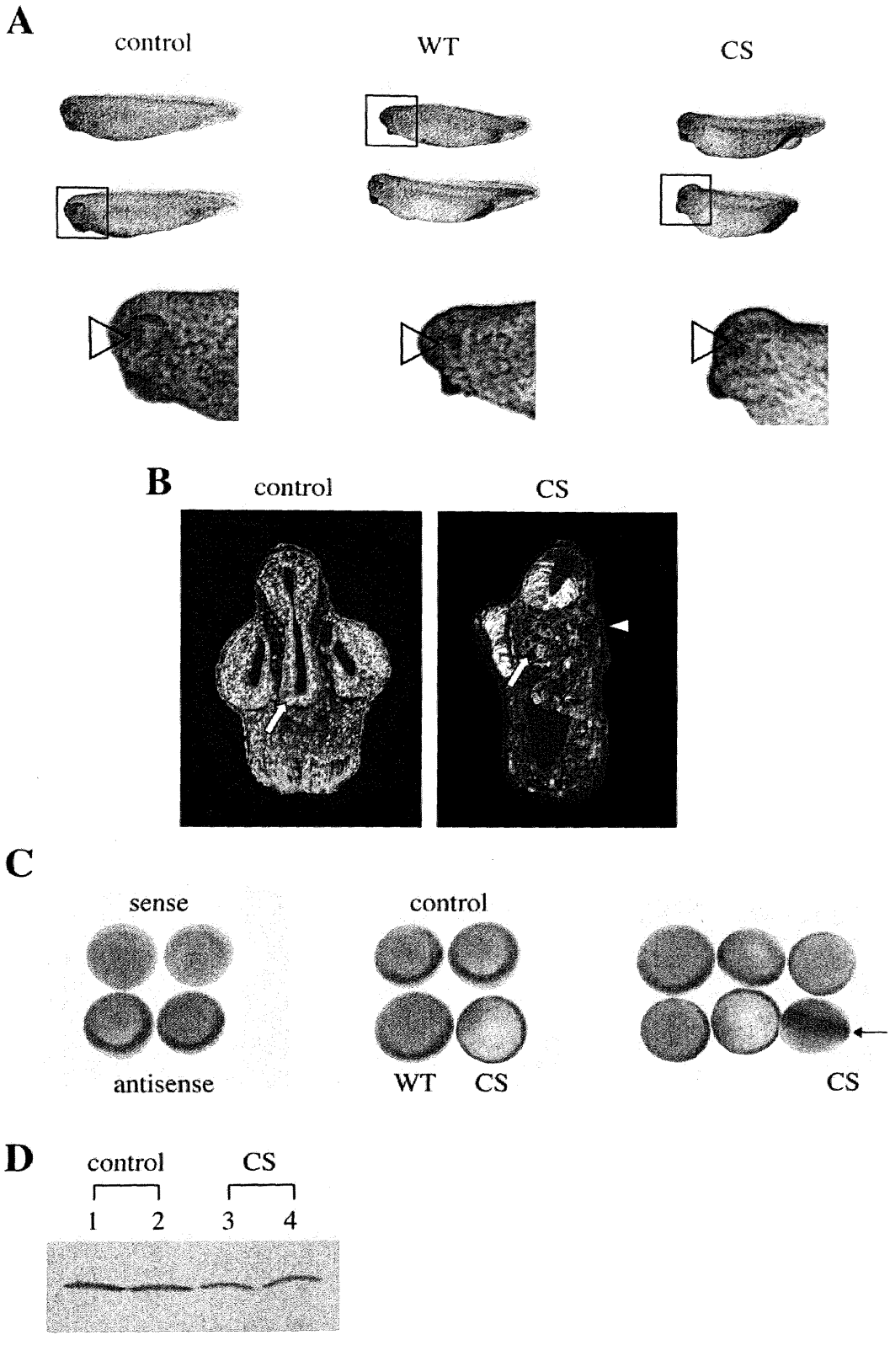
A
control
WT
CS
B
control
CS
C
sense
antisense
control
WT
CS
CS
D
control
CS
1
2
3
4

Table I. Gastrulation defects induced by ectopic expression of wild type and CS mutant XSSHs.

Sample RNA	Dose (ng)	Normal gastruration (%)	Defective gastrulation (%)	Total number of embryos
β-gal	0.5	92.9	7.1	28
	1	86.2	13.8	29
	2	84.0	16.0	25
XSSH (WT)	0.5	28.0	72.0	25
	1	18.2	81.8	22
	2	0	100	21
XSSH (CS)	0.5	66.7	33.3	27
	1	35.7	64.3	28
	2	20.8	79.2	24

Embryos were injected with β-gal (control), XSSH (WT), or XSSH (CS) mRNAs into the both blastomeres at the 2-cell stage. Phenotype of gastrulation was scored at stage 12.